

**Influence of Modifications of the Ribose Sugar on the
Parallel Stranded Adenosine Duplex**

William Copp

A Thesis

in

The Department

of

Chemistry and Biochemistry

Presented in Partial Fulfillment of the Requirements

for the Degree of Master of Science (Chemistry) at

Concordia University

Montréal, Québec, Canada

March 2016

© William Copp, 2016

CONCORDIA UNIVERSITY
School of Graduate Studies

This is to certify that the thesis prepared

By: William Copp

Entitled: Influence of Modifications of the Ribose Sugar on the Parallel Stranded Adenosine Duplex

and submitted in partial fulfillment of the requirements for the degree of
M.Sc.

complies with the regulations of the University and meets the accepted standards with respect to originality and quality.

Signed by the final examining committee:

Dr. Rafik Naccache Chair

Dr. Sebastien Robidoux Examiner

Dr. John Oh Examiner

Dr. Christopher Wilds Supervisor

Approved by Dr. Heidi Muchall
Chair of Department or Graduate Program Director

Dr. Andre Roy
Dean of Faculty

Date 18/03/2016

Abstract

Influence of Modifications of the Ribose Sugar on the Parallel Stranded Adenosine Duplex

William D. Copp, M.Sc.

Concordia University 2016

Applications of nucleic acid nanotechnology have been expanding since the early 1980s. The specific sequence programmability of these macromolecules makes them an attractive candidate for self-assembled nanostructures. Since the discovery of the DNA double helix, numerous secondary structures have been reported including G-quadruplexes, triplexes and i-motifs which have all been investigated as a molecular switch responsive to an external stimuli that causes a conformational change. In 1961 Rich *et al.* described the structure of the polyadenylic acid duplex from the X-ray diffraction pattern of fibers. The structure was proposed to be a parallel stranded duplex which is stabilized by adenine-adenine base pairing. The duplex requires acidic conditions to form which emphasizes its suitability and attractiveness as a pH dependent nanoswitch. Modification of the nucleoside residues in the polyadenosine duplex may prove useful in increasing the functionality and stability of this structure. To examine this, oligoadenylates were synthesized with various modified nucleotides and their effect on adenosine duplex stability was evaluated by UV thermal denaturation studies. It has been observed that the substitution of adenosine (rA) with 2'-deoxyadenosine (dA) residues destabilize the rA duplex by ~ 8 °C/insert. 2'-Deoxy-2'-fluoroadenosine modifications (rfA) introduced into oligoadenylates have a destabilizing effect on duplex stability, however contrastingly to dA oligonucleotides the uniformly rfA strands are capable of hybridization. CD, NMR spectroscopy and crystallographic studies show minimal structural perturbations introduced by chemically modified nucleotides. The

environmental requirement coupled with the ability to fine tune the stability or existence of adenine-adenine base pairs based on a simple modification at the 2' position presents a novel construct for potential nanodevices.

Acknowledgements

I would like to express my gratitude to my supervisor, Dr. Christopher J. Wilds, for his relentless support and encouragement throughout my studies. Achievement of my research goals and my development into an accomplished researcher would not have been possible without his mentoring.

I would like to thank my committee members, Dr. Sébastien Robidoux and Dr. John Oh, for their insight and advice on my research project.

I must extend a special thanks to Dr. Anne Noronha, who operated the ABI 3400 and synthesized the oligonucleotides in this study. Dr. Noronha also greatly assisted me in becoming a fully competent researcher in the Wilds' lab, and having laid the groundwork for my project was always available for enthusiasm and counsel.

I am appreciative of Dr. Alexey Denisov and Jingwei Xie, whose structural NMR and X-ray crystallographic work, respectively, was of utmost importance in understanding scientific phenomena. I would also like to thank Dr. Kalle Gehring for allowing me the unique opportunity to work in his structural biology lab for an exchange.

I would like to acknowledge Alain Tessier for the ESI-MS analysis of all oligonucleotides.

Lastly, I would like to thank all my labmates, past and present, for their assistance and training, and providing a special work environment.

Dedication

I would like to dedicate this thesis to my mother, father, brother et ma grandmère.

Table of Contents

List of Abbreviations	xi
List of Figures	xiii
List of Schemes	xvi
List of Tables	xvi
Chapter 1: Introduction	
1.1 Nucleic Acid Structure	1
1.2 Alternate Structures of Nucleic Acids	7
1.3 Applications of Nucleic Acid Structures	11
1.4 Background on the Adenosine Duplex	14
Chapter 2: Research Objectives	17
Chapter 3: Influence of 2'-Deoxyadenosine Residues on the Polyadenosine Duplex	22
3.1 UV Thermal Denaturation Studies on dA Modified Oligonucleotides	22
3.1.1 Studies at pH 4 of 2'-Deoxyadenosine Modified Oligonucleotides	22
3.1.2 Studies at Neutral pH and 4.4 M NH ₄ Cl of 2'-Deoxyadenosine Modified RNA Oligonucleotides	25
3.1.3 Ability of Uniformly DNA and RNA Oligoadenylates to Hybridize At pH 3	27
3.1.4 Effect of Acidity on Uniformly DNA vs. RNA Oligoadenylates	28
3.1.5 Reversibility of Duplex Formation at pH 3 for rA ₁₁ and dA ₁₁	29
3.1.6 Evaluation of Acid Catalyzed Degradation by Denaturing PAGE	31
3.1.7 HPLC Analysis of UV Denaturation Samples at pH 3	32
3.2 Native PAGE Analysis of the Adenosine Duplex in RNA and Sugar Modified Oligonucleotides	33

3.2.1 Native Polyacrylamide Gel Electrophoresis on RNA vs. DNA	
Oligoadenylates	33
3.2.2 Threshold pH for Adenosine Duplex Formation	36
3.2.3 Exploring pH and Molar Ratio Effects on Triplex vs. Duplex	
By Native PAGE	38
3.3 Extraction of van't Hoff Thermodynamic Parameters from	
Concentration Studies	41
3.3.1 Thermodynamics of RNA:DNA Chimera Duplex Formation	
at pH 4	42
3.3.2 Alternate Explanations of 2'-Deoxyadenosine Induced	
Adenosine Duplex Destabilization	43
3.4 Structural Insights into RNA/DNA Chimera Adenosine Duplexes	45
3.4.1 NMR Spectroscopy	45
3.4.2 X-ray Crystallography	46
3.4.3 Circular Dichroism Spectroscopy	48
Chapter 4: Effect of Chemically Modified Sugars on the Polyadenosine Duplex	51
4.1 C2'-Fluoro Modified Oligonucleotides	51
4.1.1 Thermal Stability of 2'-Fluorinated Oligonucleotides at pH 4	51
4.1.2 pH Dependence of the T_m for rA ₁₆ vs. rfA ₁₆	54
4.1.3 Melting Temperature Dependence on Oligonucleotide Concentration	56
4.1.4 UV Thermal Experiments on 2'-Fluoro Oligonucleotides at Neutral pH	
and High Ammonium Salt	57
4.1.5 X-Ray Crystallography of Fluorinated Adenosine Duplex	58
4.1.6 Circular Dichroism Spectroscopy of Fluorinated Oligonucleotides	60

4.2 Influence of ANA and F-ANA Modifications	62
4.2.1 UV Thermal Denaturation Experiments	62
4.2.2 Native PAGE on Uniformly Modified Arabinose Oligoadenylates	63
4.3 Adenosine Duplexes Containing 2'-O-Methylated Residues	65
4.3.1 UV Thermal Denaturation Studies on 2-O-Methyl Modified Oligonucleotides	65
4.3.2 Thermodynamic Parameters of 2'-O-Methylated Adenosine Duplex at pH 4	67
4.3.3 Influence of pH on 2'-O-Methyl Adenosine Duplex Stability	68
4.4 Influence of a 2'-5' versus 3'-5' Phosphodiester Bond	70
4.5 Self-Association of Native and Modified Branched Oligoadenylates	72
Chapter 5: Conclusions and Future Work	76
Chapter 6: Materials and Methods	79
6.1 Materials	79
6.2 Solid Phase Oligonucleotide Synthesis	79
6.3 Deprotection of Oligonucleotides	81
6.4 Purification of Oligonucleotides	82
6.5 Quantitation of Oligonucleotides	82
6.6 qTOF-ESI Mass Spectrometry	83
6.7 Enzymatic Digest Characterization	83
6.8 UV Thermal Denaturation Studies	84
6.9 Van't Hoff Analysis	85
6.10 Circular Dichroism Spectroscopy	85
6.11 Native Polyacrylamide Gel Electrophoresis	86

6.12 PABP RRM23 (98-269) Purification and Overexpression	86
6.13 Crystal Drop Setup for X-Ray Crystallography (Or Diffraction)	87
References	88
Appendix	95

List of Abbreviations

ABI: Applied Biosystems Inc.

ACN: Acetonitrile

ANA: Arabinonucleic acid

aA: Arabinoadenosine

afA: 2'-Deoxy-2'-fluoroarabinoadenosine

afI: 2'-Deoxy-2'-fluoroarabinoinosine

aI: Arabinoinosine

bp: Base-pair

C: Cytosine

CD: Circular dichroism

CIAP: Calf intestinal alkaline phosphatase

CPG: Controlled pore glass

C_t: Single strand concentration

dA: 2'-Deoxyadenosine

DCM: Dichloromethane

DMT: Dimethoxytrityl

DNA: Deoxyribonucleic Acid

dT: Thymidine

DTT: Dithiothreitol

EDTA: Ethylenediaminetetraacetic acid

FRET: Fluorescence resonance energy transfer

IEX: Ion exchange

G: Guanine

GST: Gluthathione S-transferase

HEPES: 4-(2-Hydroxyethyl)-1-piperazineethanesulfonic acid

HPLC: High performance liquid chromatography

NaCaco: Sodium cacodylate

NaOAc: Sodium acetate

NMR: Nuclear magnetic resonance
OD: Optical density
PABP: Poly(A)-binding protein
PAGE: Polyacrylamide gel electrophoresis
rA: Adenosine
rA^{2'-OMe}: 2'-O-Methyladenosine
RNA: Ribonucleic acid
rU: Uridine
RP: Reverse Phase
RRM: RNA recognition motif
TBDMS: *tert*-Butyldimethylsilyl
TBE: Tris Boric Acid EDTA Buffer
TEA: Triethylamine
TEMED: Tetramethylethylenediamine
qTOF-MS: Quadrupole-time of flight mass spectrometry
 T_m : Melting temperature
UV: Ultraviolet

List of Figures

Figure 1.1: (A) Primary structure of nucleic acids (B) Structure of the DNA double helix (C) Watson-Crick hydrogen bonding	2
Figure 1.2: Common conformations of the pentofuranose sugar	3
Figure 1.3: A, B and Z form nucleic acid duplexes	4
Figure 1.4: Asymmetry of base-pairing leads to major and minor grooves	5
Figure 1.5: Yeast tRNA illustrates various RNA secondary structures	6
Figure 1.6: Hoogsteen hydrogen bonding sites of (A) Adenine (B) Guanine	7
Figure 1.7: Hydrogen bonding pattern of (A) T·A:T and (B) C*·G:C motifs	8
Figure 1.8: (A) Hydrogen bonding pattern between guanines (B) Topology of an intramolecular G-quadruplex	9
Figure 1.9: (A) C*·C i-Motif base pairing (B) Intercalated i-motif tetramer	10
Figure 1.10: (A) Four way junction designed by Seeman (B) Depiction of a DNA cube (C) AFM image of DNA smiley face	11
Figure 1.11: $\text{Co}(\text{NH}_3)_6^{3+}$ Responsive B→Z-DNA nanomechanical device	12
Figure 1.12: (A) Illustration of i-motif→single strand conversion (B) Correlation between pH and fluorescence intensity of i-motif nanoswitch	13
Figure 1.13: (A) Adenine-adenine base pairing (B) Schematic depiction of adenosine duplex	15
Figure 1.14: (A) Continuous adenosine helix in the crystal (B) Role of ammonium cations in adenosine duplex stabilization	16
Figure 2.1: Adenosine and 2'-deoxyadenosine residues	17
Figure 2.2: 2'-Deoxy-2'-fluoroadenosine, arabinoadenosine and 2'-deoxy-2'- fluoroarabinoadenosine residues	19

Figure 2.3: 2'- <i>O</i> -Methyl, 2'-5' linked and branched adenosine modifications	20
Figure 3.1: UV thermal denaturation profiles of dA-rA chimera 9mers at pH 4	23
Figure 3.2: UV thermal denaturation profiles of dA-rA chimera 16mers at pH 4	24
Figure 3.3: UV thermal denaturation melts on rA ₁₆ with varying NH ₄ Cl at pH 7	25
Figure 3.4: UV thermal denaturation profiles of rA-dA chimera 16mers at pH 7, 4.4 M NH ₄ Cl	26
Figure 3.5: UV thermal denaturation profiles of RNA and DNA at pH 3	27
Figure 3.6: UV thermal denaturation profiles at varying pH of (A) dA ₁₁ (B) dA ₁₅	29
Figure 3.7: UV thermal denaturations from 15-95°C, followed by 95-30°C of (A) rA ₁₁ (B) dA ₁₁	30
Figure 3.8: Denaturing PAGE of degraded RNA and DNA samples	32
Figure 3.9: IEX chromatograms of pH 3 <i>T_m</i> samples of (A) rA ₁₆ and (B) dA ₁₆	33
Figure 3.10: Native polyacrylamide gel electrophoresis at pH 4	35
Figure 3.11: Native polyacrylamide gel electrophoresis at pH 7	35
Figure 3.12: Native PAGE at pH 5	37
Figure 3.13: Native PAGE at pH 5.5	37
Figure 3.14: Native PAGE at pH 6	38
Figure 3.15: Native PAGE at (A) pH 4 (B) pH 7 (C) pH 5.25 (D) pH 5.30 (E) pH 5.35	40
Figure 3.16: Hydrogen bonding pattern of rU·rA:rU at (A) Neutral pH (B) Acidic pH	41
Figure 3.17: Sugar-sugar contacts in backbone of adenosine duplex	44
Figure 3.18: Model of dT-rA ₄ -dA-rA ₃ determined by structural NMR spectroscopy	46
Figure 3.19: X-ray crystallographic data of rA ₅ -dA-rA ₅	47
Figure 3.20: Circular dichroism spectra of 2'-deoxy modified oligoadenylates at pH 4	48
Figure 3.21: Circular dichroism spectra of 2'-deoxy modified oligoadenylates at pH 7,	

4.4 M NH ₄ Cl	49
Figure 4.1: UV thermal denaturation profiles of rA-rfA chimera at pH 4	53
Figure 4.2: pH dependence of melting temperature of native and fluorinated oligonucleotides	55
Figure 4.3: UV Thermal denaturation experiments of fluorinated RNA at neutral pH, 4.4 M NH ₄ Cl	57
Figure 4.4: Hydration of the 2' group in rA vs. rfA duplexes	58
Figure 4.5: UV Thermal denaturation experiments of fluorinated RNA in crystallization conditions	59
Figure 4.6: Circular dichroism spectrum of native and fluorinated oligoadenylates at pH 4	60
Figure 4.7: Circular dichroism spectrum of native and fluorinated oligoadenylates at pH 7 and 4.4 M NH ₄ Cl	61
Figure 4.8: UV thermal denaturation spectrum of arabinose modified oligonucleotides at pH 4	62
Figure 4.9: Native PAGE of ribo and arabino oligoadenylates	64
Figure 4.10: UV thermal denaturation spectrum of 2'-O-methylated oligonucleotides at pH 4	66
Figure 4.11: UV thermal denaturation spectrum of 2'-O-methylated oligonucleotides at pH 7, 4.4 M NH ₄ Cl	67
Figure 4.12: pH dependence of melting temperature of native and methylated oligonucleotides	69
Figure 4.13: UV thermal denaturation spectrum of 2'-5' linked oligonucleotides at pH 4	70
Figure 4.14: UV thermal denaturation spectrum of 2'-5' 16mer at pH 4, 4.4 M NH ₄ Cl	72
Figure 4.15: UV Thermal denaturation experiments of branched DNA-RNA chimera at pH 4	73
Figure 4.16: UV Thermal denaturation experiments of fluorinated branched oligoadenylates at pH 4	74

Figure 4.17: UV Thermal denaturation experiments of native vs. fluorinated branched oligoadenylates at pH 4, 4.4 M NH ₄ Cl	75
Figure 5.1: Ribose sugar modifications to investigate in adenosine duplex stability	78
Figure 6.1: Sample chromatogram: RP HPLC trace of digest of dT-rA ₄ -dA-rA ₃	84

List of Schemes

Scheme 1: Steps in automated oligonucleotide synthesis <i>via</i> β-cyanoethylphosphoramidite chemistry	80
Scheme 2: Cleavage of fluorinated oligonucleotides from solid support	81

List of Tables

Table 2.1: Oligonucleotides synthesized to study the effect of 2'-deoxyadenosine residues	18
Table 3.1: Melting temperature of rA-dA chimera at pH 4	23
Table 3.2: Melting temperature of rA-dA chimera at pH 4	24
Table 3.3: Melting temperature of rA-dA chimera at pH 7 and 4.4 M NH ₄ Cl	26
Table 3.4: Thermodynamic parameters of duplex formation of oligoadenylates with dA inserts at pH 4	42
Table 4.1: 2'-Fluorinated oligonucleotides investigated in this study	52
Table 4.2: Melting temperature of native and fluorinated oligonucleotides at pH 4	54
Table 4.3: Thermodynamic properties of duplex formation of rA ₁₁ and rfA ₁₁ at pH 4	56
Table 4.4: Melting temperature of rA-rfA chimera at pH 7 and 4.4 M NH ₄ Cl	58
Table 4.5: Melting temperature of rA-rfA chimera at pH 5 and 3.0 M NH ₄ Cl	59
Table 4.6: Melting temperatures of arabinose modified oligoadenylates at pH 4	63
Table 4.7: Melting temperatures of 2'-O-methylated oligonucleotides at pH 4	65

Table 4.8: Melting temperatures of 2'- <i>O</i> -methylated oligonucleotides at pH 7, 4.4 M NH ₄ Cl	66
Table 4.9: Thermodynamic properties of duplex formation of 2'- <i>O</i> -methylated oligoadenylates at pH 4	68
Table 4.10: Melting temperatures of 2'-5' linked oligonucleotides at pH 4	70
Table 4.11: Melting temperature of branched oligonucleotides at pH 4	73

Chapter 1: Introduction

1.1 Nucleic Acid Structure

More than 60 years ago the secondary structure of DNA was solved by Watson and Crick¹. Although Watson and Crick are the household names associated with the DNA double helix, they stood on the shoulders of many others who had integral roles in deciphering the structure. The biological ramifications of this discovery continue to unfold; they were awarded the Nobel Prize in 1962 for their work. While initially met with some controversy, it is now common knowledge that DNA is the molecule responsible for physiological information storage, or genetic information. This is based on the ability of DNA to act as a template for messenger RNA strands, which copy the information contained by the DNA strand and translate it into building a specific protein. This is known as The Central Dogma of Molecular Biology.

A nucleic acid strand is a long polymer consisting of nucleotide building blocks. Each nucleotide unit is composed of a sugar and phosphate group which are connected to form the backbone of the structure with an aromatic nucleobase attached to the sugar (Figure 1.1).² The sugar is a pentofuranose, in the case of RNA it is ribose, or in the case of DNA the 2' hydroxyl group is substituted with a hydrogen and the sugar is known as 2'-deoxyribose. It is the nitrogenous heterocycle which gives the identity of the nucleotide, and it is covalently linked at the C1' atom;

known as the β -glycosidic bond. The four most abundant nucleobases are divided into two categories, the purines (adenine, guanine) and the pyrimidines (thymine, cytosine), and it is known that the genetic integrity during replication is retained by specific base pairing. The high fidelity exists due to the hydrogen bonding between the bases where adenine specifically base pairs with thymine (uracil in the case of RNA) and guanine with cytosine (Figure 1.1C). It is this hydrogen bonding between nucleic acid strands which is responsible for the specificity in double helix hybridization.

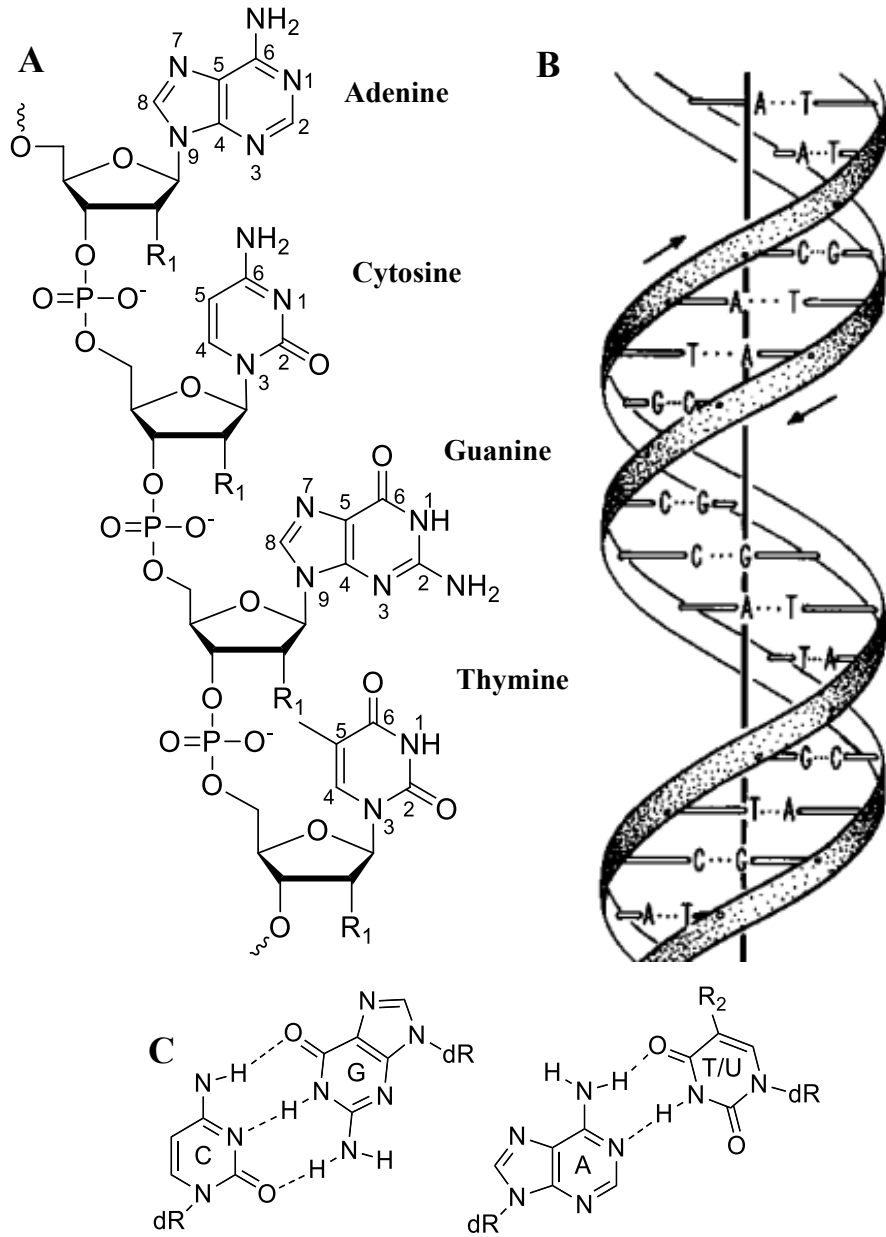


Figure 1.1: (A) Primary structure of nucleic acids (R₁: H [DNA], OH [RNA]) (B) Structure of the DNA double helix⁴ (C) Watson-Crick hydrogen bonding (R₂: CH₃ [T], H [U]). (Reproduced with permission from Elsevier).

An important aspect of nucleic acid structure is the conformation of the ribose sugar. The sugar is not rigidly planar as typically depicted however it is *puckered*, with one or more of the ring atoms above or below the plane of the other atoms of the pentofuranose sugar. While many dihedral angles can exist, in general the most populated conformations are C3'- or C2'-endo, which describes the positions of the atoms in the ring (Figure 1.2). The conformational equilibrium in RNA favors the C3'-endo (north) form, due to the presence of the 2'OH group.³ In DNA, however, the 2'-deoxy ribose sugar is significantly more flexible, and more subject to external influences. In general, the south (C2'-endo) conformer is more prevalent in solution; however conditions of low humidity/high salt can promote a population shift to the north conformer.³

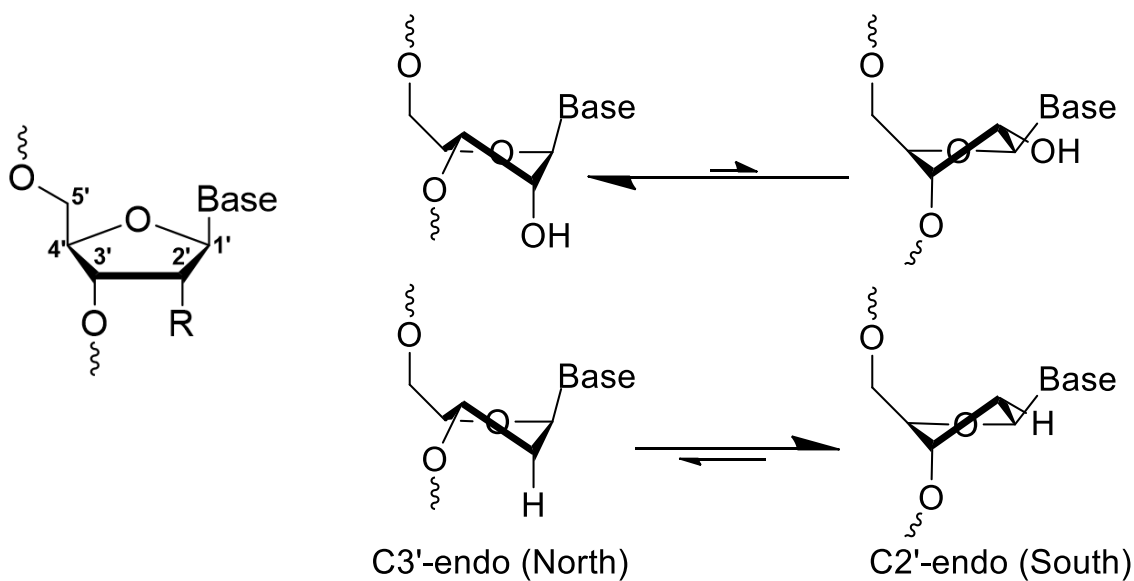


Figure 1.2: Common conformations of the pentofuranose sugar.

In the standard RNA or DNA double helix, the two hybridizing strands run antiparallel (opposite strand polarity); that is to say one strand runs 5'-3' and the complementary strand runs with the opposite orientation, 3'-5'. The previously described sugar pucker has important ramifications in the global topology of the nucleic acid helix (Figure 1.3). Due to the fact that the RNA ribose sugar almost exclusively adopts the C3'-endo sugar pucker, this leads to RNA only forming what is known as the A-form duplex. In conditions of high salt or low humidity DNA can also form this helix due to adopting the north sugar conformation.⁴ The X-ray diffraction pattern revealed that the A-form structure is characterized by a distance of 28 Å between repeating units; this is known as the pitch. The distance between successive base pairs, the rise, is 2.56 Å and therefore to avoid Van der Waals repulsion the bases are tilted out of the plane to maintain the

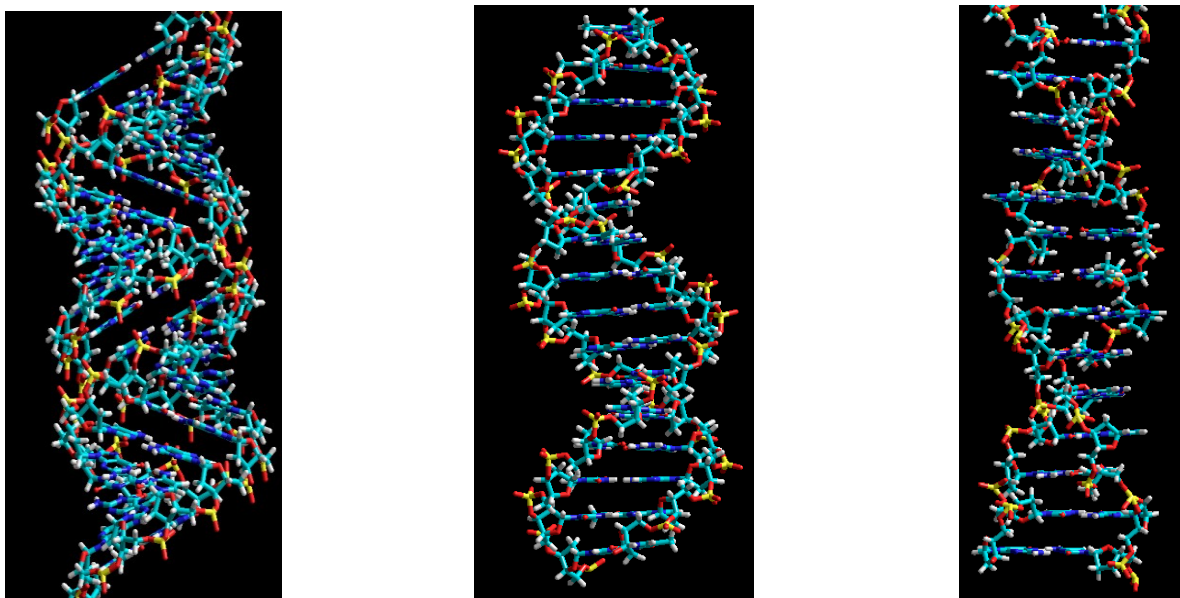


Figure 1.3: A, B and Z form nucleic acid duplexes. Models were drawn in Hyperchem™.

energetically favourable 3.4 Å separation. Although DNA can exist in either form, it is predominantly found in B-form. B-form DNA is characterized by being more elongated than A-form, with a helical pitch of 34 Å. In contrast to A-form the bases are perpendicular to the helical

axis and are able to retain the optimal 3.4 Å of separation. It should be mentioned that along with hydrogen bonding one of the most fundamental forces in duplex stability is the intra and intermolecular π - π stacking between the aromatic heterocycles. There is an asymmetry in the base pairing which leads to what are known as major and minor grooves (Figure 1.4). In A-RNA/DNA the major groove is quite deep and narrow, while the minor groove is shallow and wide. In B-DNA however both have similar depths whilst the major groove is wider. Importantly these grooves provide various sites for small molecules and proteins to interact with the nucleobases, and have had broad implications in biological processes as well as therapeutics.^{5,6} The terms A and B form more so refer to the average structure observed, and the local structure depends on environmental and base sequence variability.^{7,8} The polymorphism of DNA and importance of sequence on structure was illustrated by the discovery of Z-DNA (Figure 1.3C).⁹ Interesting structural features of the duplex are its left-handedness (as opposed to the standard right handed DNA duplex), the requirement of GC repeats, dG nucleobase oriented in a syn orientation, and an ion dependence (it was found to form in the presence of Mg^{2+} ions).

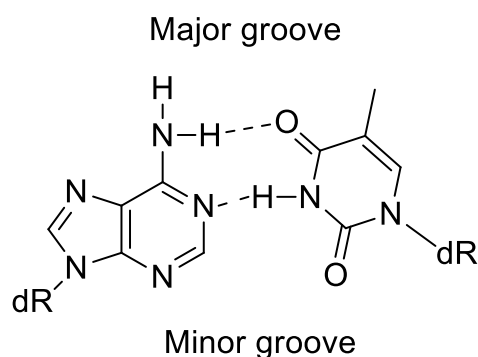


Figure 1.4: Asymmetry of base-pairing leads to major and minor grooves.

RNA secondary structure is distinguishable from DNA due to its ability to fold back upon itself and form various intramolecular motifs. tRNA, a key macromolecule involved in peptide

1.2 Alternate Structures of Nucleic Acids

The DNA double helix is by a wide margin the most well-known secondary nucleic acid structure, where the complementary nucleobases on each strand are engaged in Watson-Crick base pairing. In the above example of alternate RNA structures such as tRNA, what is important to note is that standard A:U and G:C base pairing interactions are ubiquitous. As early as 1957,¹¹ however, using various concentration and divalent cation dependence studies, it was found that a structure with a stoichiometry of 2 uridine strands to 1 adenosine strand was forming in solution. The logical rationale is that there are various hydrogen bond acceptor and donor sites on what has been termed the *Hoogsteen* face of the purines (Figure 1.6).

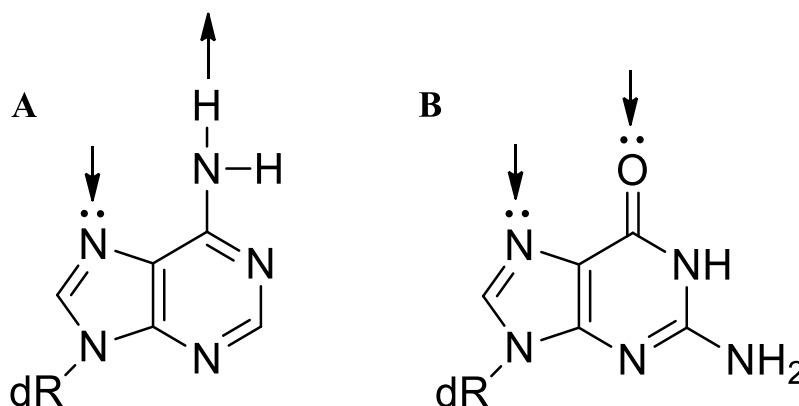


Figure 1.6: Hoogsteen hydrogen bonding sites of A) Adenine B) Guanine.

Since then it has been established that various triplex motifs exist such as A·A:U,¹² G·G:C¹³ and C*· G:C¹⁴ (which requires slightly acidic conditions to protonate the third cytosine rich strand).ⁱ Through structural evidence from X-ray crystallography¹⁵ and NMR spectroscopy hydrogen bonding on the Hoogsteen base of the purine has been confirmed (Figure 1.7). A major

ⁱ • refers to Hoogsteen H-Bonding, : Watson-Crick H-Bonding and * protonation

difference in the various motifs is that when the third strand is a purine it hybridizes in an antiparallel orientation to the purine strand; in contrast the third pyrimidine strand does so in a parallel orientation.

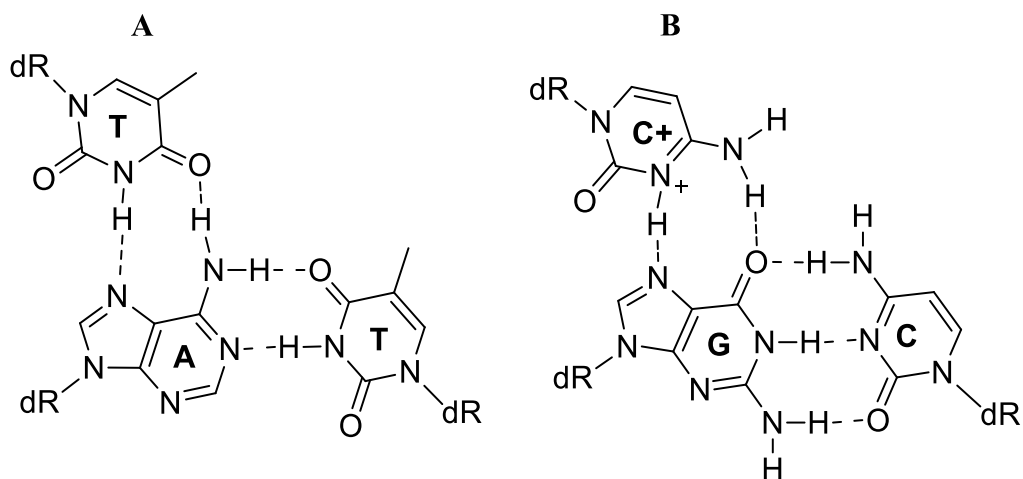


Figure 1.7: Hydrogen bonding pattern of parallel (A) T·A:T and (B) C*·G:C motifs.¹⁵

Another advance in nucleic acid chemistry was the observation of homopolymers to self-associate and form unique structures under certain conditions. In 1962¹⁶ a molecular structure of guanylic acid was solved and the four stranded structure has since been known as a G-quadruplex (or G-tetrad). Since its discovery it has been established that there is a plethora of potential antiparallel or parallel orientations in the single or multiple guanine rich strands.¹⁷ In all cases however the hydrogen bonding motif is clear and importantly a large monovalent cation is required; displacement of ions such as potassium causes a denaturation of the G-quadruplex. As illustrated in Figure 1.8 the guanine-guanine base pairing engages the Hoogsteen and Watson-Crick faces of the nucleobase. There is a rotational axis of symmetry, and the large monovalent cation (in this case potassium) sits in the helical cavity. Research into these structures has escalated due to the fact that the sequence of telomeres and the promoter region of certain oncogenes have

been shown to form intramolecular G-quadruplexes.¹⁸ G-quadruplexes are known to adopt a wide variety of various intra/inter molecular as well as parallel/antiparallel orientations.¹⁷

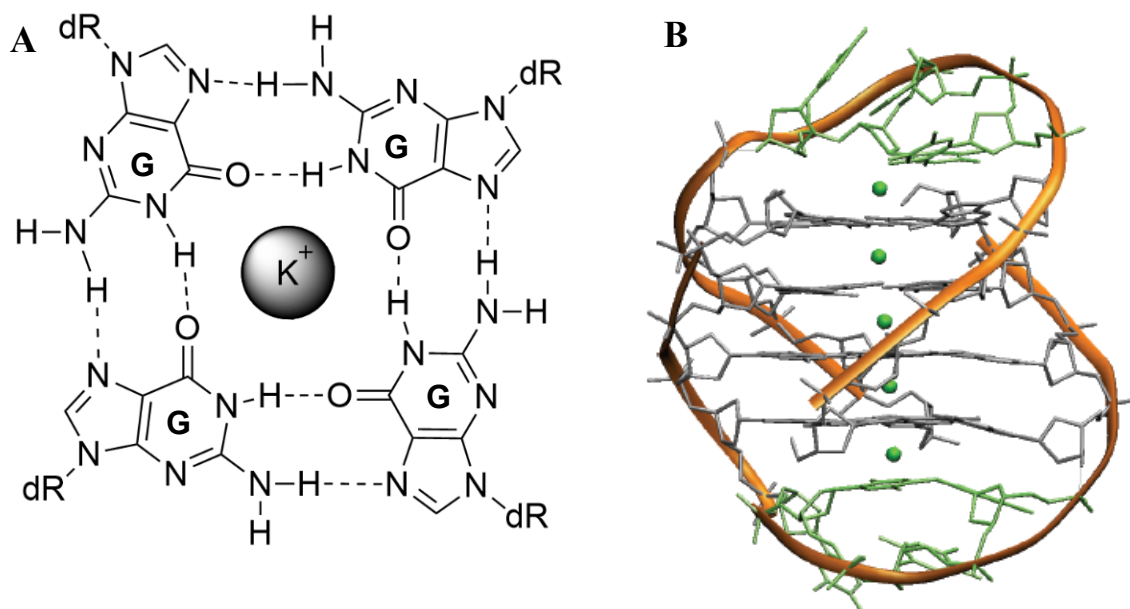


Figure 1.8: (A) Hydrogen bonding pattern between guanines (B) Topology of an intramolecular G-quadruplex.¹⁷ (Reproduced with permission from Oxford University Press).

Another well studied structure is known as the i-motif, first elucidated by Gehring¹⁹ and co-workers in 1993 by studying d(TC₅) by NMR spectroscopy. The i-motif is stabilized by cytosine-cytosine base pairing (Figure 1.9A), however requirement of protonation of one of the cytosines (hemiprotonation) is necessary for a third hydrogen bond to occur therefore slightly acidic conditions are an environmental requirement. In contrast to the nucleic acid double helix, base pairing occurs across parallel oriented nucleic acid strands. The i-motif is not a simple bimolecular structure, and actually has a tetrameric stoichiometry where the base pairs of the two hydrogen bonded strands are intercalated (Figure 1.9B). Similar to the G-quadruplex, i-motifs can occur both inter and intra²⁰ molecularly. Of course for every G rich sequence in the human genome there is a C-rich sequence (Watson-Crick base pairing), and this has led to research into the

biological relevance of the i-motif in telomeric^{20,21} and promoter regions of oncogenes.¹⁸ While it was thought that there was a conserved nature (two parallel duplexes intercalated in antiparallel fashion) of the i-motif despite sequence context, it has been shown that several²² C+T rich sequences form a duplex (lacking a tetrad intercalation). Recent research^{21,23} shows there is an i-motif population in less acidic conditions, and that there could be intermediate i-motif structures depending on the pH.²⁴ The fact that DNA forms the i-motif but not RNA²⁵ (likely due to the hydroxyl group involved in a steric clash) warrants further investigation of the role of the 2'-hydroxyl group in other unusual nucleic acid structures.

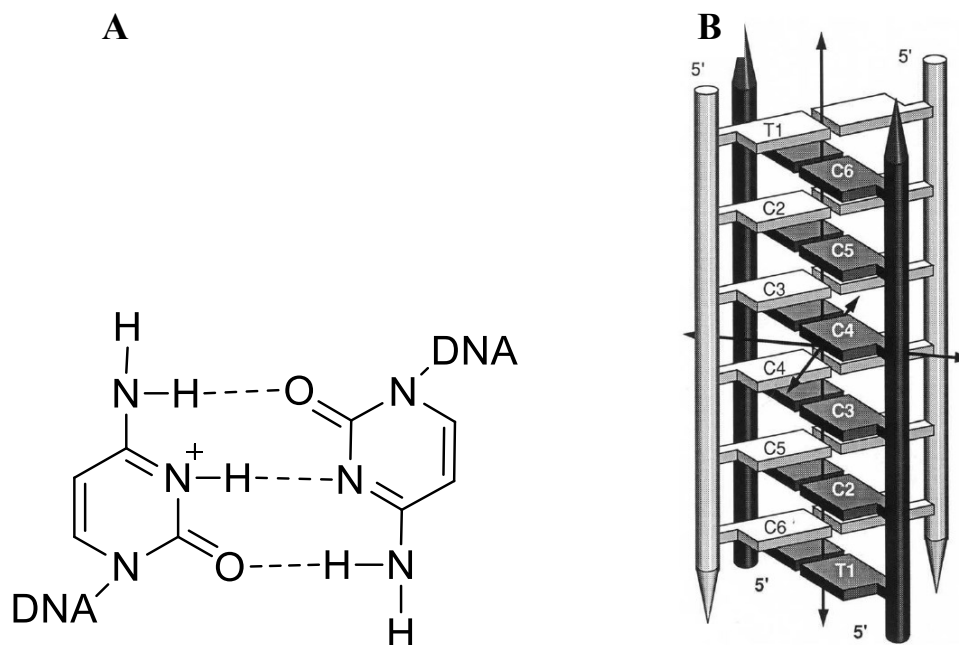


Figure 1.9: (A) C*:C i-Motif base pairing (B) Intercalated i-motif tetramer.¹⁹ (Reproduced with permission from Nature Publishing Group).

1.3 Applications of Nucleic Acid Structures

While nucleic acids are most commonly associated with being information carrying biomacromolecules, in the early 1980s Dr. Nadrian Seeman²⁶ sought to exploit short DNA sequences for the construction of various simple architectures on the nanoscale. This dawned the addition of DNA to the field of nanotechnology, which is a suitable candidate due to its sequence programmability; knowledge of Watson-Crick base pairing allows one to design a DNA sequence to specifically hybridize to other strands. Additionally, knowledge of the Van der Waals separation of base pairs (3.4 Å) allows one to fine tune length of a particular strand. The powerful tool that DNA strands can self-assemble based on simple base pairing rules has been exploited to construct simple shapes such as a cube²⁷ (Figure 1.10B) or even on the more macro scale designs such as a smiley face (Figure 1.10C).²⁸ Important to the growth of the field are advances in chemical oligonucleotide synthesis²⁹ which is commonly automated, and oligonucleotides can be synthesized up to ~150 nucleotides with ease.

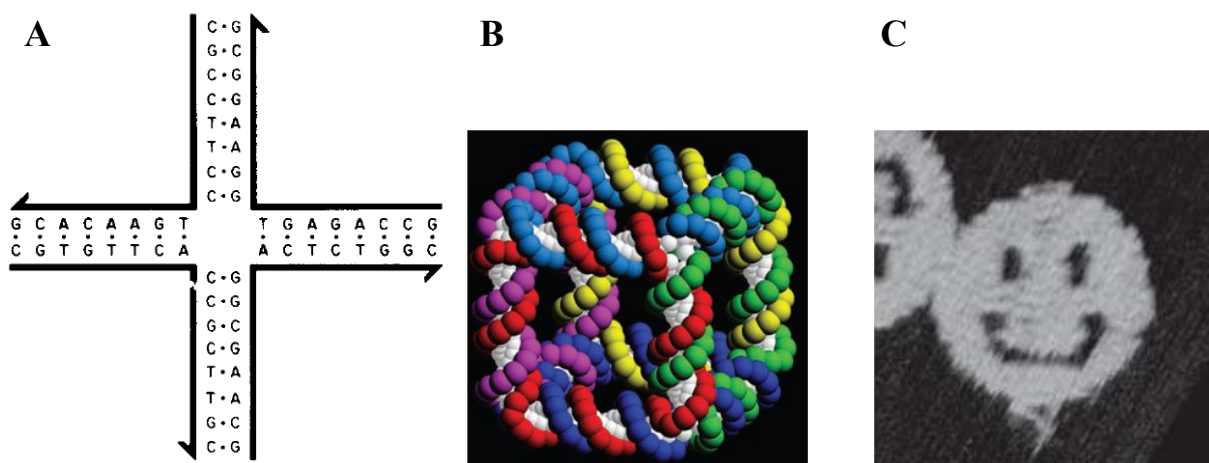


Figure 1.10: (A) Four way junction designed by Seeman²⁶ (B) Depiction of a DNA cube⁹⁰ (C) AFM image of DNA smiley face.²⁸ (Reproduced with permission from Elsevier, Annual Reviews and Nature Publishing Group).

While these nanoarchitectures are interesting from an academic sense and have potential applications such as drug delivery,³⁰ research has been shifting towards *molecular switches*: a molecule which undergoes a conformational change upon an external stimulus. One of the first examples of a molecular switch involved connecting two “double-cross over” DNA domains (a rigid DNA motif to properly monitor FRET) by a (GC)₁₀ duplex domain (Figure 1.11).³¹ As mentioned in section 1.1 GC rich sequences can form left handed duplexes under certain conditions (Section 1.1), and indeed Seeman *et al.* showed by FRET and CD that the complex could be reversibly oscillated between two architectures by adding/removing Co(NH₃)³⁺ cations.

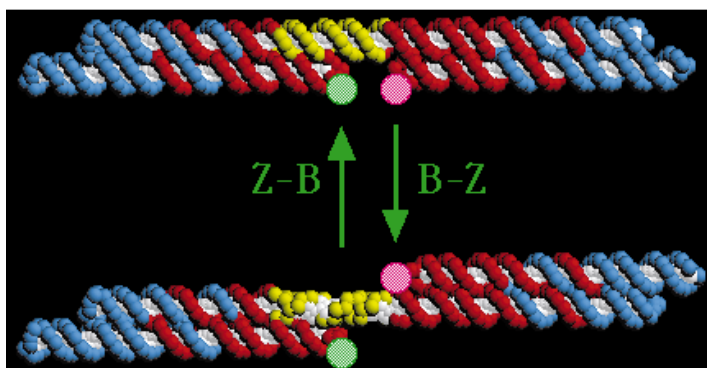


Figure 1.11: Co(NH₃)₆³⁺ Responsive B→Z-DNA nanomechanical device.³¹ (Reproduced with permission from Nature Publishing Group).

Applications of these molecular switches has focused into developing a biosensor; nucleic acid strands have been developed as sensors for various metal ions,^{32,33} and small molecules.³⁴ This section will elaborate more on nucleic acid structures which have been exploited as nanoswitches due to their pH dependence. Simmel and coworkers developed a reversible proton dependent oscillator utilizing the previously described i-motif.³⁵ They covalently tethered a cytosine rich oligonucleotide to a gold nanolayer, and labeled the oligonucleotide with a fluorescent moiety at the 3'-end. The length was designed such as that at low pH, the 3'-end moiety's fluorescence was quenched by the gold nanolayer due to its close proximity (Figure 1.12). At higher pH however, deprotonation of the N3 atoms of the cytidines cause the i-motif to collapse,

and the increase in fluorescence was monitored by the induced flexibility of the single strand. As Figure 1.12B illustrates, they were able to oscillate reversibly between i-motif and single stranded structures. Nanoswitches such as this demonstrate the proof of principle and are important to fundamental research with *in vivo* applications starting to emerge. While the macro pH of bodily fluids is understood, there is ongoing research into cellular pH mapping. In fact, Krishnan *et al*³⁶ were able to map time and spatial dependent regions of lower pH by creating a FRET based i-motif switch. Given that the microenvironment in tumours is acidic,³⁷ there exists a great potential for pH dependent nucleic acid based therapeutics.

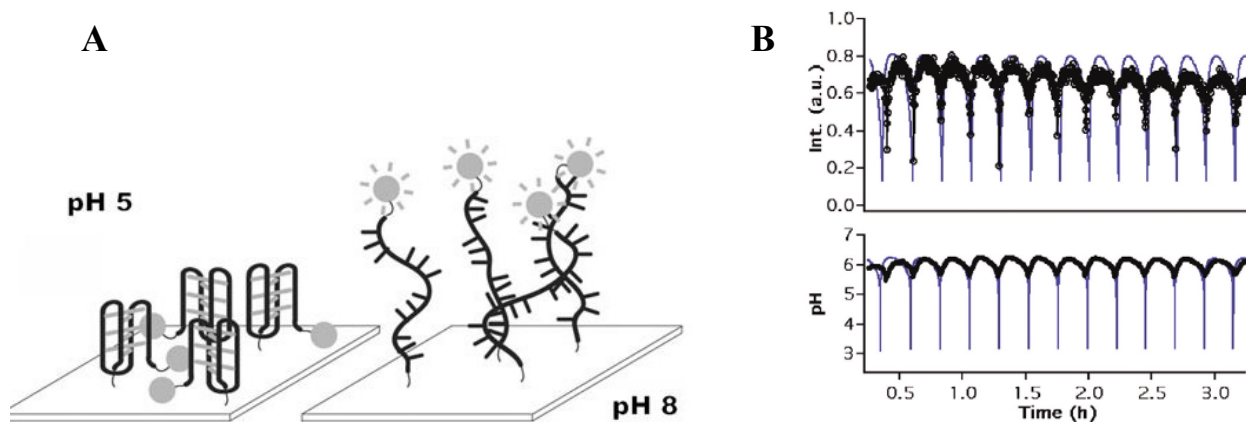


Figure 1.12: (A) Illustration of i-motif→single strand conversion (B) Correlation between pH and fluorescence intensity of i-motif nanoswitch. Grey spheres represent fluorescent tags.³⁵ (Reproduced with permission from John Wiley and Sons).

1.4 Background on the Adenosine Duplex

In 1961, Rich and coworkers³⁸ solved the molecular structure of polyadenylic acid from the fibers' X-ray diffraction pattern. The polyadenosine duplex was found to be a parallel stranded right handed duplex, stabilized by adenine-adenine base pairing. The base pairing involves the Hoogsteen face of the adenine bases, with the exocyclic amine group base pairing with the opposing strand's N7 ring atom (Figure 1.13). It is said to be N7-amino symmetric, as there is a 180° rotational symmetry in the hydrogen bonding pattern. An interesting property of the structure is it only forms under acidic conditions, which is due to the protonation of the N1 atom of adenine. Once protonated the positively charged N1 atom is in optimal position to electrostatically interact with the negatively charged backbone of the opposing strand; this is what is believed to lead to its overall compact structure. These geometric features do not result in major-minor grooves as found in a typical duplex, and lead to grooves of equal dimensions. While the structure solved by Rich and co-workers was done on the RNA duplex, recently³⁹⁻⁴¹ the DNA "A-motif" has been exploited as a potential pH responsive nanoswitch however concrete structural data of this structure remains elusive.

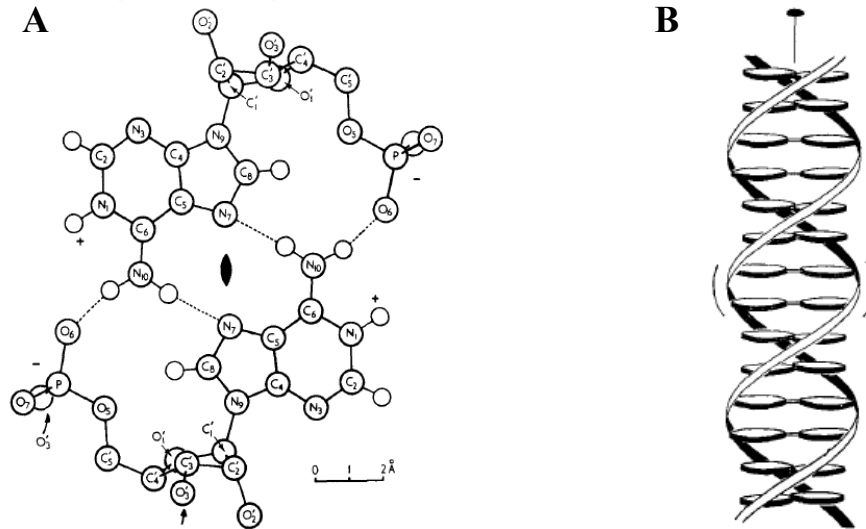


Figure 1.13: (A) Adenine-adenine base pairing (B) Schematic depiction of adenosine duplex.³⁸ Ribbons represent sugar-phosphate backbone, disks the nucleobases. (Reproduced with permission from Elsevier).

In 2013,⁴² the Gehring and Wilds labs succeeded in crystallizing the rA₁₁ duplex. However the crystals were grown at neutral pH, as opposed to the perceived environmental requirement of low pH. The crystal structure was unique in that the oligoadenylates were stabilized by 10 adenine base pairs, with the 11th nucleotide overhang able to hydrogen bond with an adenine overhang on another duplex; this leads to a continuous helix in the crystal structure (Figure 1.14). Electron density was observed for a tightly bound molecule for 18 of the nucleotides in the duplex. It is believed that these molecules are ammonium cations, which were present in high concentration in the crystallization set up. The positioning of these ammonium cations would allow each cation to form hydrogen bonds with the N1 atom of an adenine, and two of the phosphate oxygens of the opposing strand (Figure 1.14). This is analogous to the N1 protonation (in acidic conditions) which allows the adenine base to electrostatically interact with the other strand's backbone (termed an "inner salt effect"). UV thermal denaturation melts (to be discussed later) at neutral pH confirmed the importance of NH₄⁺ ions and no evidence of duplex was noted when they were absent. The

newfound environmental factor (NH_4^+ cations) warrants further investigation into the duplex's potential as a molecular switch.

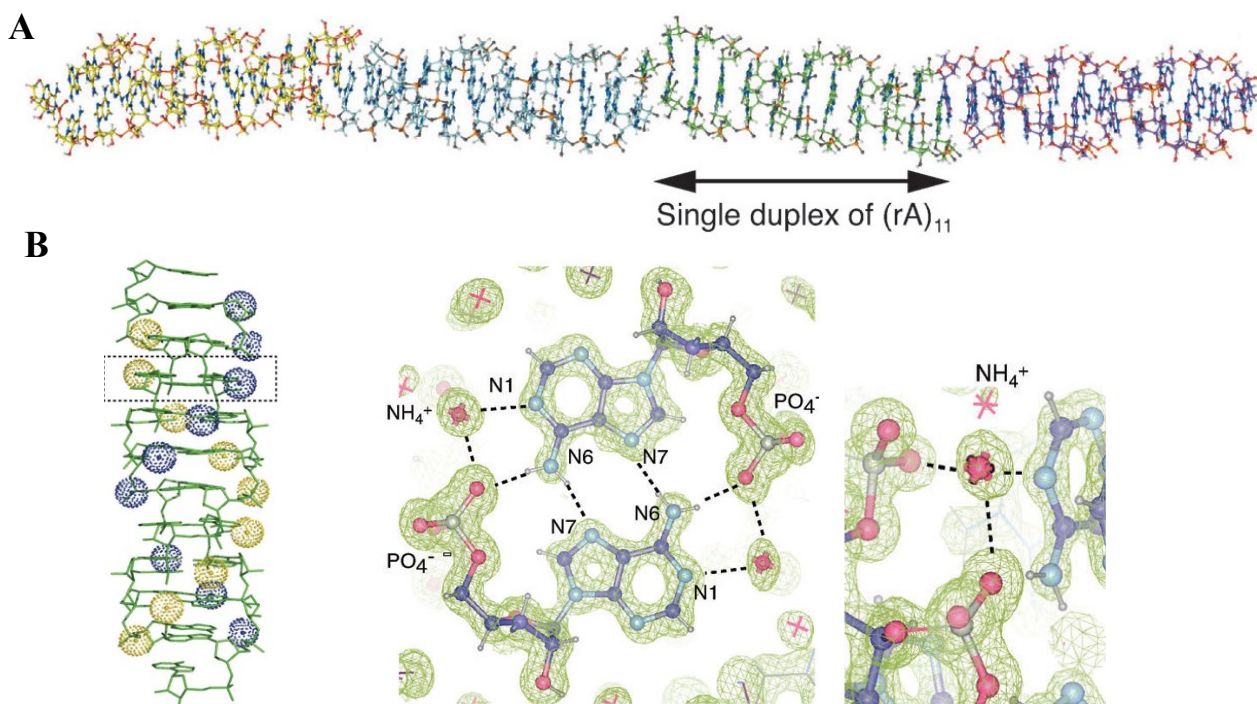


Figure 1.14: (A) Continuous adenosine helix in the crystal (B) Role of ammonium cations in adenosine duplex stabilization.⁴² (Reproduced with permission from John Wiley and Sons).

Chapter 2: Research Objectives

The ability of adenosine (rA) to form the polyadenosine (poly rA) duplex at low pH and neutral pH (with 4.4 M NH₄Cl) is well established.^{38,42} There have also been studies investigating 2'-deoxyadenosine's capability of forming a parallel stranded homoduplex.⁴⁰ However to date little is known on the effect of modifying the adenosine nucleoside on the poly rA duplex structure. To address this, the influence of dA and chemical modifications at the 2'-position of the ribose sugar on the poly rA duplex will be explored in this thesis. A common technique used to evaluate duplex stability is UV thermal denaturation; a key experiment performed throughout this research project. Secondary structure formation was evaluated by native polyacrylamide gel electrophoresis. Solution structure determination was done in collaboration with Dr. Alexey Denisov by NMR spectroscopy (Concordia University). Attempts to grow crystals and structure determination by high resolution X-ray crystallography was performed in collaboration with Professor Kalle Gehring (McGill University).

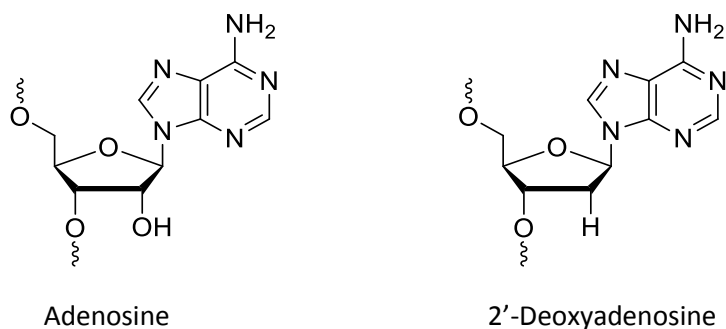


Figure 2.1: Adenosine and 2'-deoxyadenosine residues.

The first modification examined, 2'-deoxyadenosine (dA), has a hydrogen as opposed to the hydroxyl group at the C2'-atom (Figure 2.1). This modification has demonstrated drastic

differences in nucleic acid secondary structure due to the flexibility of the pentofuranose sugar and a general preference for the C2' endo sugar pucker.²

Oligonucleotides 9, 11 and 16 nucleotides in length were synthesized (Table 2.1) to investigate the influence of dA substitution. Oligonucleotides containing an increasing number of dA residues were prepared in addition to a uniformly modified DNA strand. The purpose of synthesizing different lengths is to note whether trends can be interpolated, and it should be noted the pH 7, 4.4 M NH₄Cl conditions require *exclusively* longer lengths for duplex formation.

Sequence (5'-3')		
dT-rA ₈	}	9mers
dT-rA ₄ -dA-rA ₃		
dT-rA ₃ -dA ₂ -rA ₃		
dT-rA ₃ -dA ₃ -rA ₂		
dT-dA ₈	}	11mers
rA ₅ -dA-rA ₅		
rA ₅ -dA ₂ -rA ₄		
rA ₄ -dA ₃ -rA ₄		
dA ₁₁	}	16mers
rA ₁₆		
rA ₁₀ -dA-rA ₅		
rA ₉ -dA ₂ -rA ₅		
rA ₁₀ -dA-rA ₃ -dA-rA		
rA ₉ -dA ₃ -rA ₄		
dA ₁₆		

Table 2.1: Oligonucleotides synthesized to study the effect of 2'-deoxyadenosine residues.

Another modification that was evaluated is 2'-deoxy-2'-fluoroadenosine (rfA, Figure 2.2). This analogue was of interest for the adenosine duplex study due to the presence of the most electronegative atom, fluorine, at the 2' position which has been described to further rigidify the sugar in C3' endo pucker relative to RNA.^{43,44} Almost ubiquitously in the literature the 2'-fluoro modification is stabilizing to canonical A-form RNA duplexes, as observed from increased duplex thermal stability.^{43,45-47} Furthermore, the fluoro substituent has been shown to be well tolerated in

other higher order nucleic acid structures such as parallel stranded i-motifs⁴⁸ and G quadruplexes.⁴⁹ Oligonucleotides containing the ribofluoro substituent have been shown to be more stable to acid catalyzed depurination and degradation under basic conditions than their unmodified counterparts.⁵⁰ Phosphorothioates in tandem with this fluoro moiety have shown promise as antisense agents *in vivo*, and due to their increased ability to activate RNAse H in chimeric gapmers.⁵¹ Additionally, phosphorothioates are more resistant to degradation by various nucleases.⁵²

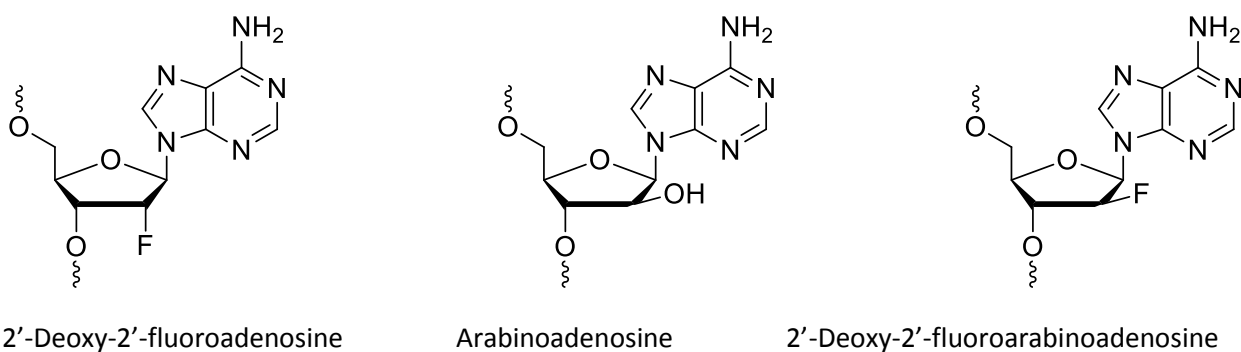


Figure 2.2: 2'-Deoxy-2'-fluoroadenosine, arabinoadenosine and 2'-deoxy-2'-fluoroarabinoadenosine residues.

The influence of arabino (aA) and 2'-deoxy-2'-fluoroarabino (afA) adenosine inserts (Figure 2.2) on the adenosine duplex were also investigated. The 2' epimer of ribose (and 2'-fluoro) offers a more rigid DNA mimic, with the less flexible arabinose sugar occupying conformations of C2' and O4' endo sugar pucker.⁵³⁻⁵⁵ The population distribution is driven by the 2' substituent and environmental factors such as salt and hybridization.⁵³ It is believed that oligoarabinonucleotides' ability to activate RNAse H^{56,57} is due the tendency of the arabinose sugar to emulate the 2'-deoxyribose sugar conformation.

The final set of modifications explored were the 2'-*O*-methyl, the 2'-5'-backbone linked series and branched oligonucleotides (Figure 2.3). The 2'-*O*-methyladenosine (rA^{2'-OMe}) modified nucleotides are similar to the fluoro modification in that they offer a more rigid RNA analogue.^{58,59} Additionally they have been shown to have more resistance to degradation by nucleases and chemical degradation⁶⁰ and stabilizing to "standard" A-form and hybrid duplexes.^{61,62}

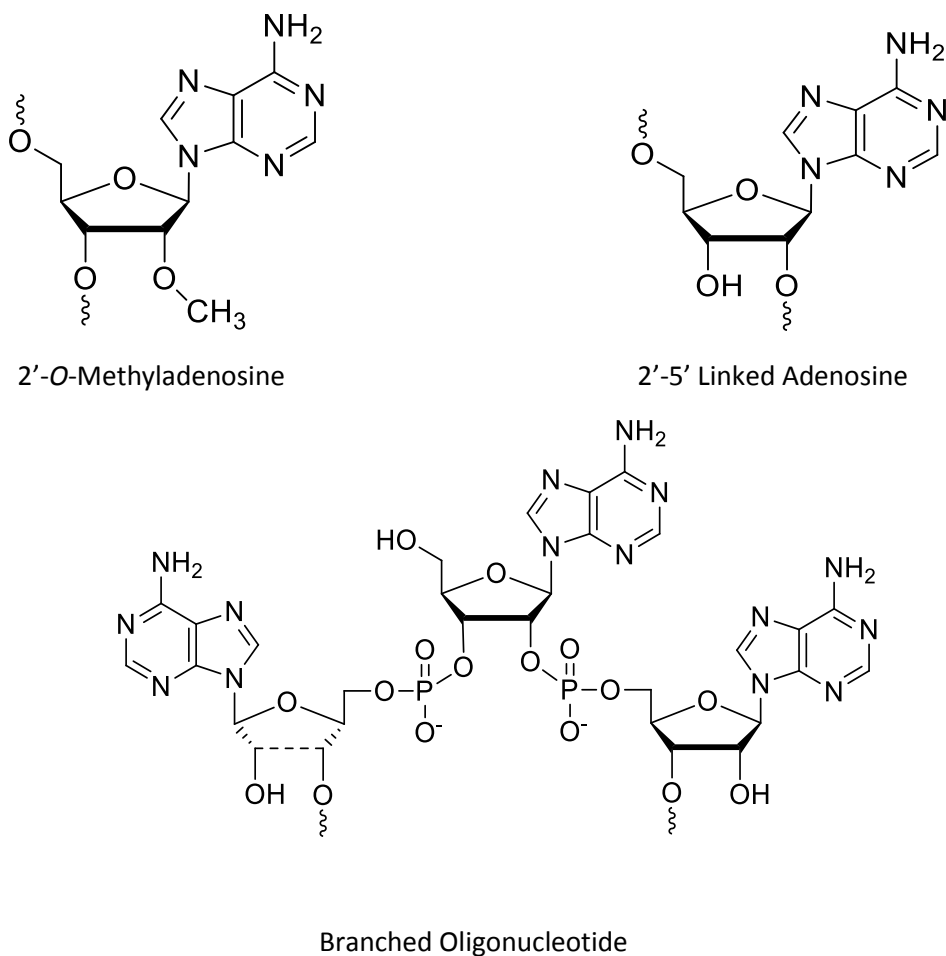


Figure 2.3: 2'-*O*-Methyl, 2'-5' linked and branched adenosine modifications.

The 2'-5' modified RNA has the adjacent nucleotides in a strand linked by the 2' as opposed to the 3' oxygen atom. For the branched oligonucleotide two parallel adenosine strands are covalently held in geometric juxtaposition by a branching adenosine nucleoside through the 2' and 3' oxygen atoms.

Chapter 3: Influence of 2'-Deoxyadenosine Residues on the Polyadenosine Duplex

3.1 UV Thermal Denaturation Studies on dA Modified Oligonucleotides

One of the main techniques of measuring duplex stability is the UV thermal denaturation experiment, where one measures absorbance (typically at 260 nm) as a function of temperature.⁶³ This relies on the property that random coils of DNA/RNA absorb more light at this wavelength than when in a complex: referred to as a hyperchromic transition. This is chiefly the result of the unstacking of the nucleobases, which are responsible for absorbing light at this wavelength. In this study the melting temperature (T_m) is measured as the temperature where the slope (dA/dT) is at a maximum ($dA^2/d^2T=0$): corresponding to 50% random coil:50% complex. It should be noted that in this thesis *fraction of maximum absorbance* is given on the y-axis which corresponds to % hyperchromic transition.

3.1.1 Studies at pH 4 of 2'-Deoxyadenosine Modified Oligonucleotides

The influence of 2'-deoxyadenosine (dA) inserts on the stability of the adenosine duplex in oligonucleotides 9 nucleotides in length was evaluated. The control oligonucleotide contained 8 adenosine residues with a 5' thymidine, for the purpose of introducing asymmetry for structural studies by NMR spectroscopy (to be discussed later). The amount of dA inserts was increased stepwise to a uniform dA sequence (Table 3.1). The UV thermal denaturation experiments revealed a destabilizing effect of $\sim 8^\circ\text{C}/\text{dA}$ insert at pH 4, with the uniformly dA oligonucleotide showing no clear sigmoidal transition (Figure 3.1)

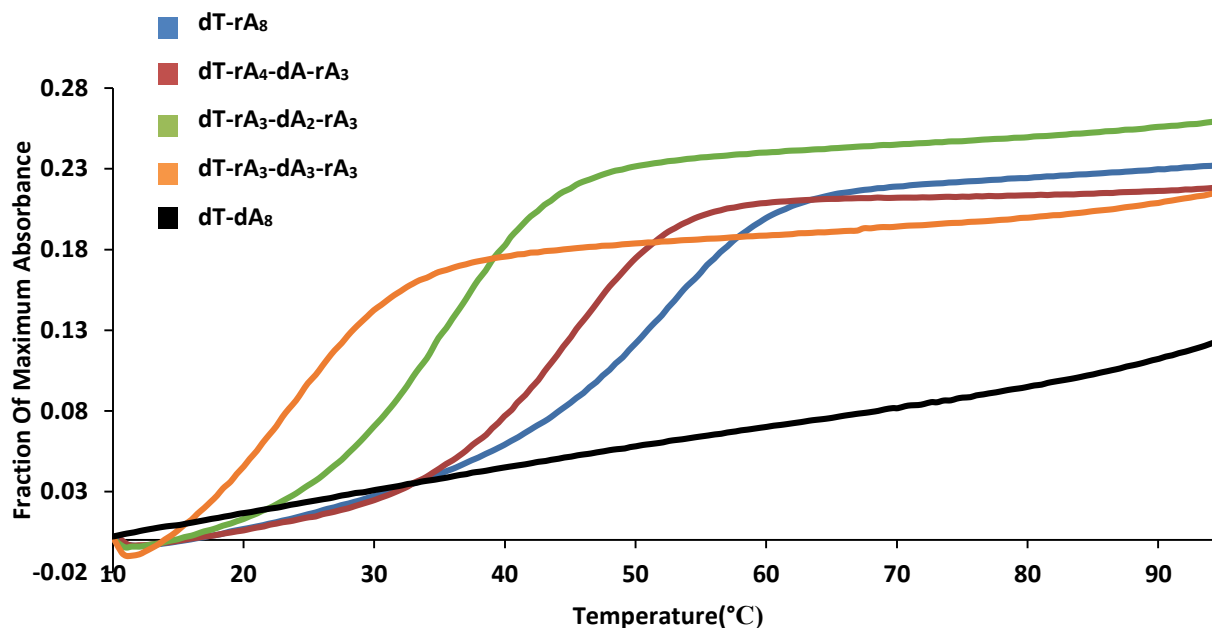


Figure 3.1: UV thermal denaturation profiles of dA-rA chimeric 9mers at pH 4 (Buffer: 50 mM NaOAc). 4.2 μ M single strand concentration.

Sequence (5'-3')	T_m ($^{\circ}$ C)	ΔT_m ($^{\circ}$ C)
dT-rA₈	53	
dT-rA₄-dA-rA₃	45	-8
dT-rA₄-dA₂-rA₃	37	-16
dT-rA₄-dA₃-rA₃	<24	<-29
dT-dA₈	NA	NA

Table 3.1: Melting temperature of rA-dA chimera at pH 4.

To further investigate this trend, oligoadenylates 16 nucleotides (16mer) in length were studied. Following similar rationale, the dA content of each oligoadenylates was increased systematically (Table 3.2). One single dA insert has a less pronounced effect in the 16mer, decreasing the T_m by 2° C. The location of multiple dA inserts in an oligonucleotide appears to have a slight effect on the stability. Two consecutive dA inserts results in a diminished reduction in stability relative to separating them with rA nucleotides. The uniform DNA oligonucleotide

exhibited no sigmoidal transition at pH 4, which suggests that no duplex formed under these conditions (Figure 3.2).

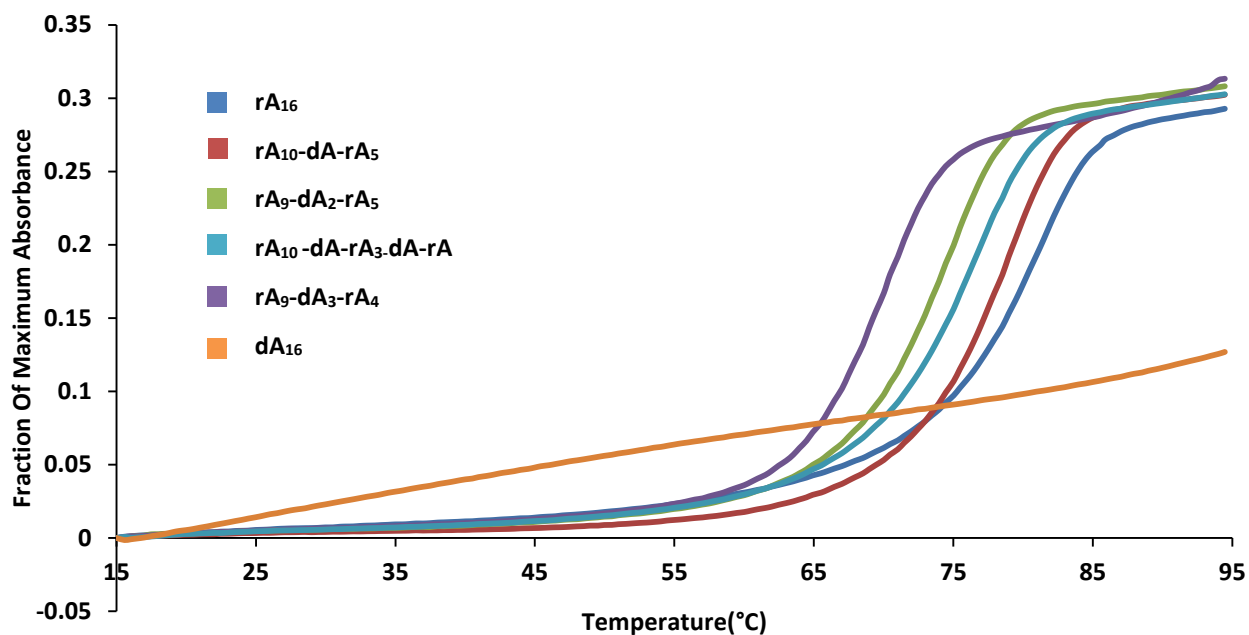


Figure 3.2: UV thermal denaturation profiles of dA-rA chimera 16mers at pH 4 (Buffer: 50 mM NaOAc). 2.3 μ M single strand concentration.

Sequence (5'-3')	T_m ($^{\circ}$ C)	ΔT_m ($^{\circ}$ C)
rA ₁₆	82	
rA ₁₁ -dA-rA ₅	80	-2
rA ₉ -dA ₂ -rA ₅	75	-7
rA ₁₀ -dA-rA ₃ -dA-rA	77	-5
rA ₉ -dA ₃ -rA ₄	71	-11
dA ₁₆	NA	NA

Table 3.2: Melting temperature of rA-dA chimera at pH 4.

3.1.2 Studies at Neutral pH and 4.4 M NH₄Cl of 2'-Deoxyadenosine Modified RNA Oligonucleotides

The influence of varying the NH₄Cl concentration on the melting temperature of the RNA 16mers at neutral pH was evaluated. Buffers were prepared with increasing NH₄Cl concentration at neutral pH and UV thermal melts were performed (Figure 3.3). No sigmoidal transition was observed in the buffers evaluated other than the one containing 4.4 M NH₄Cl which was used for subsequent studies.

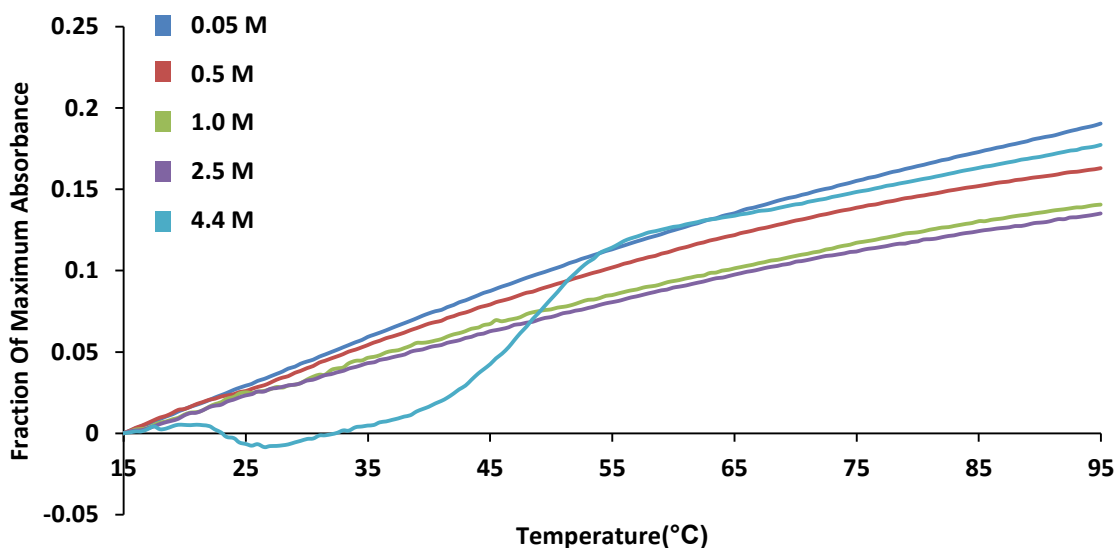


Figure 3.3: UV thermal denaturation melts on rA₁₆ with varying NH₄Cl at pH 7 (Buffer: 40 mM Na₂HPO₄, 30 mM citric acid).

To evaluate if the 2'-deoxyadenosine destabilization trend was consistent for adenosine duplex formation (4.4 M NH₄Cl and neutral pH) UV thermal denaturation studies were performed. Duplex formation under these conditions required longer oligonucleotides, as the T_m is generally too low to evaluate with shorter oligonucleotides (data not shown). Oligonucleotides containing a single dA insert exhibit similar destabilization to the 9mer oligonucleotides at acidic pH (7-8°C), and the trend is consistent with an increasing amount of inserts. As observed under previous

conditions, dA₁₆ did not show a sigmoidal transition, which suggests it is not forming a duplex at neutral pH in the presence of 4.4 M NH₄Cl (Figure 3.4).

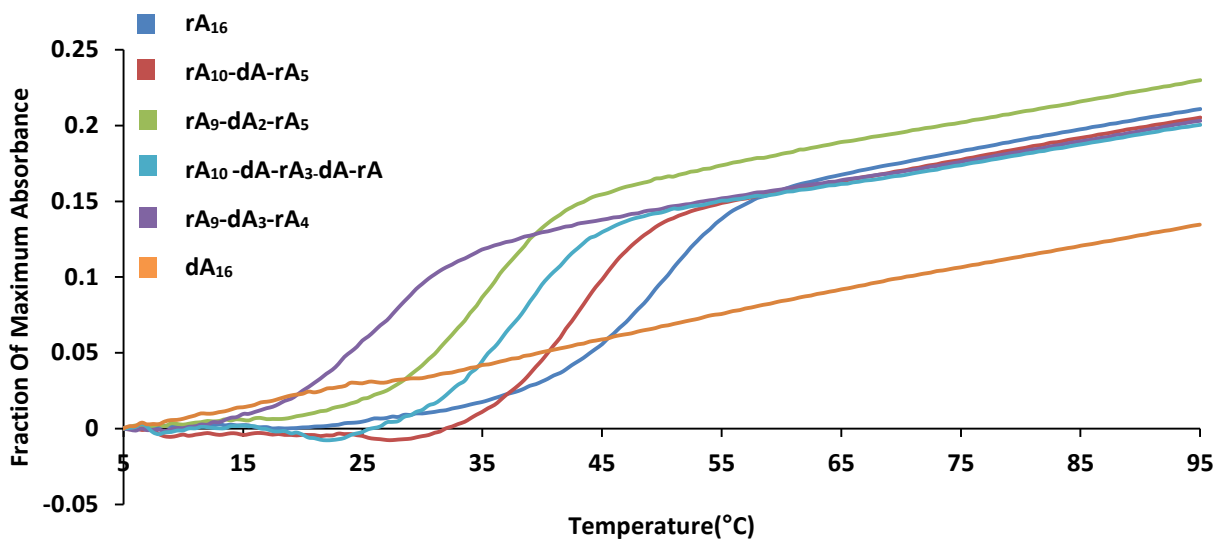


Figure 3.4: UV thermal denaturation profiles of rA-dA chimera 16mers at pH 7, 4.4 M NH₄Cl (Buffer: 40 mM Na₂HPO₄, 30 mM citric acid). 2.3 μM single strand concentration.

Sequence (5'-3')	T_m (°C)	ΔT_m (°C)
rA ₁₆	51	
rA ₁₁ -dA-rA ₅	42	-9
rA ₉ -dA ₂ -rA ₅	36	-15
rA ₁₀ -dA-rA ₃ -dA-rA	39	-12
rA ₉ -dA ₃ -rA ₄	28	-23
dA ₁₆	NA	NA

Table 3.3: Melting temperature of rA-dA chimera at pH 7 and 4.4 M NH₄Cl.

3.1.3 Ability of Uniform DNA and RNA Oligoadenylates to Hybridize at pH 3

Due to reports in the literature of the formation of a DNA A-motif³⁹⁻⁴¹, UV thermal denaturation studies were performed at pH 3 on dA vs. rA homopolymers to see if sigmoidal transitions could be observed. Heating at 95°C for ten minutes to ensure proper annealing was not performed due to increased risk of degradation *via* the depurination mechanism for the 2'-deoxyadenosine series. The samples were allowed to anneal for 1 hour, instead of the standard overnight.

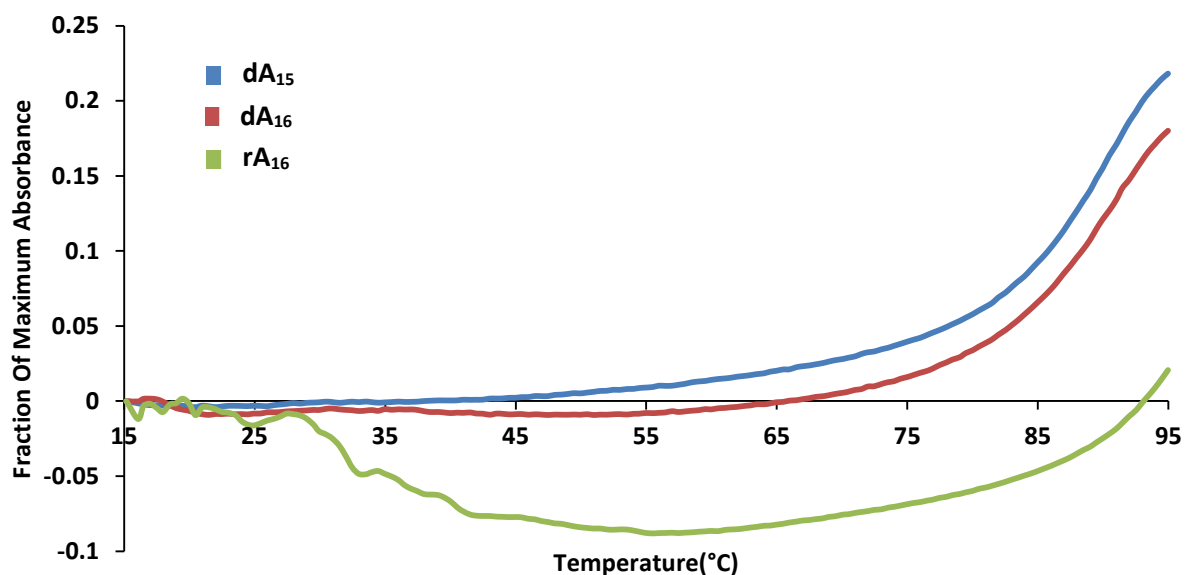


Figure 3.5: UV thermal denaturation profiles of RNA and DNA at pH 3 (Buffer: 10 mM NaH₂PO₄). 2.3 μM single strand concentration.

Analysis of the UV thermal denaturation curves at pH 3 reveals a transition suggesting possible duplex-single strand transition for the DNA species (Figure 3.5). However with no upper plateau the T_m could not be accurately determined. The need for lower pHs for DNA to form the adenosine duplex was surprising considering the N1 atom of adenine in DNA has been reported to be more basic than its RNA counterpart.⁶⁴ The slight decrease in absorbance for rA₁₆ can be

considered negligible, and it is likely that the duplex is too stable: the hyperchromic transition would occur above 100°C.

3.1.4 Effect of Acidity on Uniformly DNA vs. RNA Oligoadenylates

In order to obtain measurable T_m data for uniformly DNA species, buffers ranging in pH between 3 and 4 were evaluated. UV thermal denaturation experiments were performed for both dA₁₁ and dA₁₅ (Figure 3.6). Analysis of UV thermal denaturation curves of dA₁₁ reveals no sigmoidal hyperchromic transition above pH 3.25, and for the dA₁₅ series no transition can be observed above pH 3.7. It was interesting to note the higher threshold pH of duplex formation for longer species, however it is consistent with the observation that longer oligonucleotides form a more stable duplex.

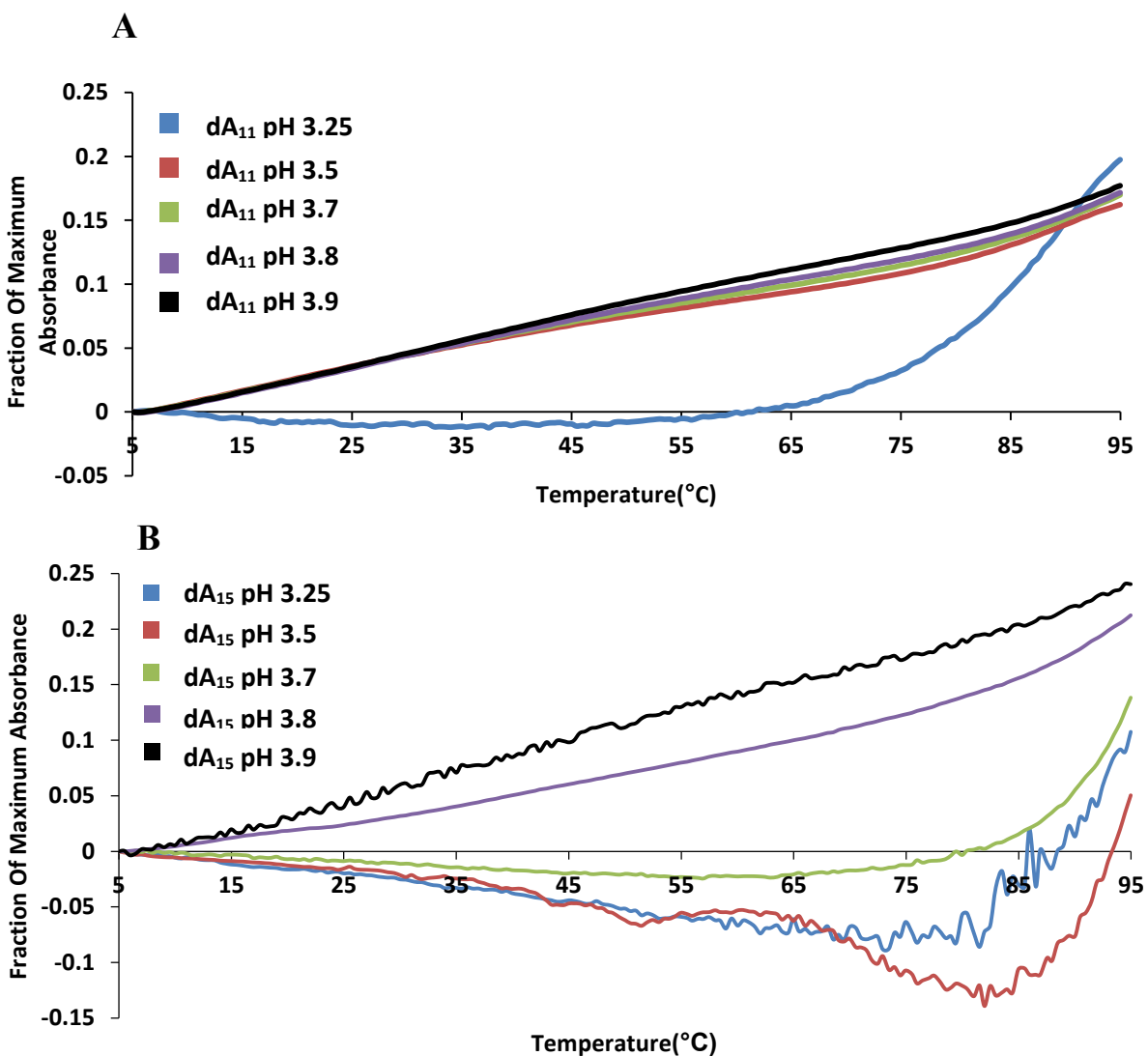


Figure 3.6: UV thermal denaturation profiles at varying pH of (A) dA₁₁, 3.3 μM single strand concentration (B) dA₁₅, 2.3 μM single strand concentration. (Buffer: 90 mM Na₂HPO₄, 120 mM citric acid).

3.1.5 Reversibility of Duplex Formation at pH 3 for rA₁₁ and dA₁₁

The lack of upper plateau independent of pH or oligonucleotide length suggested the possibility of other phenomena occurring at higher temperature and at pH 3. If only the process of denaturation was occurring at higher temperatures, it should be reversible and a *hypochromic* transition should be observed upon lowering the temperature. Ideally a molecular nanoswitch should undergo a reversible transition from one form to another and not susceptible to forming

multiple structures. To investigate this, UV thermal denaturation studies were performed on rA₁₁ and dA₁₁ ramping the temperature upwards and then downwards (Figure 3.7).

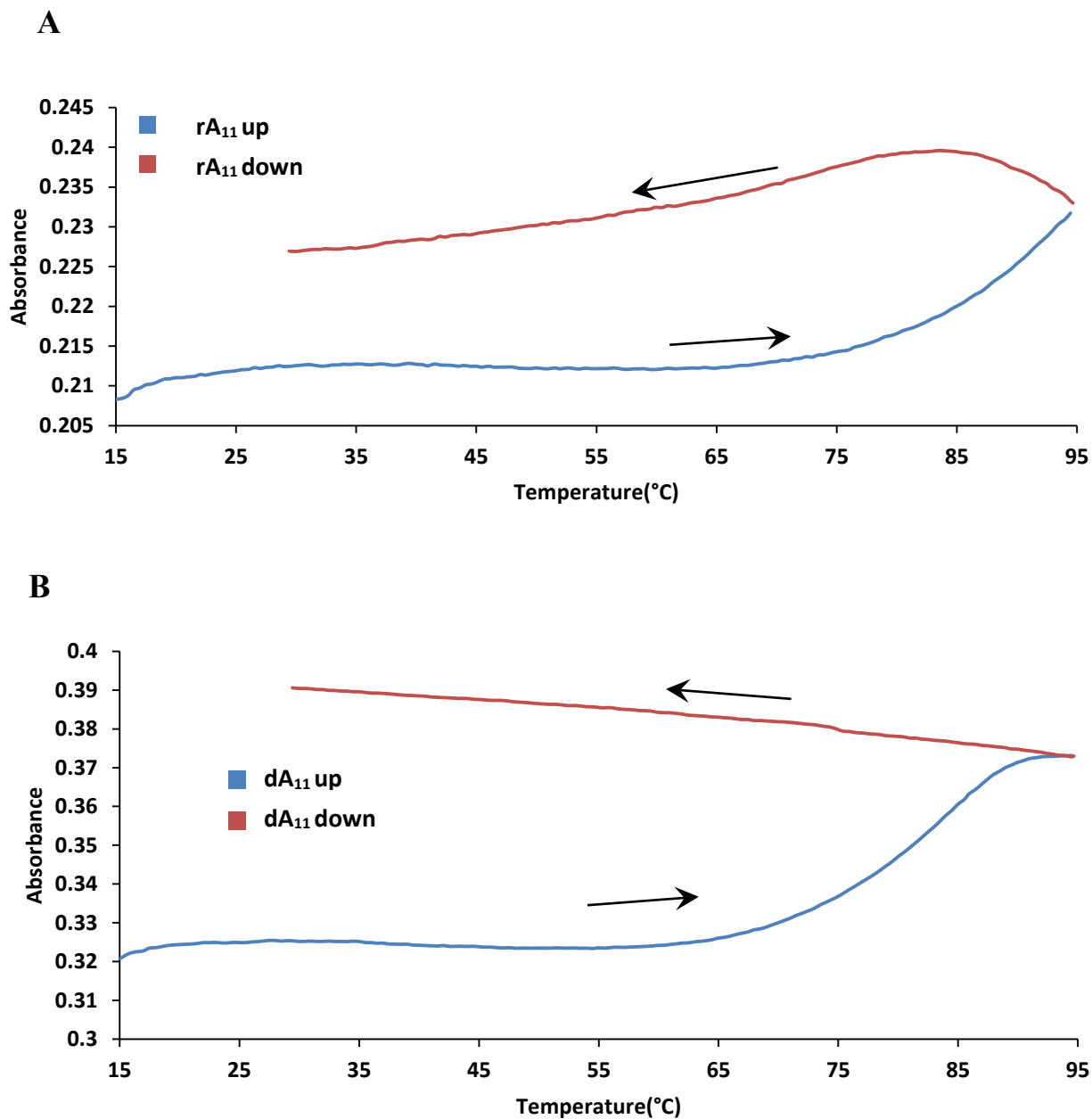


Figure 3.7: UV thermal denaturation from 15-95°C, followed by 95-30°C at pH 3 of (A) rA₁₁ (B) dA₁₁ (Buffer: 10 mM NaH₂PO₄).

For both the RNA and DNA an increase in absorbance at 260 nm is observed at approximately 75°C, with a slight upper plateau for the dA series. However upon lowering the temperature rA₁₁ shows a decrease in absorbance possibly less pronounced due to slow annealing (hysteresis). However, the dA series does not show any evident decrease in absorbance upon decreasing the temperature. While it is possible that the kinetics of duplex formation for DNA are slower than RNA, another possible conclusion is that the DNA is degrading by the acid catalyzed depurination after heating to higher temperatures.

3.1.6 Evaluation of Acid Catalyzed Degradation by Denaturing PAGE

To investigate the stability of RNA vs. DNA in acidic conditions, denaturing PAGE was performed after samples were treated with 1) Formamide 2) 4°C overnight 3) 10 mins at 95°C 4) 1 hour at 95°C. The formamide samples would serve as intact (undegraded) controls, and those incubated at 95°C for an hour would be the degraded controls. Analysis of the RNA bands reveals minimal degradation in all conditions except when heated at 95°C for an hour (Lane E). For the DNA species instead of an intact band smearing can be observed when heated for only 10 minutes at pH 3, suggesting degradation. Additionally there is a band still in the well, which may be the free purine base as it is no longer a polyanionic nucleic acid (and therefore should not be expected to migrate towards the positively charged electrode). While concrete conclusions upon the increase in the UV absorbance about heating the DNA samples should be drawn with caution, there is evidence of degradation at pH 3 of the DNA oligonucleotides by PAGE in conditions that did not degrade RNA (95°C for 10 minutes).

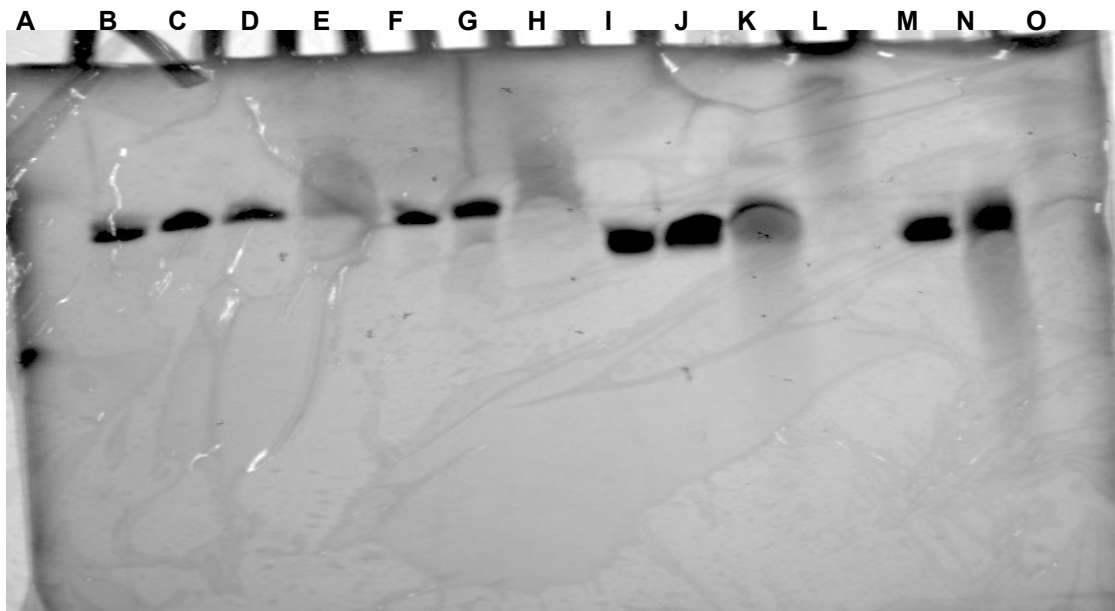


Figure 3.8: 20 % Acrylamide (19:1) PAGE (A) marker dye (B) rA₁₆ formamide (C) rA₁₆, pH 3, 4°C overnight (D) rA₁₆, pH 3, 95°C for 10 minutes (E) rA₁₆, pH 3, 95°C for 1 hour (F) rA₁₆, pH 4, 4°C overnight (G) rA₁₆, pH 4, 95°C for 10 minutes (H) rA₁₆, pH 4, 95°C for 1 hour (I) dA₁₆, formamide (J) dA₁₆, pH 3, 4°C overnight (K) dA₁₆, pH 3, 95°C for 10 minutes (L) dA₁₆, pH 3, 95°C for 1 hour (M) dA₁₆, pH 4, 4°C overnight (N) dA₁₆, pH 4, 95°C for 10 minutes (O) dA₁₆, pH 4, 95°C for 1 hour.

3.1.7 HPLC Analysis of UV Denaturation Samples at pH 3

Ion-exchange HPLC was performed on samples of rA₁₆ and dA₁₆ at pH 3 that had been heated to 95°C for UV thermal denaturation studies to investigate qualitatively degradation by the proposed depurination. As shown in Figure 3.9, several peaks are present in both chromatograms, however in the DNA sample there is clearly a larger peak eluting at 2 minutes versus ~23 minutes (likely the 16mer). It is hypothesized that the peak at 2 minutes is the free adenine base, which absorbs UV light at 260 nm, and elutes quickly due to its uncharged nature. In the case of RNA however, the oligonucleotide appears to be fully intact. While this does not necessarily explain the “sigmoidal” increase in absorbance on the UV thermal denaturation studies, it does support the

view that that dA_n strands are unstable at high temperature and acidic conditions; this would render them impractical as a reversible pH switch if indeed dA strands are capable of self-hybridization.

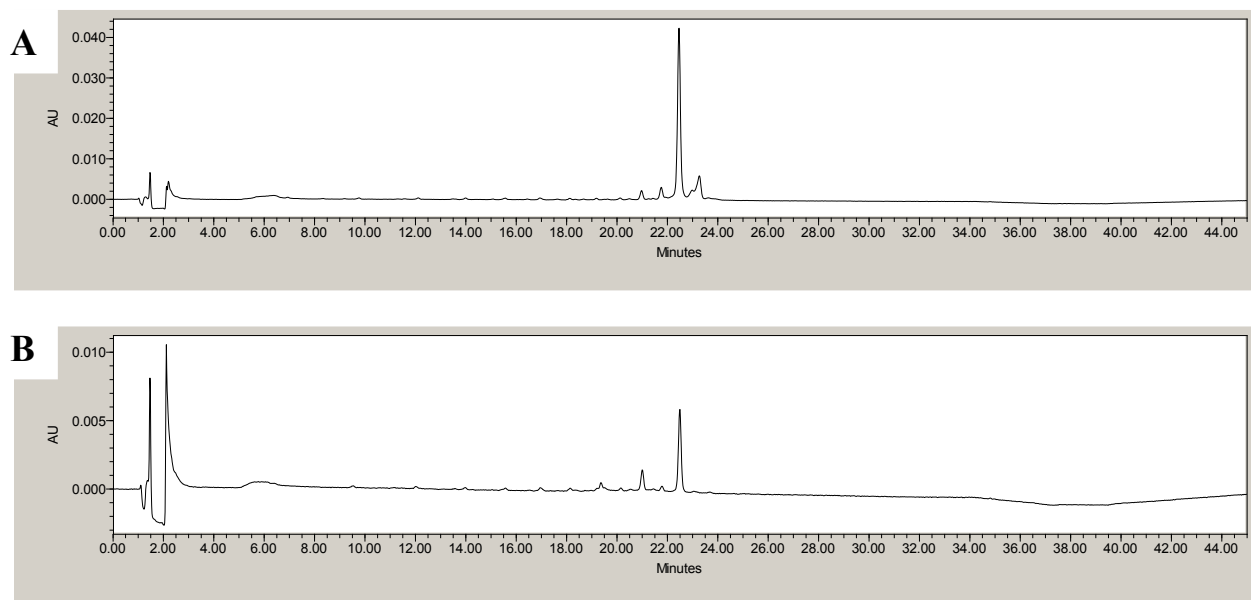


Figure 3.9: IEX chromatograms of (A) rA_{16} and (B) dA_{16} on samples which had been heated to 95°C at pH 3 (Buffer: 10 mM NaH_2PO_4).

3.2 Native PAGE Analysis of Adenosine Duplex in RNA and Sugar Modified Oligonucleotides

3.2.1 Native Polyacrylamide Gel Electrophoresis on RNA vs. DNA Oligoadenylates

Duplex formation was also evaluated by native polyacrylamide gel electrophoresis (PAGE). Oligothymidines (dT_x) and oligouridines (rU_x) were synthesized as single stranded controls as these homopolymers do not assemble into higher order structures (see Appendix). The 2'-hydroxyl group and sugar pucker has an effect on electrophoretic mobility where the 2'-deoxyribose oligomers are observed to migrate further than their RNA counterparts. For these reasons it is necessary to compare the thymidine oligomers to

2'-deoxyadenosine and the uridine oligomers to adenosine. The native conditions used in the experiments were pH 4 and pH 7; with the goal of observing relative differences in migration.

One would expect an adenosine duplex to migrate slower on a gel relative to a less bulky single stranded oligonucleotide. Inspection of the polyacrylamide gel at pH 4 (Figure 3.10) shows migration of dT₁₁ and dT₁₆ are quite similar to dA₁₁ and dA₁₆, respectively. In sharp contrast the rU single strand controls migrate further than their rA counterparts. This suggests formation of the adenosine duplex, which would have lower mobility in the polyacrylamide gel, relative to the single stranded 2'-deoxyadenosine. Under neutral conditions, different conclusions can be drawn (Figure 3.11). As at pH 4 the dT oligomers run similarly to their dA analogue. Observing the rU vs the rA bands at pH 7 similar mobility is seen, which was not observed at pH 4. This implies all lanes contain single stranded oligonucleotides at neutral pH, which was expected. The slightly reduced mobility of the single stranded control species has been reported in the literature,⁶⁵ and it is believed this is due to the nucleobase's interaction with the gel matrix.

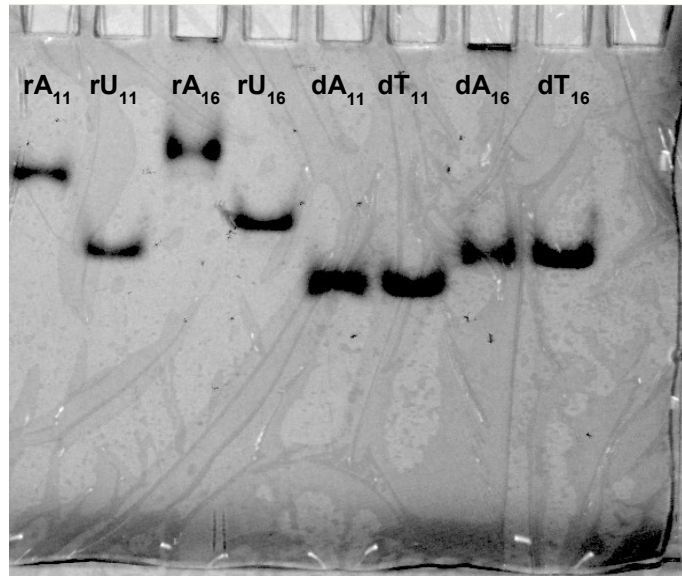


Figure 3.10: Native polyacrylamide gel electrophoresis at pH 4. 20% Acrylamide/bisacrylamide (19:1), 80 V for 3 hours, (39 mM Na₂HPO₄, 31 mM citric acid, 1.1 mM EDTA).

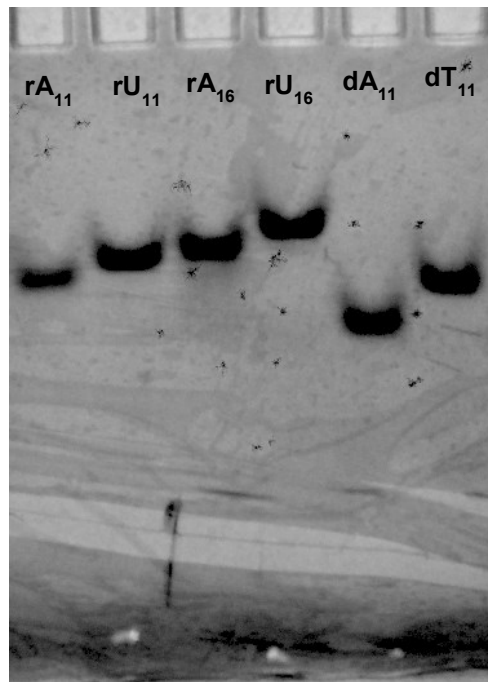


Figure 3.11: Native polyacrylamide gel electrophoresis at pH 7. 20% Acrylamide/bisacrylamide (19:1), 80 V for 3 hours, (39 mM Na₂HPO₄, 31 mM citric acid, 1.1 mM EDTA).

3.2.2 Threshold pH for Adenosine Duplex Formation

Having established that the rA duplex can form at pH 4, the next undertaking was finding the threshold pH at which the duplex forms, and is it possible to find an operating pH where both single strand and double stranded species exist? To investigate, buffers were prepared at pH 5, 5.5 and 6 as this is known to be the threshold region of duplex formation based on UV denaturation melts and native PAGEs were run with dA₁₁, rA₁₁, rA₁₆, rU₁₁ and rU₁₆ oligonucleotides. As an attempted double stranded control rA₁₆ was allowed to hybridize with its rU₁₆ complement (DNA ladders were considered unreliable due to A] Lack of a bulky hydroxyl group which facilitates further migration B] Such ladders are not calibrated for acidic conditions). Surveying the pH 5 gel shows that similar to pH 4 a reduced migration of the rA species relative to the single strands controls is observed, indicating the duplex is still being formed (Figure 3.12). Surprisingly the double stranded control showed two bands, one with even lower mobility than the adenosine duplex. It is believed that this slower migrating band is the bulkier rU·rA:rU triplex motif, which has been described in the literature.¹¹ Evidently at pH 5.5 and pH 6 the single stranded controls have a similar mobility to the adenosine lanes, indicating that the threshold region is in the pH 5-5.5 region (see following section).

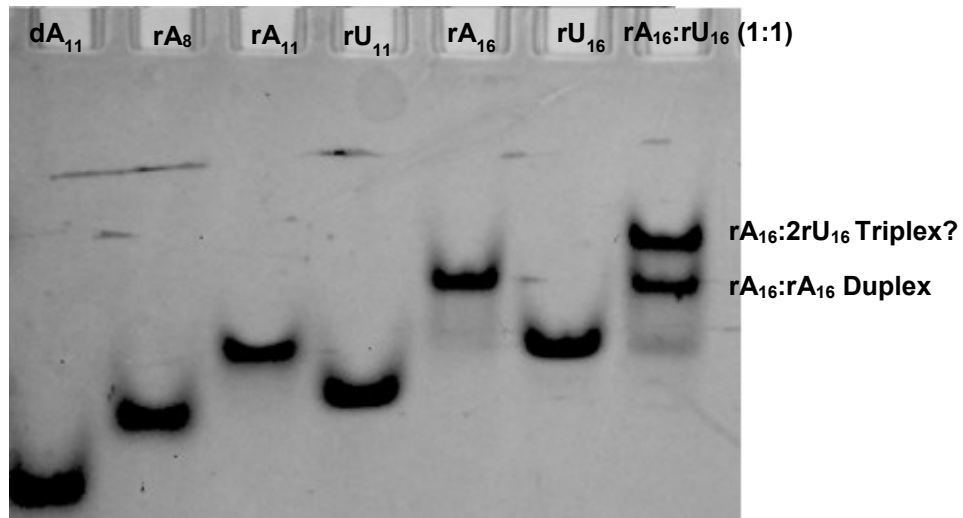


Figure 3.12: Native PAGE at pH 5 (51 mM Na_2HPO_4 , 26 mM citric acid, 5.5 mM EDTA), run at 80 V.

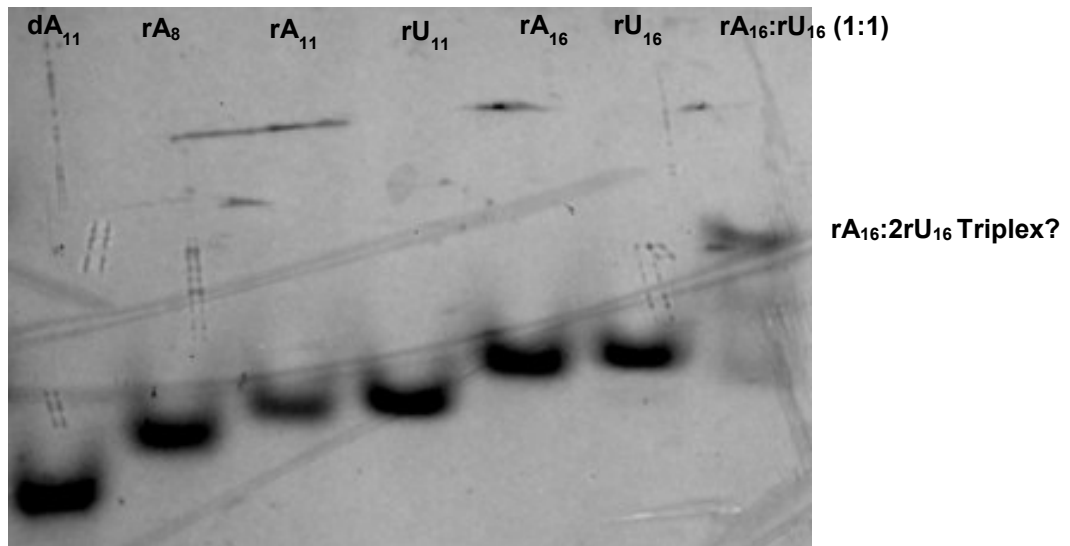


Figure 3.13: Native PAGE at pH 5.5 (56 mM Na_2HPO_4 , 22 mM citric acid, 5.5 mM EDTA), run at 80 V.

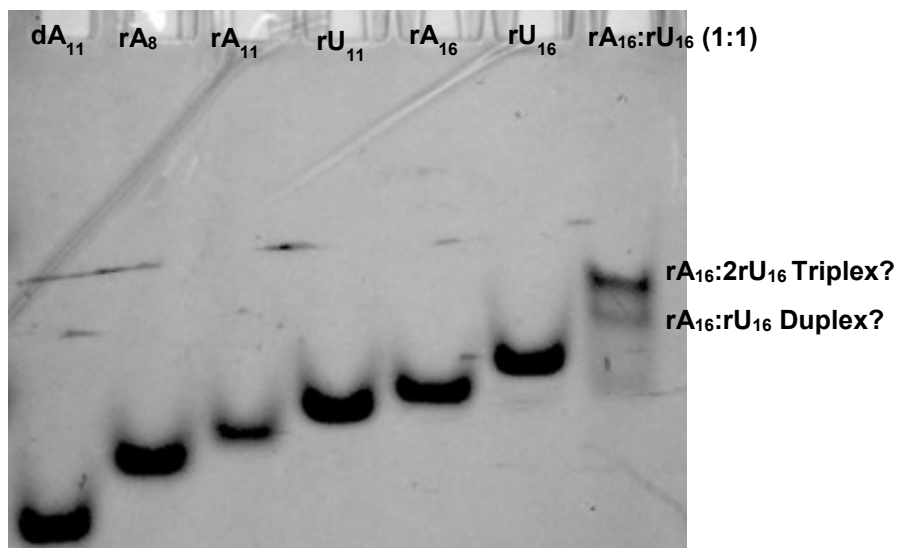


Figure 3.14: Native PAGE at pH 6 (64 mM Na₂HPO₄, 18 mM citric acid, 5.5 mM EDTA), run at 80 V.

3.2.3 Exploring pH and Molar Ratio Effects on Triplex vs. Duplex Formation by Native PAGE

The serendipitous observation of potential RNA triplex warranted further investigation. Typical methods of investigating triplex include modifying the buffer (pH, salt) or stoichiometry of the interacting oligonucleotides;^{11,66} this is due to the fact that it is expected that there are two uridine strands for every adenosine strand in the expected triplex motif. In the competing conditions of adenosine duplex vs. triplex however adjusting pH is more applicable. Other lanes contained adenosine and uridine oligonucleotides as controls and to further investigate threshold pH of adenosine duplex formation buffers were prepared with pH 4, 5.25, 5.30, 5.35 and 7. The last lane had an adjusted stoichiometry of 5 uridines to 1 adenosine which should assist in pushing the equilibrium towards triplex formation. As figure 3.15A shows, even the higher concentration of uridine, triplex formation is not favoured at pH 4. The gel at pH 7 however, offers no concrete conclusions; the slower migrating species seen in the uridine:adenosine lanes is likely the rA:rU duplex

and it is possible the triplex may have dissociated at the gel operating temperature (native gels were not performed maintaining constant temperature). The gel at pH 5.25 however, shows possibly both the rA duplex and a slower migrating species. In fact, at pH 5.30 there are three apparent bands which are hypothesized to be the triplex, rA:rU duplex and rA:rA duplex (from lowest to highest migration). The lack of adenosine duplex band in Figure 3.15E suggests the pH is higher than the required threshold. The lane with a higher uridine stoichiometry has a more intense band with the lowest migration, which supports the triplex theory. Unfortunately, UV thermal denaturation studies do not offer a clear cut characteristic biphasic transition at 260 nm for rA:rU samples (data not shown) in these conditions to corroborate triplex formation.

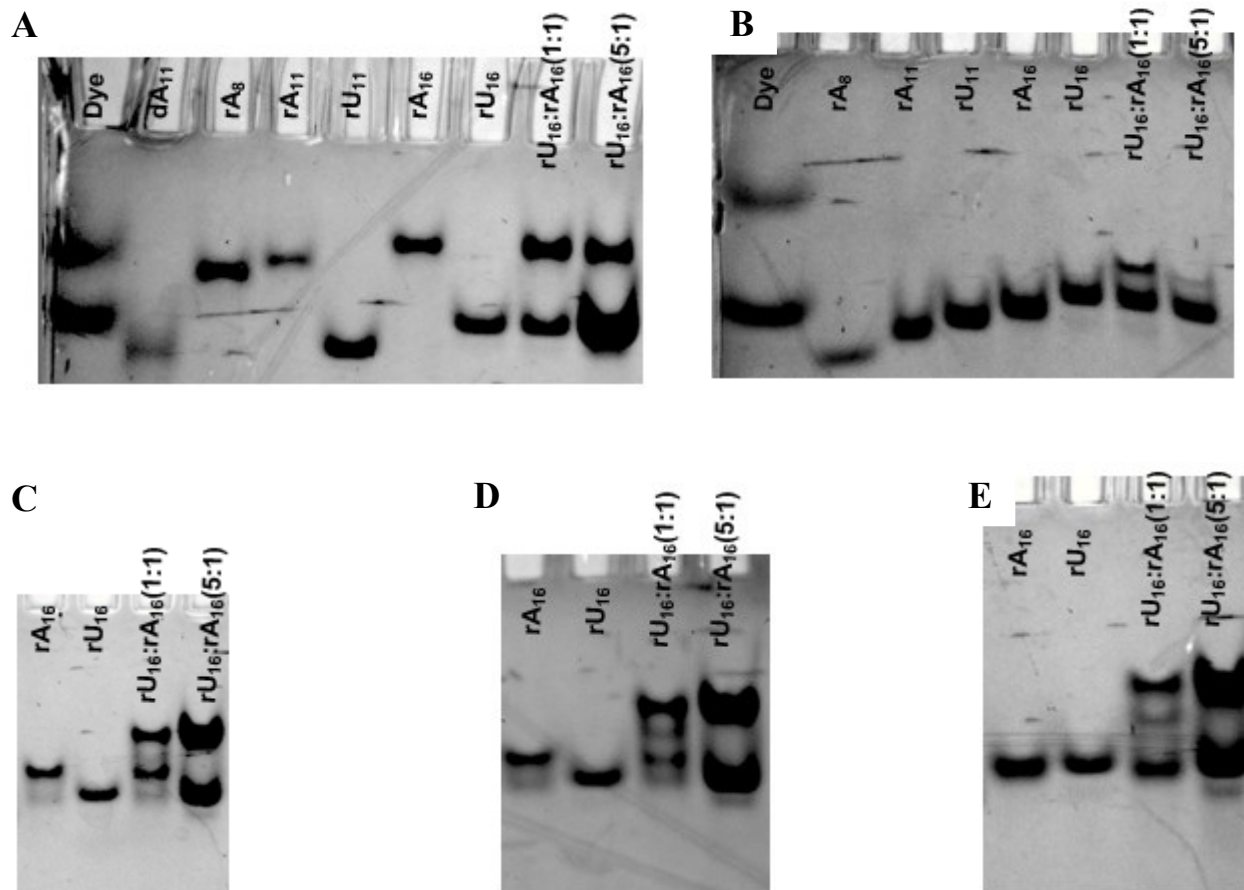


Figure 3.15: Native PAGE at (A) pH 4 [39 mM Na₂HPO₄, 31 mM citric acid, 5.5 mM EDTA] (B) pH 7 [87 mM Na₂HPO₄, 6.5 mM citric acid, 5.5 mM EDTA], NOTE 5:1 lane used 1/5 the OD quantity compared to the other lanes (C) pH 5.25 [52 mM Na₂HPO₄, 23 mM citric acid, 5.5 mM EDTA] (D) pH 5.30 [56 mM Na₂HPO₄, 23 mM citric acid, 5.5 mM EDTA] (E) pH 5.35 [56 mM Na₂HPO₄, 23 mM citric acid, 5.5 mM EDTA].

Structure distribution between adenosine duplex and the triplex can be illustrated by Figure 3.16. Theoretically, lowering the pH, therefore protonating the N1 atom of adenine disrupts Watson-Crick base pairing with uridine and therefore adenosine duplex is energetically favoured. As pH is increased however, N1 protonation becomes less likely relative to the rU·rA:rU triplex.

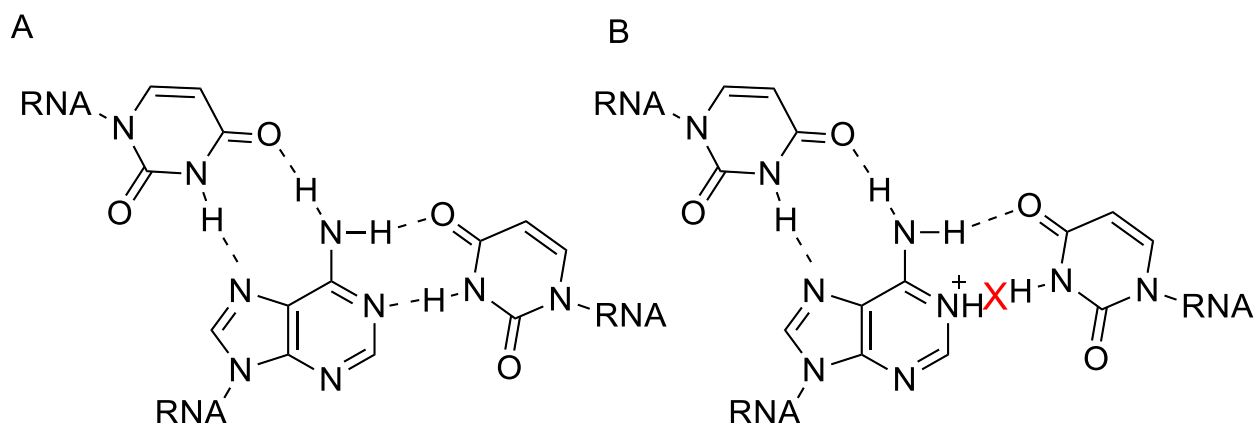


Figure 3.16: Hydrogen bonding pattern of rU·rA:rU at (A) Neutral pH (B) Acidic pH.

3.3 Extraction of van't Hoff Thermodynamic Parameters from Concentration Studies

To examine the source of destabilization from dA inserts at pH 4, van't Hoff analyses were performed to extract enthalpic, entropic and Gibbs' free energy components of adenosine duplex formation. These parameters are obtained from a derived linear relationship of the melting temperature to the natural logarithm of oligonucleotide concentration (Equation 1) for a self-complementary biomolecular system.

$$\frac{1}{T_m} = \frac{R}{\Delta H^\circ} \ln(C_t) + \frac{\Delta S^\circ}{\Delta H^\circ} \quad (1)$$

Equation 1 allows one to determine the change of enthalpy (ΔH°) from the slope and entropy (ΔS°) from the y-intercept. Afterwards the change in Gibbs' free energy of hybridization is acquired from equation 2. It should be noted that the values should not be viewed absolutely, and are to be used in a relativistic analysis.

$$\Delta G^\circ = \Delta H^\circ - T\Delta S^\circ \quad (2)$$

3.3.1 Thermodynamics of RNA: DNA Chimera Duplex Formation at pH 4

The melting temperature concentration dependence of the native RNA 9mer, as well as those with single and two 2'-deoxyadenosine inserts was exploited to determine the van't Hoff thermodynamic parameters (Table 3.4). The data for the oligonucleotide containing three dA inserts was not included as the lack of lower plateau did not allow for an accurate determination of the melting temperature.

Series (5'-3')	ΔH° (kJmol ⁻¹)	$\Delta\Delta H^\circ$	ΔS° (JK ⁻¹ mol ⁻¹)	$\Delta\Delta S^\circ$	ΔG° (kJmol ⁻¹) at 25 °C	T_m (°C) (4μM)
dT-rA ₈	-249±32		-665±87		-50.9	53
dT-rA ₄ -dA-rA ₃	-293±44	50	-816±124	151	-49.3	45
dT-rA ₃ -dA ₂ -rA ₃	-313±10	64	-904±30	239	-43.0	37

Table 3.4: Thermodynamic parameters of duplex formation of oligoadenylates with dA inserts at pH 4 (Buffer: 50mM NaOAc).

Evidently, the negative change of Gibbs' free energy is greater in magnitude as the T_m increases: indicative of a more stable duplex. The thermodynamic source of the destabilization appears to be entropic as there is a larger loss of entropy as the dA content is increased. A potential reasoning for this lies in the concept of conformational preorganization.^{55,67} The NMR and crystal structures⁴² have revealed that the ribose sugars adopt a C3'-endo conformation in the adenosine duplex. The presence of the 2'-hydroxyl group in RNA is responsible for rigidifying the sugar in C3'-endo,² and therefore the sugar is already conformationally "preorganized" to form the adenosine duplex. In the case of DNA however, the sugar is significantly more flexible and in general prefers the south conformation. Therefore rigidifying the 2'-deoxy ribose sugars (in the duplex *vs.* single strand) carries an additional entropic penalty which does not apply for the rA residues, and could potentially explain the destabilization effect on the adenosine duplexes.

3.3.2 Alternate Explanations of 2'-Deoxyadenosine Induced Adenosine Duplex Destabilization

An alternate theory of why the dA inserts are destabilizing could be related to stereoelectronic effects of the electron withdrawing effect of the 2' hydroxyl substituent in RNA (which is absent in DNA). Whilst initial inspection of the group shows it to be solvent exposed and not in a position to interact with other moieties, it has been reported in the literature that it is responsible for polarizing the geminal hydrogen. The crystal structure reported by Safaee *et al*⁴² reveals (Figure 3.17) that this hydrogen is in an appropriate position to interact with the O4' oxygen of an adjacent nucleotide. Traditional hydrogen bonds in biological systems are typically characterized by a hydrogen bond donor (N-H,

O-H) and a lone pair acceptor (usually N or O). Typically C-H has not been considered a hydrogen bond donor due to the similar electronegativities of carbon and hydrogen. Computational studies⁶⁸ have shown that polarized hydrogen bound to carbons can form hydrogen bonds to water molecules with energies of $\frac{1}{4}$ the magnitude of the traditional water-water hydrogen bond. Due to there being a multitude of these weak interactions, the cumulative effect could have significant stabilizing effects. A weak C1'-H...O4' sugar-sugar contact has been implicated as factor in i-motif self-assembly.⁶⁹ Indeed, in the case of the adenosine duplex the C-H...O bond distance (2.2 Å) and angle (155 °) lie in the optimal range for a pseudo hydrogen bond, and the interaction would be negligible in DNA due to the lack of electronegative 2' moiety.

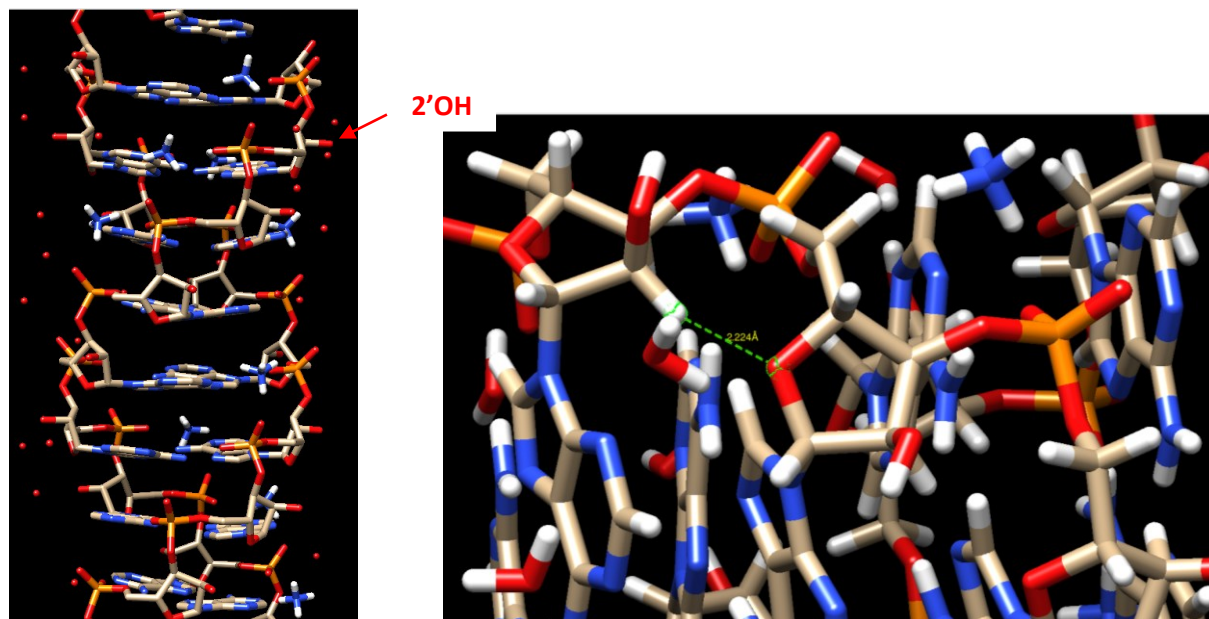


Figure 3.17: Sugar-sugar contacts in backbone of adenosine duplex.

3.4 Structural Insights into RNA/DNA Chimera Adenosine Duplexes

3.4.1 NMR Spectroscopy

NMR spectroscopy was performed by Dr. Alexey Denisov (Concordia University) to elucidate the structure of the adenosine duplex with the sequence dT-rA₄-dA-rA₃. The structure was closely compared to the rA₁₁ duplex determined by X-ray crystallography to gain insights into the influence of the dA insert. Examination of a superimposition of the two structures show geometric similarity; the RMSD for heavy atoms is 0.64 Å. While RNA ribose sugars naturally adopt the North sugar pucker, based on NMR evidence the single dA insert conforms to its RNA environment; this suggests that the destabilization is not due to structural perturbations such as less optimal base stacking/hydrogen bonding.

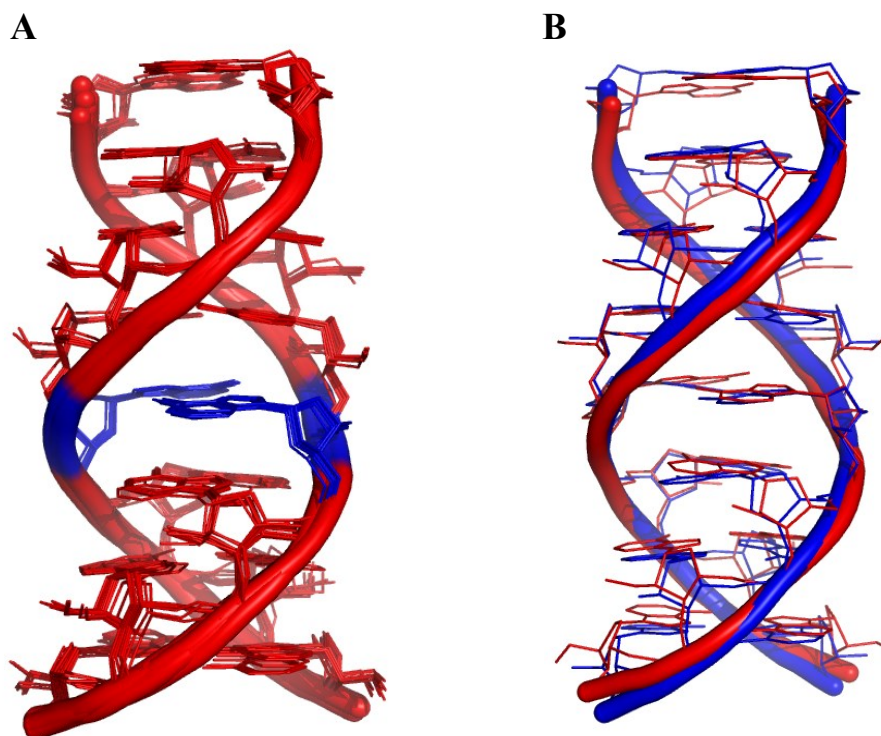


Figure 3.18: (A) 10 convergent structures of dT-rA₄-dA-rA₃ (rA: red, dA: blue) (B) Overlay of rA₁₁ X-ray structure (red) and dT-rA₄-dA-rA₃ NMR structure (blue), RMSD for heavy atoms= 0.64 Å.

3.4.2 X-ray Crystallography

Crystals of rA₅-dA-rA₅ were grown in the lab of Dr. Kalle Gehring at McGill University to determine the structure in the presence of ammonium cations. The crystals were grown in the presence of PABP (RRM23), which is known⁴² to assist in crystallizing the adenosine duplex. The crystal structure was solved by Jingwei Xie (Gehring Lab, McGill University) from the X-ray diffraction pattern (resolved to 1 Å) of rA₅-dA-rA₅ crystals. Similar to the solution structure determined by Dr. Denisov, the dA insert conforms to its RNA environment and adopts a C3'-endo sugar pucker. As in the previous

study, the ammonium cations occupy regular sites on the backbone, and are hydrogen bonded to the N1 of an adenine and two of the phosphate groups on the opposing strand's backbone. Although the crystals were grown at pH 5, measurements of the internal adenine C2-N1-C6 angle corresponds to the absence of ring protonation.⁷⁰ Importantly, the similarity in the native RNA and single dA insert adenosine duplexes is in support of the hypothesis that the destabilization is not structural in origin.

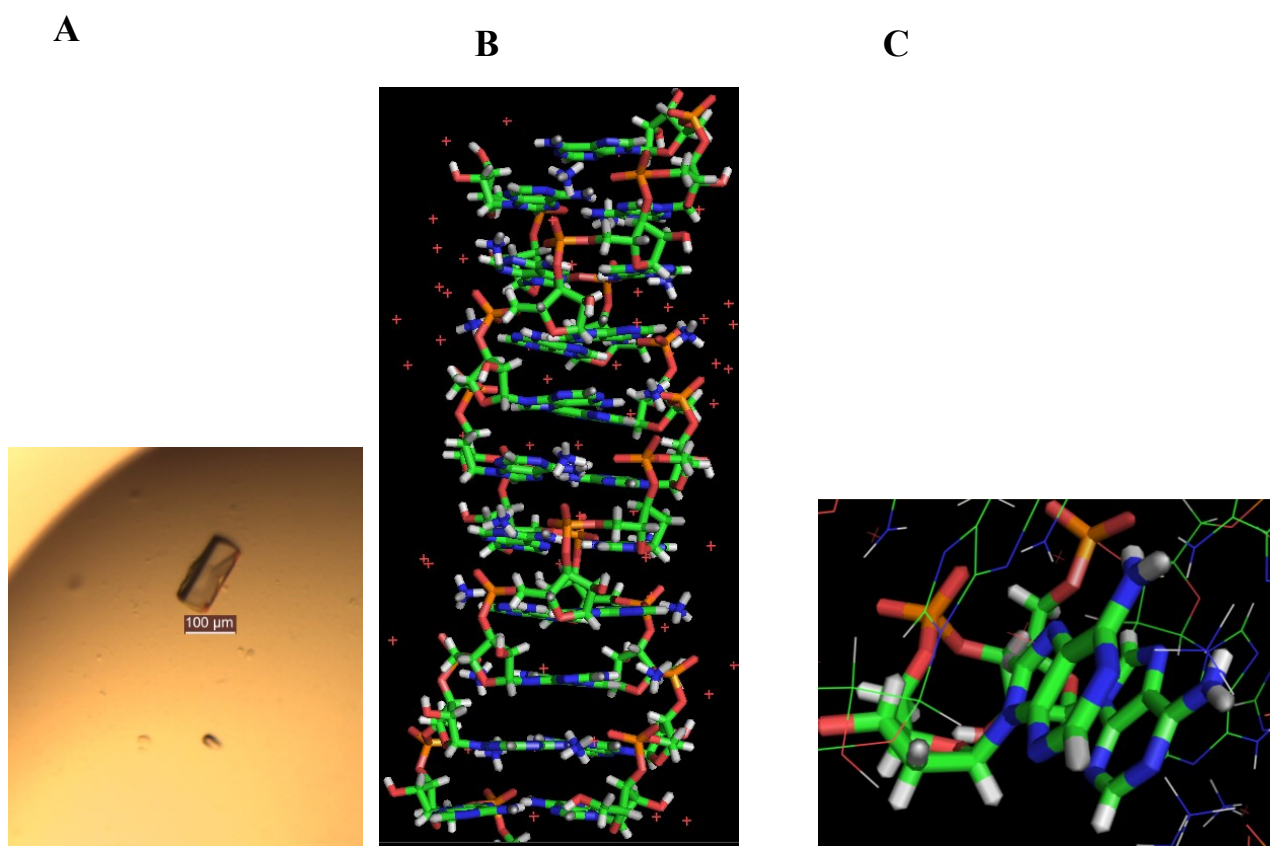


Figure 3.19: (A) Image of rA₅-dA-rA₅ crystal (crystallization conditions: 1.6 M (NH₄)₂SO₄, 0.1 M citric acid, pH 5, 0.47 mM RNA (RRM23:RNA 1:1) (B) Molecular model of RNA-DNA chimeric adenosine duplex from X-ray diffraction pattern (C) 2'-Deoxyadenosine sugar adopts C3'-endo sugar pucker.

3.4.3 Circular Dichroism Spectroscopy

To elucidate structural information of the adenosine duplex with increasing 2'-deoxyadenosine inserts, circular dichroism spectra were acquired at pH 4 at 10°C to ensure the duplex was being observed. Circular dichroism spectroscopy functions by measuring the difference in absorbance of right and left handed circularly polarized light scanning the middle-near UV range of the electromagnetic spectrum. This technique is used as a *qualitative* analysis for nucleic acid secondary structure, and is used to compare an observed spectrum with one already empirically determined,⁷¹ therefore allowing one to identify structures such as A-form vs. B-form. The polyadenosine duplex spectrum has been noted⁴⁰ to exhibit a positive maximum around 260 nm, and a less intense minimum around 245 nm.

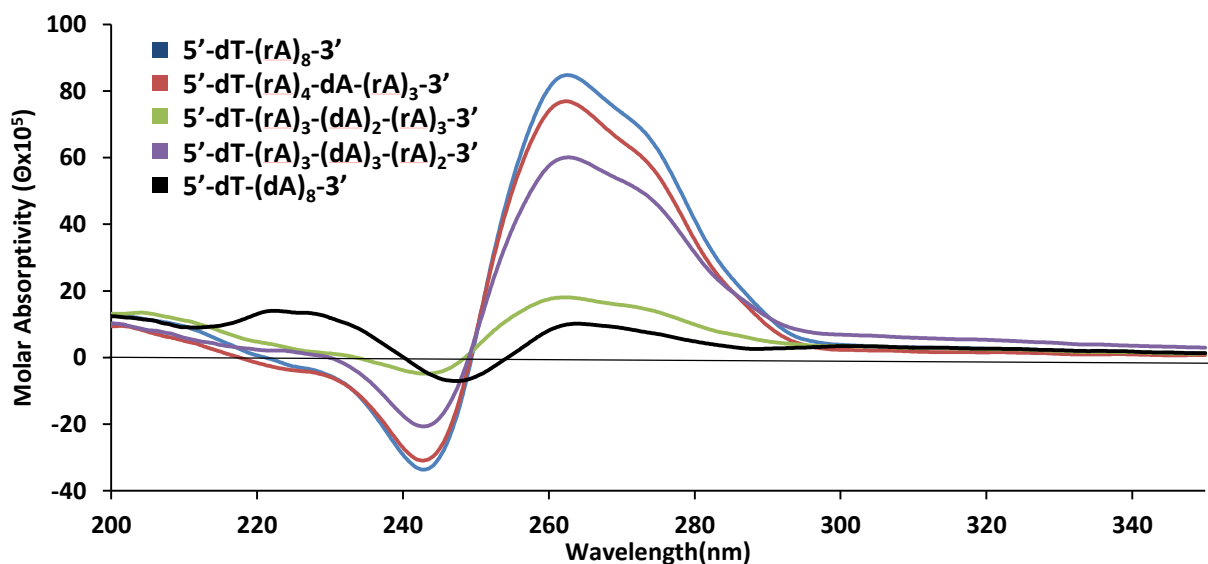


Figure 3.20: Circular dichroism spectra of 2'-deoxy modified oligoadenylates at pH 4 (Buffer: 50mM NaOAc, pH 4).

In the case of dT-rA₈ a similar profile is observed to that reported in the literature for the polyA duplex, with a convincing positive maximum at 266 nm, and a broad shoulder in the 270-290 nm region. A negative absorption at 241 nm is also present. With increasing dA content (1-3 inserts) the overall profile is similar suggesting that the structure is conserved. This is in agreement with the similarity shown by the NMR structure. The CD signature of the dT-dA₈ series, which is believed not to form a duplex at pH 4 based on UV thermal denaturation and native PAGE experiments, shows a rather different profile with a slight broad maximum at around 225 nm, a slight negative peak at 250 nm (as opposed to the more pronounced peak at 240 nm seen for the adenosine duplex) and where a significant maximum was seen for the dT-rA₈ sequence a minimal broad peak is observed.

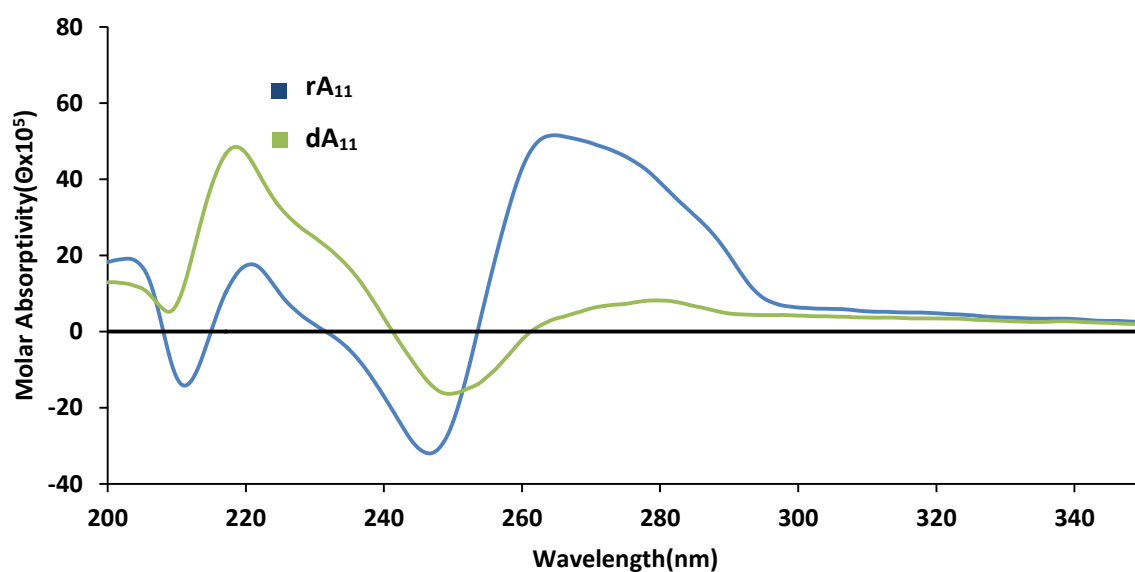


Figure 3.21: Circular dichroism spectra of 2'-deoxy modified oligoadenylylates at pH 7, 4.4 M NH₄Cl (Buffer: 10 mM NaH₂PO₄).

CD spectra were also acquired for the 11mers (rA₁₁ and dA₁₁) at neutral pH and 4.4 M NH₄Cl to compare and contrast global structural features (Figure 3.21). The rA₁₁ duplex

shows a similar broad positive peak around 265 nm, and the negative peak at 245 nm that were seen in the adenosine duplex at pH 4. A slight maximum and minimum are apparent at 220 and 210 nm respectively, possibly due to it being a different sequence than the low pH spectra (no 5' thymidine and 3 additional adenosines) or the buffer containing a 4.4 M NH_4Cl rather than the low pH. dA_{11} shows a significantly reduced maximum, and a red shift of the minimum similar to that observed at pH 4; the data suggests there is some global structural difference between the DNA and RNA at pH 4 and pH 7.

In summary, 2'-deoxyadenosines are destabilizing to the RNA adenosine duplex by $\sim 8^\circ\text{C}/\text{insert}$ in the 9mer series at pH 4, and the 16mers at pH 7 and 4.4 M NH_4Cl . The inability of a uniform dA oligonucleotide to form the adenosine duplex at pH 4 is corroborated by migration on a native PAGE. Likewise, its inability to form at pH 7 and 4.4 M NH_4Cl is corroborated by a lack of a sigmoidal transition by UV thermal denaturation experiments. The results obtained from NMR spectroscopy, X-ray crystallography and circular dichroism all suggest that single inserts are structurally tolerated, and the source of destabilization appears to be entropic in origin based on concentration studies.

Chapter 4: Effect of Chemically Modified Sugars on the Polyadenosine Duplex

4.1 C2'-Fluoro Modified Oligonucleotides

Having established that dA inserts are destabilizing to the adenosine duplex the next modification evaluated was 2'-deoxy-2'-fluoroadenosine. In addition to the attributes stated in the research objectives (Chapter 2), the fluoro group allows one to further probe the possibility of a backbone C-H...O hydrogen bond contributing to the stabilization of the poly rA duplex. Fluorine being the most electronegative element should be responsible for further polarizing H2'', and therefore a stronger hydrogen bond donor. This has some precedent in the literature in nucleic acid double helices where the strands run antiparallel to each other: Gonzalez *et al.*⁴⁷ have measured the chemical shift of the H2'' proton and its signal is 1-2 ppm downfield of its hydroxylated analogue. The more pronounced downfield shift is directly related to deshielding and polarization. Additionally, by sequence design they showed that disrupting the sugar-sugar contact led to significant destabilization.

4.1.1 Thermal Stability of 2'-Fluorinated Oligonucleotides at pH 4

To evaluate the influence of these modifications on duplex stability, UV thermal denaturation experiments were performed. Similar to the study investigating the influence of 2'-deoxyadenosine inserts, rfA content was systematically increased centrally in oligoadenosine (rA) to a uniformly rfA oligonucleotide (Table 4.1).

Sequence (5'-3')
dT-rA₈
dT-rA₄-rfA-rA₃
rA₁₁
rA₅-rfA-rA₅
rA₅-rfA₂-rA₄
rA₄-rfA₃-rA₄
rfA₁₁
rA₁₆
rA₁₀-rfA-rA₅
rfA₁₆

Table 4.1: 2'-Fluorinated oligonucleotides investigated in this study.

Evaluation of the UV thermal denaturation experiments at pH 4 (Figure 4.1) on the 9mer series reveals that a single fluoro insert in the center of the oligonucleotide is well tolerated as the reduction in the T_m is within the margin of error (typically 1-2°C). The influence of one rfA insert on the T_m value appears to be minimal and within the limit of the margin of error for the 11mer series. As the content is increased to 2 and 3 rfA residues a clear destabilizing trend can be observed (Table 4.2). However in contrast to the dA series the uniformly fluorinated oligonucleotide shows a clear sigmoidal transition (Figure 4.1), albeit destabilized by 15°C.

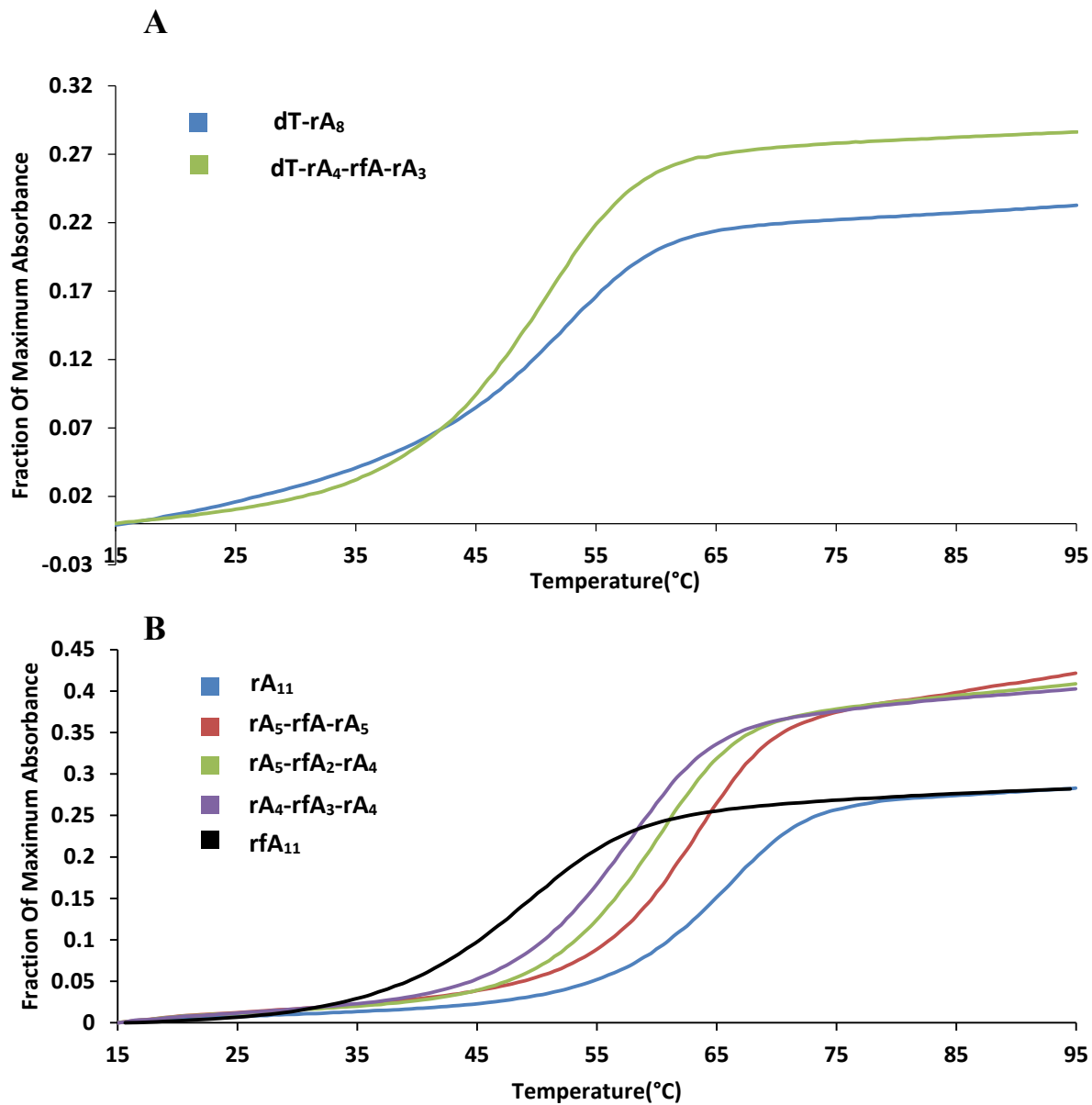


Figure 4.1: UV thermal denaturation profiles of rA-rfA chimera at pH 4 (Buffer: 50 mM NaOAc) of (A) 4.2 μ M single strand concentration (B) 3.3 μ M single strand concentration.

Sequence (5'-3')	T_m (°C)	ΔT_m (°C)
dT-rA₈	53	
dT-rA₄-rfA-rA₃	52	-1
rA₁₁	66	
rA₅-rfA-rA₅	64	-2
rA₅-rfA₂-rA₄	61	-5
rA₄-rfA₃-rA₄	58	-8
rfA₁₁	51	-15

Table 4.2: Melting temperature of native and fluorinated oligonucleotides at pH 4 (Buffer: 50 mM NaOAc).

This destabilizing effect was surprising, as the 2'-fluoro modification is apparently ubiquitously stabilizing in the literature.^{45-47,49} One hypothesis is related to protonation of the N1 atom of the adenine base which is established criteria of adenosine duplex formation. Computational and small system studies have shown that the electronegative hydroxyl group can have long range inductive effects through bonds and space on the nucleobase.^{64,72} It is believed this is what is partly responsible for a higher thermal stability in RNA over DNA duplexes as the higher acidity of the N1 (guanine)/N3 (thymine/uracil) protons is proportional the hydrogen bond strength. There are fewer reports on the effects of 2'-fluoro substituent on the pK_a of the N1 of adenine, however related studies suggest that triplex destabilization is due to the decreased basicity of the N3 atom of cytosine.⁷³ This will be evaluated in more detail in the following section.

4.1.2 pH Dependence of the T_m for rA₁₆ vs. rfA₁₆

Buffers were prepared ranging from pH 3.5-6 (incrementing by 0.5 pH units) to explore differences in melting temperature between native RNA and its fluorinated analogue as a function of pH. Varying the buffer pH would allow differences in N1 protonation due to the electronegativity of the C2' substituent to be evaluated. At pH 3.5 a negligible difference between

rA₁₆ and rfA₁₆'s melting temperature indicates there is little difference between the oligonucleotides. However as the pH is increased the ΔT_m is correlated to the pH; this supports the view that there is a relationship between protonation of the N1 atom and the stability of the adenosine duplex. One can conclude based on the UV thermal denaturation melts that the uniformly fluorinated species is incapable of duplex formation at pH 5 in contrast to the native RNA oligonucleotide. At pH 5.5 or higher no sigmoidal transition was observed for either oligonucleotide.

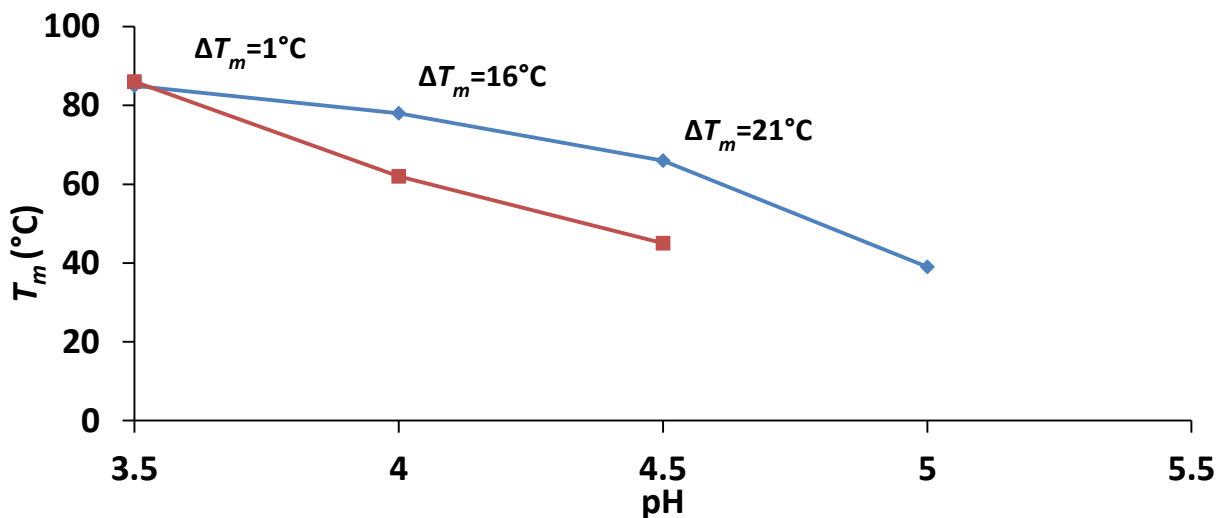


Figure 4.2: pH dependence of melting temperature of rA₁₆ (red) and rfA₁₆ (blue). 1.3 μ M single strand concentration (Buffer: 40 mM Na₂HPO₄, 30 mM citric acid).

4.1.3 Melting Temperature Dependence on Oligonucleotide Concentration

Van't Hoff experiments were performed on rA₁₁ vs. rfA₁₁ at pH 4 to gain insights into the source of destabilization. Evaluation of the parameters (Table 4.3) shows a clear correlation between the change in Gibbs' free energy of duplex formation and duplex stability (T_m).

Series	ΔH° (kJmol ⁻¹)	ΔS° (JK ⁻¹ mol ⁻¹)	ΔG° (kJmol ⁻¹) at 25 °C	T_m (°C) (at 3μM)
rA ₁₁	-297±47	-773±124	-66.7	65
rfA ₁₁	-235±28	-629±75	-48.0	47

Table 4.3: Thermodynamic properties of duplex formation of rA₁₁ and rfA₁₁ at pH 4.

The less significant loss of entropy for rfA₁₁ can be explained by the electron withdrawing group rigidifying the sugar and preorganizing the single strands relative to rA₁₁.⁴⁶ The origin of destabilization due to the 2'-fluoro moiety appears to be enthalpic in nature, with a less negative change in enthalpy for the uniformly fluorinated species. This may be related to the decreased protonation of the N1 atom of the adenine base, which would have a compromised electrostatic interaction between the oligonucleotide strands. It could also be related to a structural perturbation and effects such as reduced base stacking.

4.1.4 UV Thermal Experiments on 2'-Fluoro Oligonucleotides at Neutral pH and High Ammonium Salt

Having established a destabilizing effect in acidic conditions, the influence of the 2'-fluoro modification at neutral pH and 4.4 M NH_4Cl was evaluated. Only the 16mer series was investigated, as the 11mers are too short to form a stable enough duplex to be studied (data not shown). A single fluoro insert was observed to be well tolerated in the 16mer duplex, with the change in T_m within the experimental error (Figure 4.3). In sharp contrast to what was observed for rfA_{11} in acidic conditions, a stabilization of 13°C is observed at neutral pH with 4.4 M NH_4Cl . This is more in parallel to what has been reported in the literature, and is possibly related to the previous rationale including stronger hydrogen bonding between the bases, improved base stacking and a stronger C-H...O backbone interaction due to the high electronegativity of the fluorine atom.

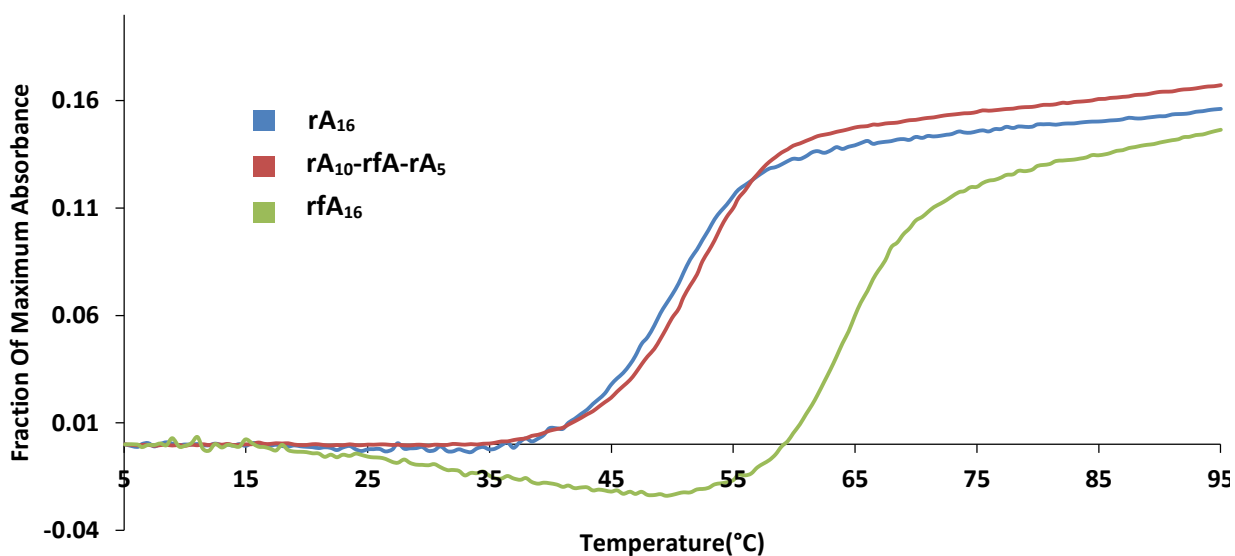


Figure 4.3: UV Thermal denaturation experiments of fluorinated RNA at neutral pH, 4.4 M NH_4Cl . 2.3 μM single strand concentration (Buffer: 10 mM NaH_2PO_4).

Sequence (5'-3')	T_m (°C)	ΔT_m (°C)
rA ₁₆	51	
rA ₁₀ -rfA-rA ₅	52	+1
rfA ₁₆	64	+13

Table 4.4: Melting temperatures of rA₁₆, rfA₁₆ and a 16-mer oligoadenylate containing a single rfA insert in 10 mM NaH₂PO₄ (pH = 7) containing 4.4 M NH₄Cl.

4.1.5 X-Ray Crystallography of the Fluorinated Adenosine Duplex

The sequences rA₅-rfA-rA₅, rA₅-rfA₂-rA₄ and rA₄-rfA₃-rA₄ were crystallized and the crystal structures solved from their X-ray diffraction pattern by the Gehring lab. The fluorinated chimera adenosine duplexes were strikingly similar to the rA₁₁ duplex. Interestingly, the crystals were grown at pH 5 and 3.0 M NH₄Cl concentration which could indicate that either the destabilization of the duplex at low pH, or stabilization at neutral pH with 4.4 M NH₄Cl are not due to structural differences. One potential hypothesis to the destabilization of the 2'-fluoro is

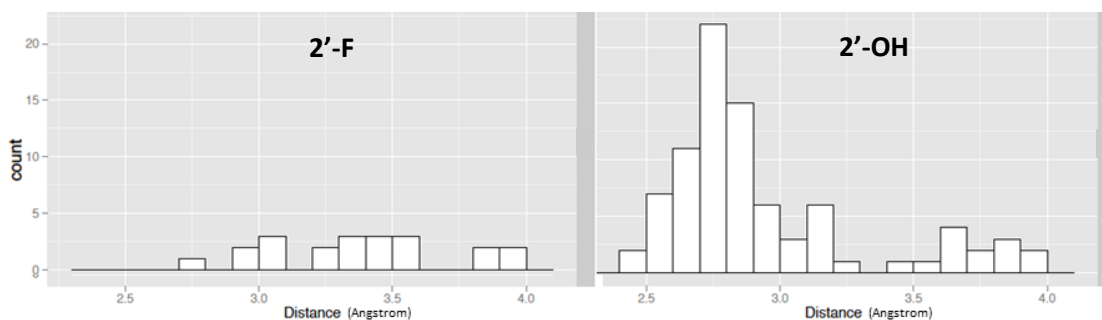


Figure 4.4: Hydration of the 2' group in rA vs. rfA duplexes (distances compiled from 4 X-ray structures).

related to poor hydration of the C2' moiety. Enthalpic hydration of water molecules bridging hydrophilic groups has been established as a stabilizing source of RNA duplexes over DNA based on crystallographic data.⁷⁴ The 2' hydroxyl group serves as a bridgehead to these water networks, and fluorine being a poor hydrogen bond acceptor has been shown to interrupt these water

networks.⁴⁵ Water to 2'hydroxyl/fluorine group distances were evaluated (Figure 4.4) and it can be concluded that the more poorly hydrated fluorines are a potential source of enthalpic destabilization. It is necessary to determine how the crystal conditions influence duplex stability, and therefore UV thermal denaturation studies were done on the rA-rfA chimera at pH 5, 3.0 M NH₄Cl. As expected, the NH₄⁺ stabilizing effect and the acidic pH destabilizing effect appear to negate each other (Figure 4.5). Nonetheless the acidic pH effect appears to prevail and the uniformly fluorinated species is destabilized by 9°C.

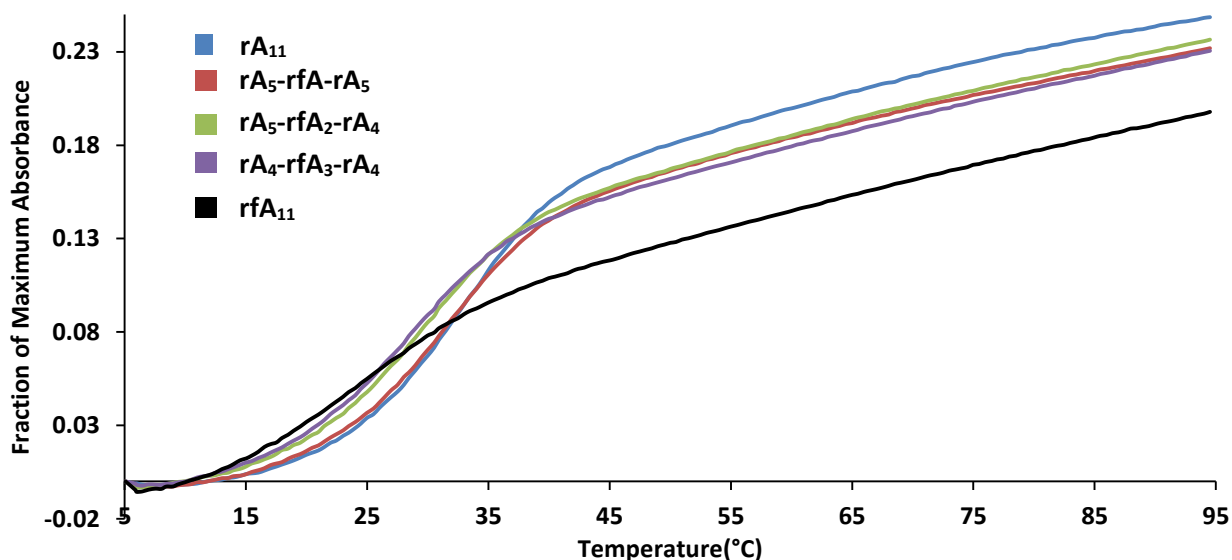


Figure 4.5: UV Thermal denaturation experiments of fluorinated RNA in crystallization conditions. 3.3 μ M single strand concentration (Buffer: 100 mM citric acid, 3.0 M NH₄Cl [pH 5]).

Sequence (5'-3')	T_m (°C)	ΔT_m (°C)
rA ₁₁	33	
rA ₅ -rfA-rA ₅	32	-1
rA ₅ -rfA ₂ -rA ₄	30	-3
rA ₄ -rfA ₃ -rA ₄	30	-3
rfA ₁₁	24	-9

Table 4.5: Melting temperatures of rA₁₁, rfA₁₁ and 11-mer oligoadenylylates containing rfA inserts in 100 mM citric acid (pH = 5) containing 3.0 M NH₄Cl.

4.1.6 Circular Dichroism Spectroscopy of Fluorinated Oligonucleotides

In order to gain insight in the structural differences between the native adenosine duplex and its 2' fluorinated counterpart, circular dichroism spectroscopy was performed. The CD profiles of both sequences (Figure 4.6) exhibit similarity in the location of maxima and minima: a maximum at ~260 nm with a broad shoulder in the ~260-295 nm range while the negative maximum for both oligonucleotides are located around 240 nm. This data supports the observations from the crystal structures; rfA residues have minimal influence on the global structure of the adenosine duplex at pH 4.

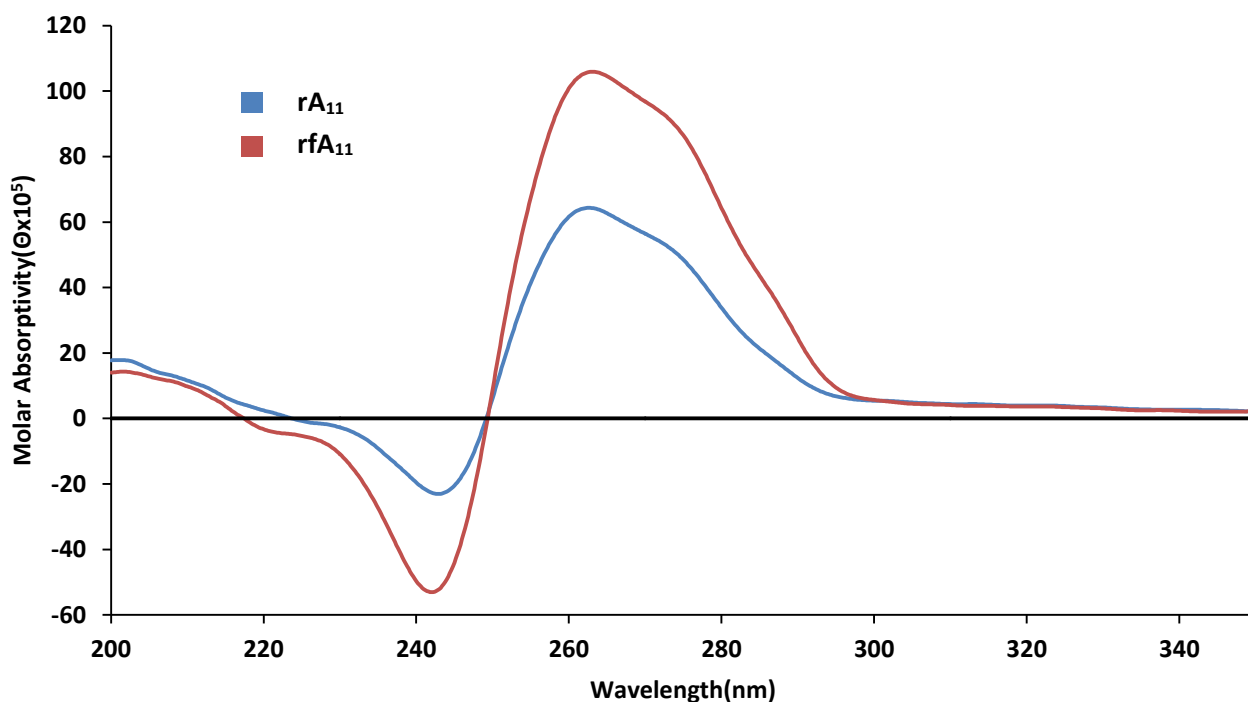


Figure 4.6: Circular dichroism spectrum of native and fluorinated oligoadenylates at pH 4. 3.3 μ M single strand concentration (Buffer: 50 mM NaOAc; spectra acquired at 20°C).

Similarly, at pH 7 and 4.4 M NH_4Cl (Figure 4.7), there is a maximum at ~ 260 nm for both oligonucleotides. In the 260-300 nm region of the spectra a broad plateau rather than a shoulder is observed relative to the spectra acquired at pH 4. The differences in intensity for these spectra acquired at 10°C could be due to the increased duplex stability for the fluorinated duplex, which is more stable at neutral pH than the RNA duplex.

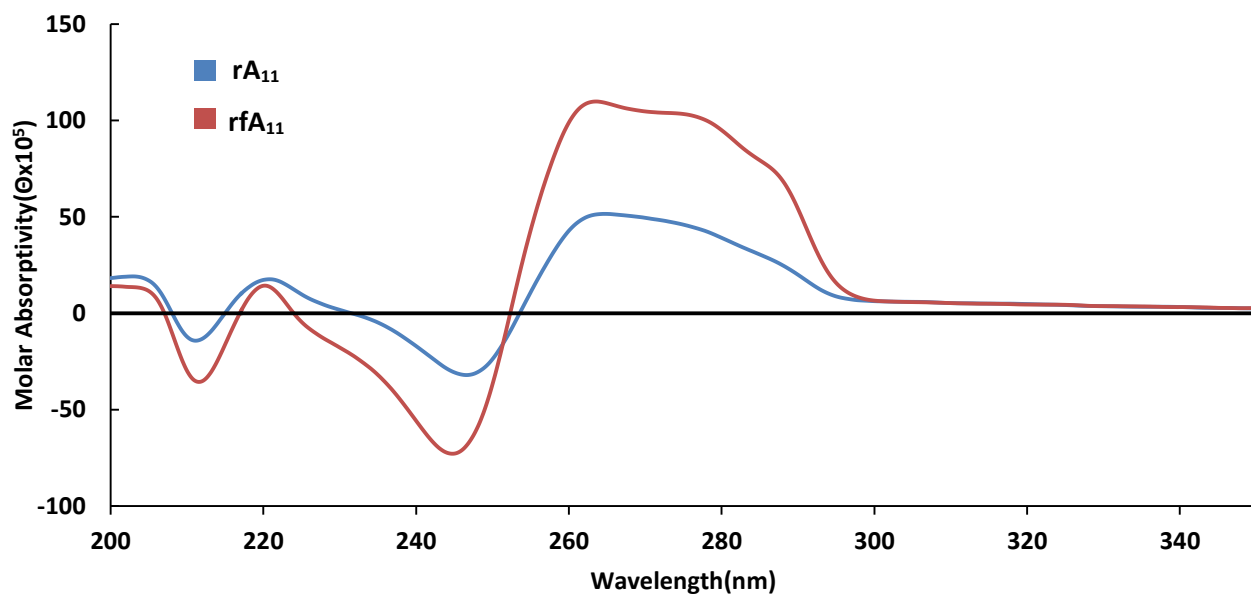


Figure 4.7: Circular dichroism spectrum of native and fluorinated oligoadenylates at pH 7 and 4.4 M NH_4Cl . $2.3 \mu\text{M}$ single strand concentration (Buffer: 10 mM NaH_2PO_4 ; spectra acquired at 10°C).

4.2 Influence of ANA and F-ANA Modifications

4.2.1 UV Thermal Denaturation Experiments

After evaluating the influence of dA and rA residues on the polyadenosine duplex, the effect of arabinose and 2' fluoro arabinose modifications were studied. Arabinose is the 2' epimer of ribose which allows for the investigation of the stereochemistry of the 2'-OH (or 2'-F) group on duplex stability. These modifications serve as a means to probe the contribution of the weak backbone C-H...O hydrogen bond in duplex formation, as this interaction should be eliminated by different conformations that these nucleotides adopt. Additionally, the more "DNA-like" sugar pucker should address whether C3'-endo is a requirement for adenosine rich strands to be self-complementary. To investigate, oligomers 9 nucleotides in length (containing a 5'-dT residue to introduce asymmetry for NMR spectroscopy), with a single aA or arafA insert or uniformly modified were synthesized.

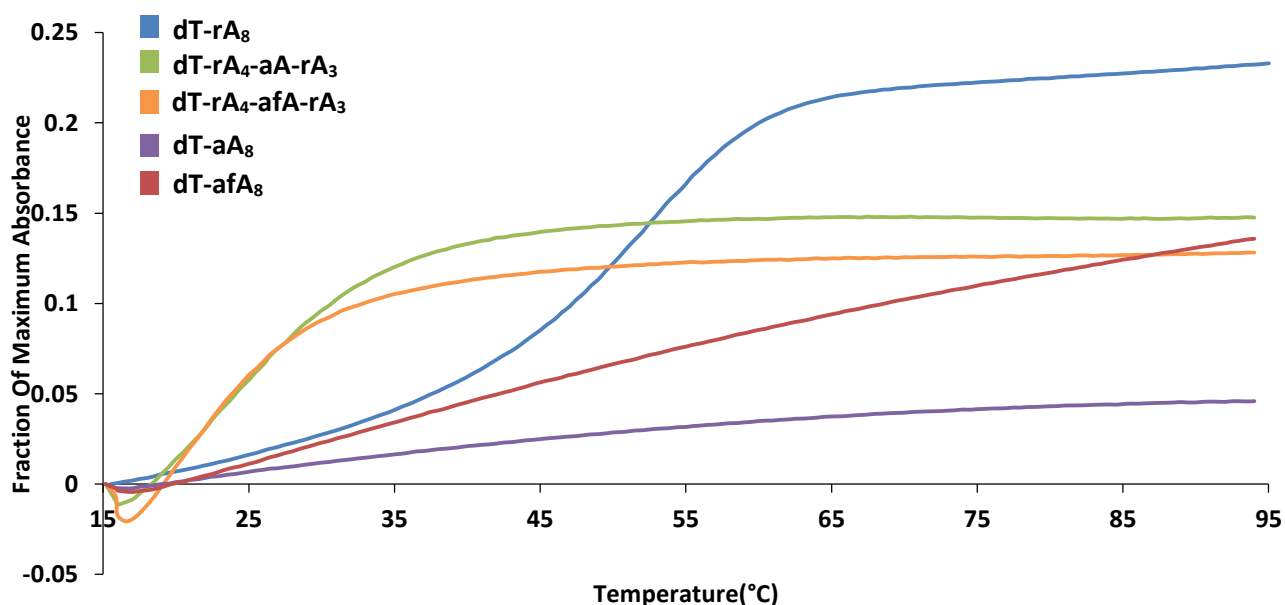


Figure 4.8: UV thermal denaturation spectrum of arabinose modified oligonucleotides at pH 4. 4.2 μ M single strand concentration (Buffer: 50 mM NaOAc).

Inspection of the UV thermal denaturation profiles at pH 4 reveals that a single aA or afA

Sequence (5'-3')	T_m (°C)
dT-rA ₈	53
dT-rA ₄ -aA-rA ₃	<25
dT-rA ₄ -afA-rA ₃	<25
dT-aA ₈	NA
dT-afA ₈	NA

Table 4.6: Melting temperatures of arabinose modified oligoadenylates (50 mM sodium acetate buffer at pH 4)

residue is strongly destabilizing relative to the rA control (Figure 4.8); the absence of a lower plateau makes it less accurate to quantify the ΔT_m . Furthermore, the uniformly arabino or 2'-

fluoroarabino adenosine oligonucleotides show no clear two-state transition suggesting they are incapable of duplex formation under the conditions studied. This result likely emphasizes the importance of the weak sugar-sugar contact present in RNA, as well as confirming the importance of the C3'-endo sugar pucker. Unfortunately the 9mer sequences were too short to observe a sigmoidal transition in the UV thermal denaturation experiments at pH 7, 4.4 M NH₄Cl (data not shown) and therefore the influence under these conditions could not be investigated.

4.2.2 Native PAGE on Uniformly Modified Arabinose Oligoadenylates

To support the results which suggest all aA oligomers are incapable of adenosine duplex formation at pH 4, native PAGE was performed as a complementary technique. Similar to the studies in section 3.2.1, the migration of a more bulky duplex is expected to be more retarded by the polyacrylamide matrix than a flexible single strand. An additional goal of this experiment is concern that partial protonation of the N1 atom of the adenine base in acidic conditions would reduce its mobility relative to the unprotonated uridine control, which may lead to erroneous conclusions about duplex formation. In this case arabino and ribo adenosine are epimers, both

should have similar N1 protonation, and therefore the native gels may alleviate concerns (reduced migration due to positive charge on N1 atom of adenine) about the Chapter 3 mobility shift experiments.

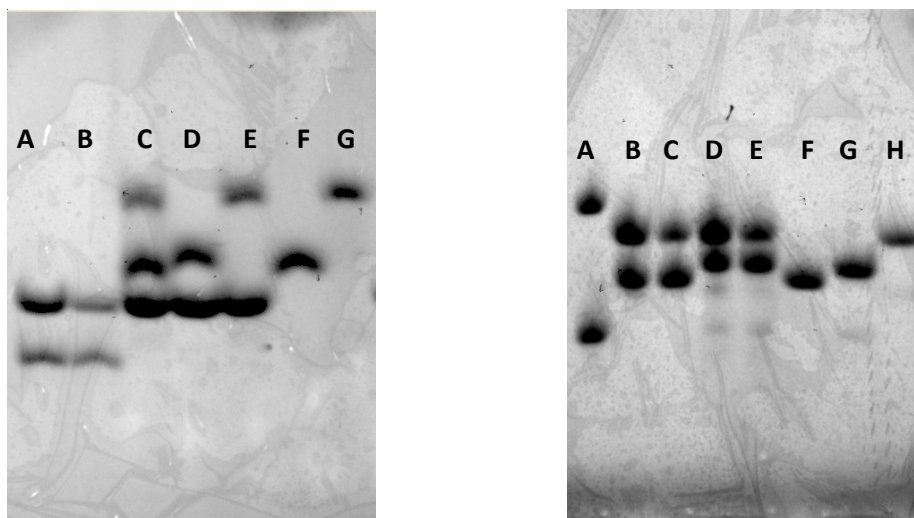


Figure 4.9: Native PAGE of ribo and arabino oligoadenylates. 20% Acrylamide (19:1), 200 V, 15°C
 1) **pH 4** A) dA₁₁:rU₁₁ [1:2] B) dA₁₁:rU₁₁ [1:1] C) dTrA₈:dTaA₈: rU₁₁ [1:1:2] D) dTaA₈:rU₁₁ [1:2] E) dTrA₈:rU₁₁[1:2] F) dTaA₈ G) dTrA₈ (Buffer: 39 mM Na₂HPO₄, 31 mM citric acid, 1.1 mM EDTA).
 2) **pH 7** A) dA₁₁:rU₁₁ [1:1] B) rU₈dA:dTaA₈ [1:2] C) rU₈dA:dTaA₈ [1:1] D) rU₈dA:dTrA₈ [2:1] E) rU₈dA:dTrA₈ [1:1] F) dTaA₈ G) dTrA₈ H) rU₈dA (87 mM Na₂HPO₄, 6.5 mM citric acid, 1.1 mM EDTA).

In this study, given that evidence which suggested that the arabinose sugar was not tolerated in the adenosine duplex, the formation of a duplex with its Watson-Crick complement (rU₁₁) or a triplex structure was evaluated by adjusting relative strand stoichiometries. The main objective on the gel at pH 4 (Figure 4.9) was to compare the relative mobilities of dT-araA₈ and dT-rA₈ (lanes F and G respectively). In agreement with UV thermal denaturation experiments, the adenosine oligonucleotide has a reduced mobility with respect to its 2' epimer counterpart. This is indicative of the fact that the more bulky adenosine duplex would be more retarded by the polyacrylamide gel matrix than the single stranded arabino oligoadenylate. As a control

experiment at pH 7, one would expect no duplex to be formed and indeed, the migration of dT-araA₈ and dT-rA₈ (lanes G and H respectively) are quite comparable. Unfortunately all attempts in both conditions at forming duplex controls or triplexes failed which is believed to be due to the lack of thermal stability at the 15°C gel operating temperature.

4.3 Adenosine Duplexes Containing 2'-*O*-Methylated Residues

4.3.1 UV Thermal Denaturation Studies on 2'-*O*-Methyl Modified Oligonucleotides

The next modification of the 2' position was replacement of the hydroxyl group with a hydrophobic *O*-methyl group. Sequence design was implemented as before; beginning initially with a native RNA species, and exploring the adenosine duplex tolerance of a central insert, as well as a uniformly 2'-*O*-methylated species. As before, the acidic conditions which promote duplex formation were examined for sequences containing a 5' dT residue for structural NMR spectroscopy studies. Inspection of the UV thermal denaturation curves at pH 4 (Figure 4.10) shows a clear stabilizing transition with a single rA^{2'-OMe} insert. While the single insert stabilizes the adenosine duplex by 4°C relative to the RNA control, the uniformly *O*-methylated species has a substantial stabilizing effect of 10°C

Sequence (5'-3')	T_m (°C)	ΔT_m (°C)
dT-rA ₈	53	
dT-rA ₄ -rA ^{2'-OMe} -rA ₃	57	+4
dT-rA ₈ ^{2'-OMe}	63	+10

Table 4.7: Melting temperatures of 2'-*O*-methylated oligonucleotides at pH 4 (Buffer: 50 mM NaOAc).

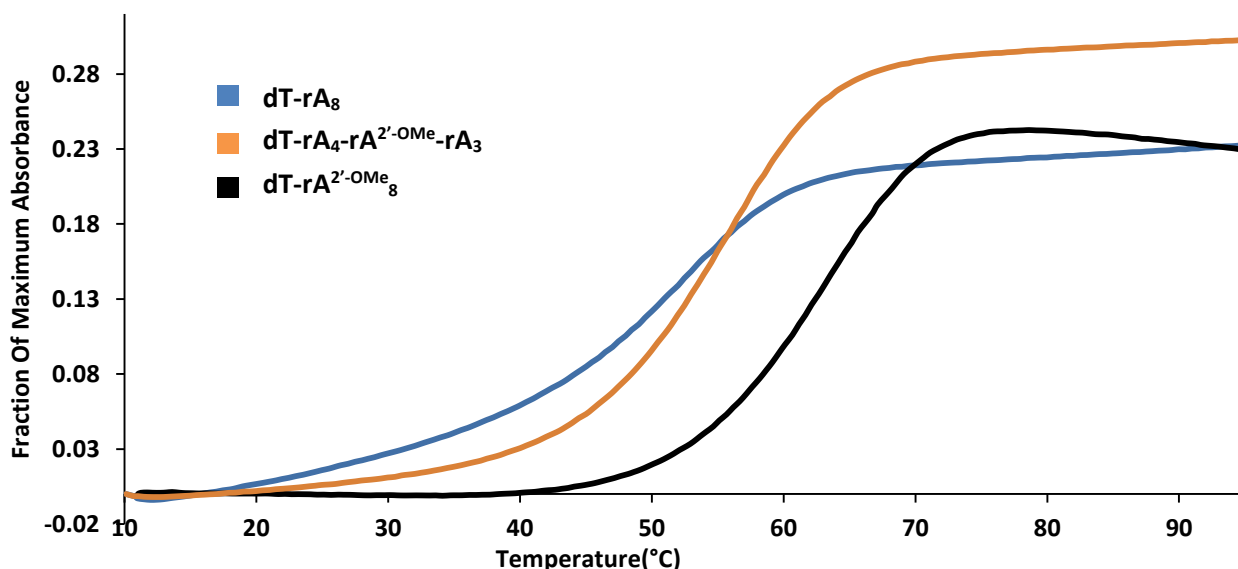


Figure 4.10: UV thermal denaturation spectrum of 2'-O-methylated oligonucleotides at pH 4. 4.2 μ M single strand concentration (Buffer: 50 mM NaOAc).

Encouraged by the 2'-O-methyladenosine's stabilizing effect at low pH, oligoadenylates and 2'-O-methylated analogues 16 nucleotides in length were synthesized to observe the effect at pH 7 in the presence of 4.4 M NH_4Cl . In contrast to what was observed at low pH, no significant difference of the T_m values obtained from the UV thermal denaturation curves was observed (Figure 4.11).

Sequence	T_m ($^{\circ}\text{C}$)	ΔT_m ($^{\circ}\text{C}$)
rA ₁₆	50	
rA ₁₆ ^{2'-OMe}	52	+2

Table 4.8: Melting temperatures of 2'-O-methylated oligonucleotides at pH 7, 4.4 M NH_4Cl (Buffer: 10 mM NaH_2PO_4).

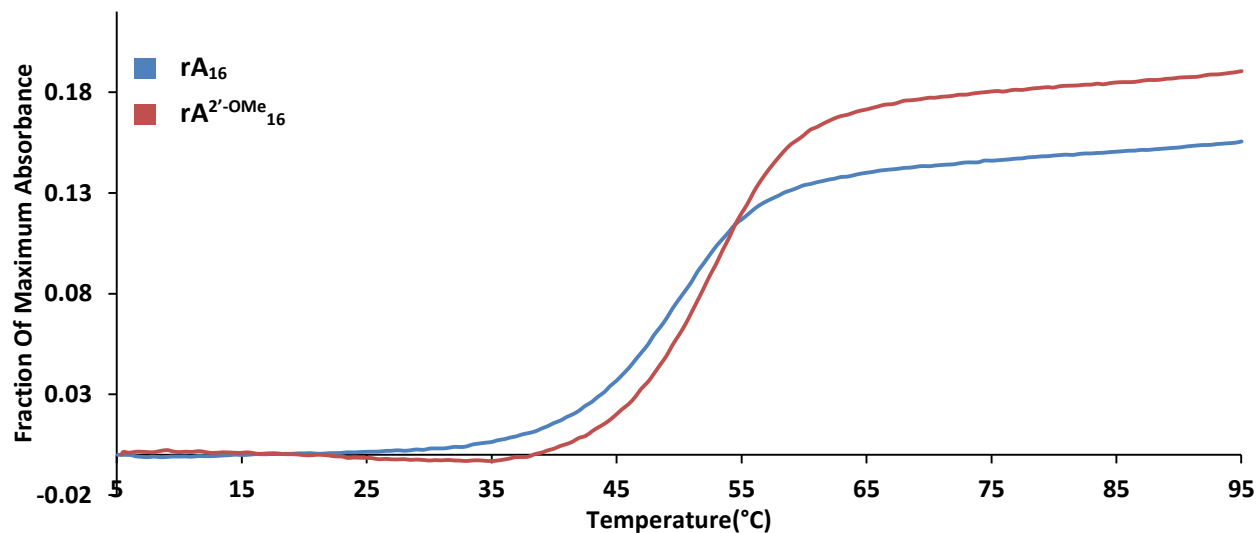


Figure 4.11: UV thermal denaturation spectrum of 2-*O*-methylated oligonucleotides at pH 7, 4.4 M NH₄Cl. 2.3 μM single strand concentration (Buffer: 10 mM NaH₂PO₄).

4.3.2 Thermodynamic Parameters of 2'-*O*-Methylated Adenosine Duplex at pH 4

Van't Hoff analysis of the native RNA, single rA^{2'-OMe} containing and uniformly methylated oligonucleotides at pH 4 reveals the uniformly 2'-*O*-methylated RNA source of stabilization to be enthalpic in nature. The thermodynamic data of dT-rA₄-rA^{2'-OMe}-rA₃ should be treated with caution, as the ΔG° of duplex formation is not proportional to the stabilizing effect on the melting temperature. Enthalpic stabilization of 2'-*O*-methyl groups is sometimes attributed to beneficial hydrophobic contacts,⁵⁸ however in the model of the adenosine duplex the 2' substituent is solvent exposed and does not appear to be in a position to form contacts with other moieties in the adenosine duplex.

Series (5'-3')	ΔH° (kJmol ⁻¹)	$\Delta\Delta H^\circ$	ΔS° (JK ⁻¹ mol ⁻¹)	$\Delta\Delta S^\circ$	ΔG° (kJmol ⁻¹) at 25 °C	T_m (°C) (4μM)
dT-rA ₈	-249±32		-665±87		-50.9	53
dT-rA ₄ -rA ^{2'-OMe} -rA ₃	-329±24	-80	-894±66	-229	-62.5	57
dT-rA ₈ ^{2'-OMe}	-269±35	-20	-695±90	-30	-62.1	63

Table 4.9: Thermodynamic properties of duplex formation of 2'-*O*-methylated oligoadenylates at pH 4 (Buffer: 50mM NaOAc).

4.3.3 Influence of pH on 2'-*O*-Methyl Adenosine Duplex Stability

While somewhat counterintuitive, reports in the literature have shown that the N1 atom of a 2'-*O*-methyl adenosine nucleotide analogue is more basic than the RNA or DNA counterpart.⁷² It has also been shown that the InAN3 atom of 2'-*O*-methyl cytosine has a higher propensity to be protonated in triplex forming oligonucleotides.⁷³ The data shows a minimal difference in thermal stability of native RNA vs. 2'-*O*-methylated at neutral pH which suggests that protonation could be responsible for the stabilizing effect in acidic conditions. Employing methodology used in section 4.1.2, buffers were prepared ranging from pH 3.5-6 to evaluate the effect of pH on melting temperature. The data reveals (Figure 4.12) a decrease in 2'-*O*-methyl adenosine duplex stability is observed, similar to the native RNA as the pH of the buffer is increased, and neither exhibits a sigmoidal transition at pHs above 5. At pH 3.5 the uniformly 2'-*O*-methylated duplex is 14°C more stable than the rA, however at pH 5 the difference is at least 8°C. This does not allow one to conclude that it is the increased basicity of the N1 atom of the modified adenosine nucleotides is responsible for the stabilization, as was the case with the fluorinated oligoadenylates (which had lower threshold pH for duplex formation).

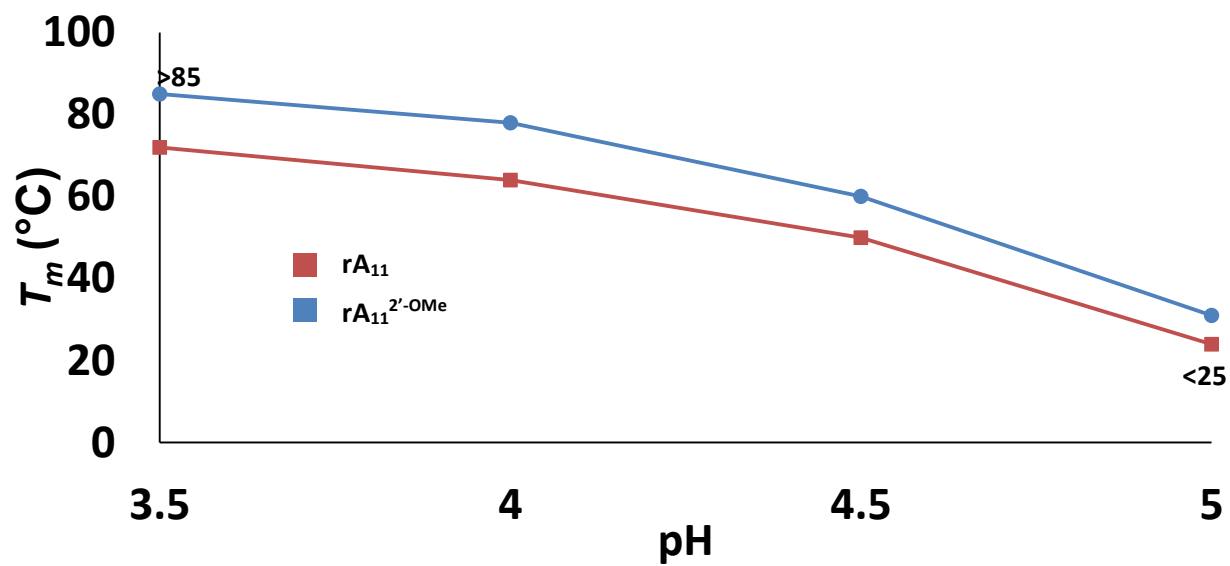


Figure 4.12: pH dependence of melting temperature of native and methylated oligonucleotides.

4.4 Influence of a 2'-5' versus 3'-5' Phosphodiester Bond

The influence of modifying the backbone to a 2'-5' phosphodiester as opposed to the standard 3'-5' linkage was evaluated. Oligonucleotides 16 nucleotides in length containing a single and uniform 2'-5' linkage were prepared. UV thermal denaturation studies (Figure 4.13) performed at pH 4 revealed a destabilizing influence of this linkage; a single 2'-5' phosphodiester linkage destabilizes the 16mer adenosine duplex by more than 30°C and the uniformly 2'-5' linked species shows no significant hyperchromic transition. This linear increase in absorbance suggests that the altered geometry of the uniformly 2'-5'rA oligonucleotide is not compatible with the parallel stranded adenosine duplex.

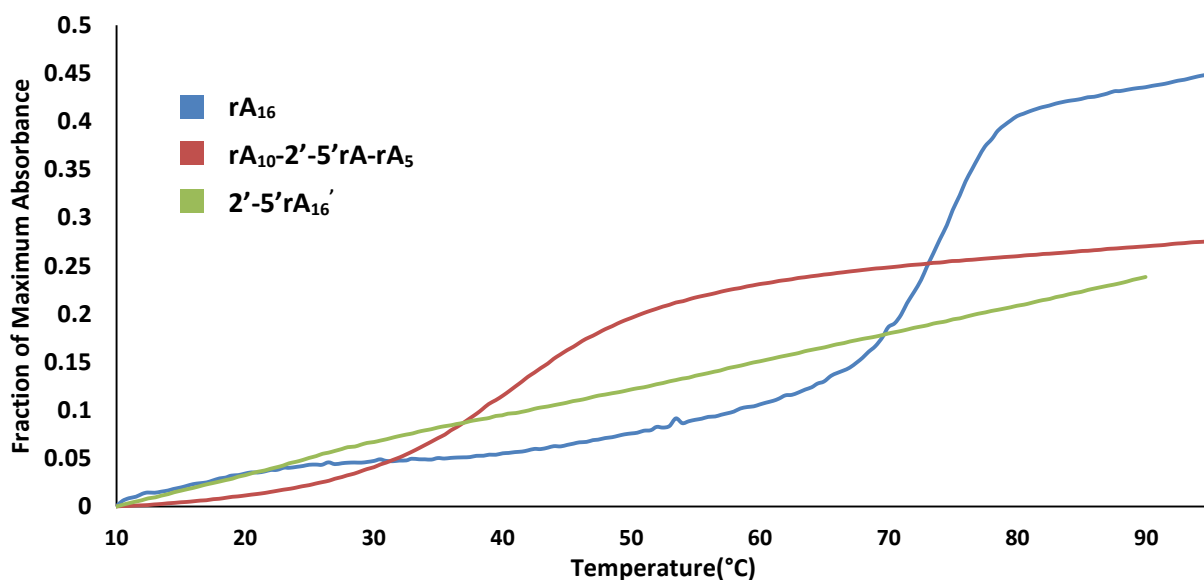


Figure 4.13: UV thermal denaturation spectrum of 2'-5' linked oligonucleotides at pH 4. 1.0 μ M single strand concentration (Buffer: 50 mM NaCaco).

Sequence (5'-3')	T_m (°C)	ΔT_m (°C)
rA ₁₆	75	
rA ₁₀ -2'-5'(rA)-rA ₅	42	-33
2'-5'(rA) ₁₆	NA	NA

Table 4.10: Melting temperatures of 2'-5' linked oligonucleotides at pH 4 (Buffer: 50 mM NaCaco).

Evaluation of the thermal stability for the oligoadenylate 16mers at neutral pH and 4.4 M NH_4Cl concentration revealed a more destabilizing effect where a single 2'-5' rA insert destabilizes the duplex with no sigmoidal transition observed (Appendix). Further studies are required to investigate why one sole insert in the middle of an adenosine strand 16 nucleotides in length renders it incapable of hybridization in the presence of ammonium cations but not in acidic conditions. While no structural information is available, one may speculate that the large destabilization in the single 2'-5' oligoadenylate is likely due to a significant distortion in the center of the duplex due to non-optimal geometry that the 2'O-P linkage introduces. This could lead to a disruption of base stacking and intermolecular hydrogen bonding, possibly also influencing the neighboring base pairs. Another possible reason as to why no duplex was detected for the single 2'-5' insert at neutral pH, 4.4 M NH_4Cl as opposed to a transition observed at low pH could be related to the proposed "inner salt effect" where an electrostatic interaction between the protonated adenine and the phosphate backbone of the opposing strand occurs. At neutral pH however, it requires an ammonium cation which may not participate so readily. The fact that at 4.4 M NH_4Cl and at pH 4 there appears to exhibit a sigmoidal transition (Figure 4.14) with a T_m of 35°C for the uniformly 2'-5' linked oligoadenylate 16mer merits additional studies. This is in contrast to either pH 4 without ammonium cations or pH 7 with, in either case no evidence of duplex was observed.

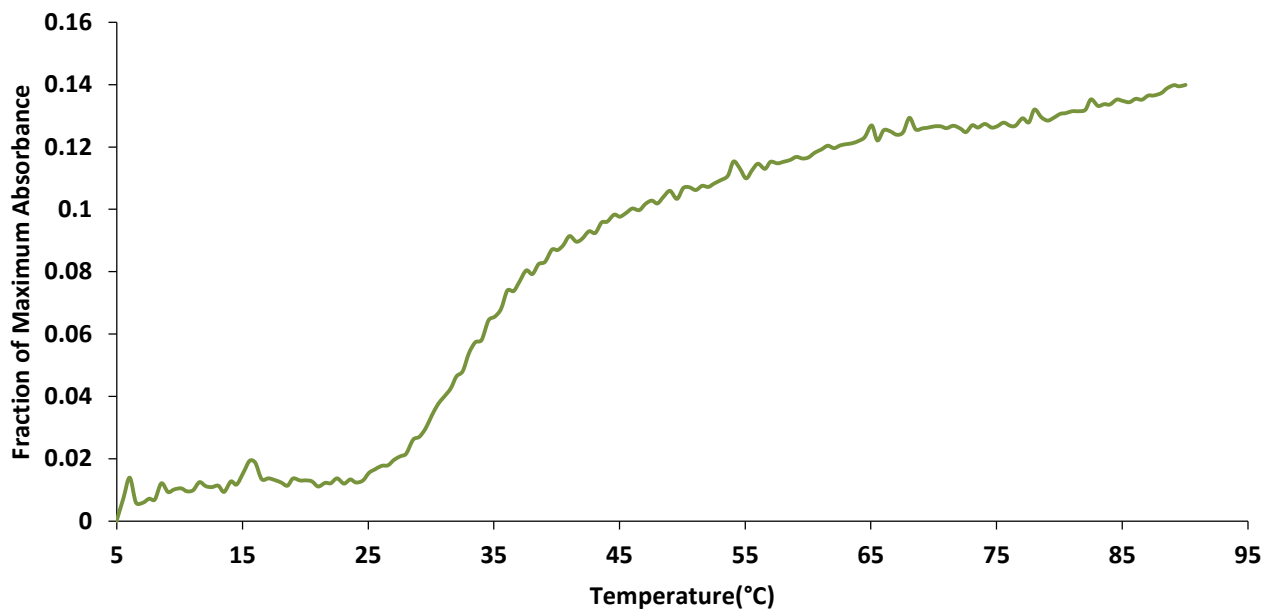


Figure 4.14: UV thermal denaturation spectrum of 2'-5' 16mer at pH 4, 4.4 M NH₄Cl. 1.0 μM single strand concentration (Buffer: 50 mM NaCaco).

4.5 Self-Association of Native and Modified Branched Oligoadenylylates

An approach to stabilize this structure by connecting the polyadenosine strands with an adenosine branch through the 2' and 3' oxygen atoms was evaluated. This geometric juxtaposition of two parallel adenosine strands is not merely a matter of academic curiosity, and has some precedent in cellular processes. In the process of post-transcriptional mRNA splicing, removal of introns proceeding *via* a 2', 3' branching point.⁷⁵ The branching introduces a reduced entropic cost of hybridization (shown in parallel stranded structures such as the i-motif)⁷⁶ and no reasoning was evident for a deviation of trends already noted for the 2' modifications. The first modification studied was the effect of a single 2'-deoxyadenosine insert in a branched oligonucleotide consisting of 8 adenosines. To view the effect of the branching the T_m analysis was also performed with a uniformly RNA and a single dA insert 8mers as controls. As seen before a drop of ~8°C is

observed with a single dA insert in the 8mer control series (Figure 4.15), and a similar drop is seen with the single dA insert in the branched 8mer series (the T_m of rA-(rA₈)₂ could not be accurately evaluated due to lack of upper plateau). The reduced entropic penalty significantly stabilized the adenosine duplex as evidenced by the ~20-30°C increase in melting temperature relative to the unbranched oligonucleotides.

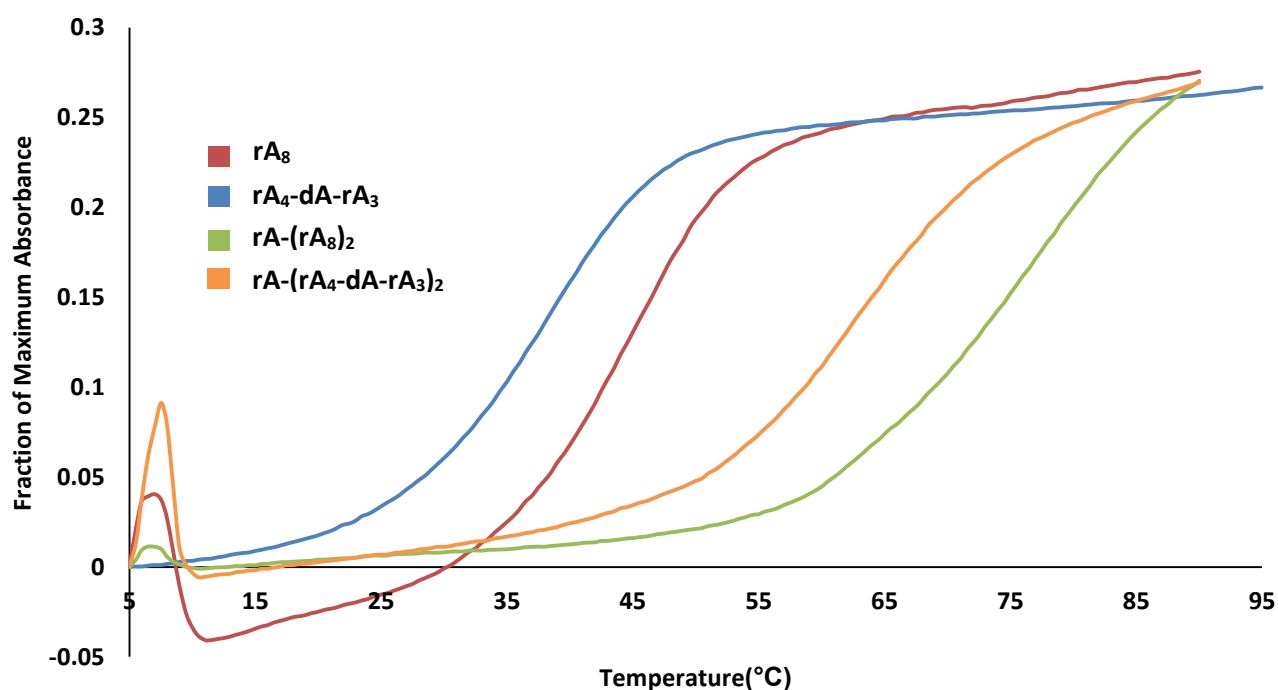


Figure 4.15: UV Thermal denaturation experiments of branched DNA-RNA chimera at pH 4. 1.8 (non-branched)/0.9 (branched) μ M single strand concentration (Buffer: 50mM NaOAc).

Sequence (5'-3')	T_m (°C)
rA-(rA ₈) ₂	>77
rA-(rA ₄ -dA-rA ₃) ₂	62
rA-(rA ₄ -rfA-rA ₃) ₂	>76
rA-(rfA ₈) ₂	NA

Table 4.11: Melting temperature of branched oligonucleotides at pH 4 (Buffer: 50 mM NaOAc).

Investigation of the fluoro modification does not lead to obvious trends. While two single fluoro inserts are well tolerated in the branched oligoadenylate (Figure 4.16), the uniformly fluorinated branched oligomer shows a very non-cooperative sigmoidal transition which warrants further investigation. A final point of interest is that the uniformly fluorinated species branched oligonucleotide was the only species (all data not shown) to exhibit a clear sigmoidal transition at pH 7 in the presence of 4.4 M NH_4Cl which reemphasizes the stabilizing effect of fluorine on adenosine duplex in those conditions (Figure 4.17).

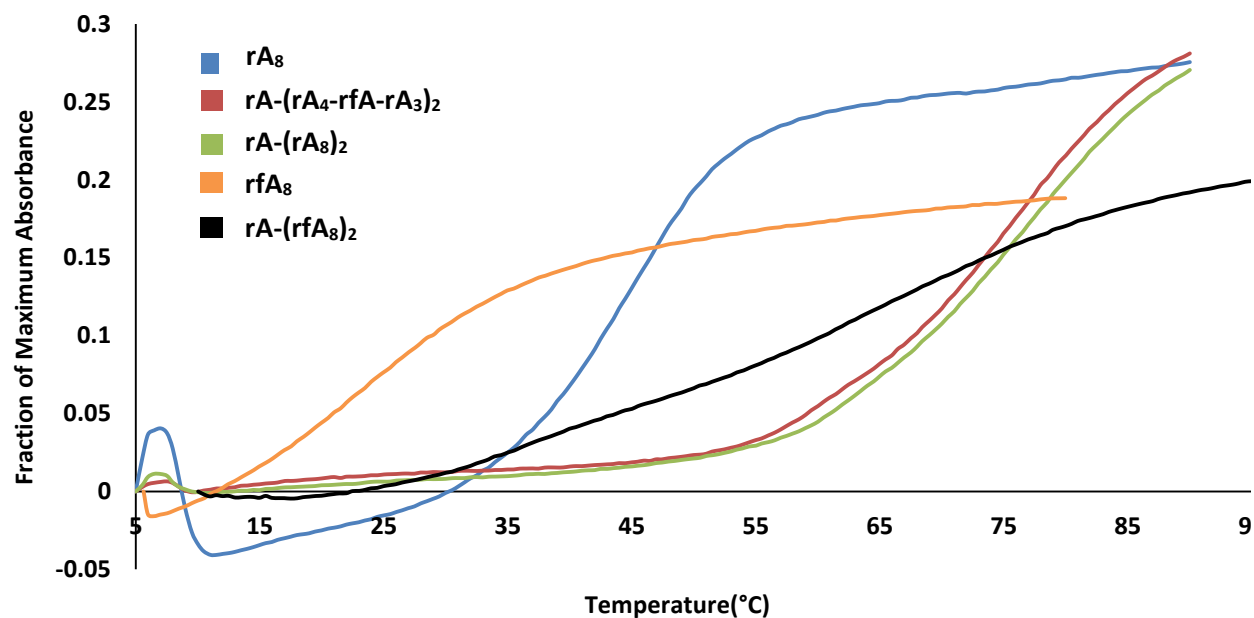


Figure 4.16: UV Thermal denaturation experiments of fluorinated branched oligoadenylates at pH 4. 1.8 (non-branched)/0.9 (branched) μM single strand concentration (Buffer: 50 mM NaOAc).

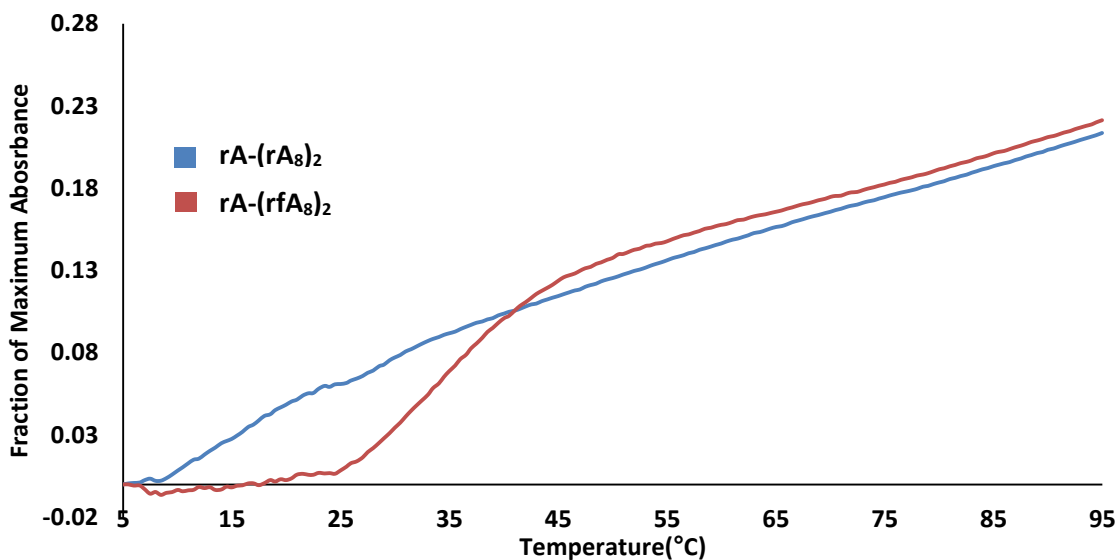


Figure 4.17: UV Thermal denaturation experiments of native *vs.* fluorinated branched oligoadenylates at pH 7 in the presence of 4.4 M NH₄Cl (Buffer: 40 mM Na₂HPO₄, 30 mM citric acid).

In summary, 2'-fluoro inserts are tolerated in the adenosine duplex but have a destabilizing influence on thermal stability at low pH but are stabilizing at neutral pH (7) in the presence of 4.4 M NH₄Cl. X-ray crystallographic studies reveal the destabilization to not be structural in origin. 2'-*O*-Methylated residues are stabilizing to the adenosine duplex at low pH, however little change in T_m is noted at neutral pH and 4.4 M NH₄Cl. The 2'-5' phosphodiester bond linked nucleotides do not appear to be compatible with adenosine duplex formation (UV thermal denaturation studies), and the reduced entropic penalty of branched oligonucleotides leads to an increase in T_m to 20-30°C relative to single stranded oligoadenylates.

Chapter 5: Conclusions and Future Work

Conclusions

2'-Deoxyadenosine (dA) inserts are destabilizing to the adenosine duplex regardless if the conditions are at pH 4, or at pH 7 with 4.4 M NH₄Cl as illustrated by UV thermal denaturation studies. The UV melt experiments on uniformly DNA oligonucleotides suggest this duplex is not stable under these conditions as supported by native PAGE where both single stranded DNA controls (dT) and dA oligonucleotides have near identical migration. NMR and X-ray crystallographic studies on the adenosine duplex containing single dA inserts show no significant perturbations to the duplex structure suggesting the destabilization is not conformational in origin. Based on the thermodynamic data the destabilization appears to be entropic in nature, which is hypothesized to be due to the entropic penalty of the 2'-deoxyribose sugar conforming to its RNA environment, and could also be related to the absence of a weak backbone C2'-H...O4' hydrogen bond.

Single 2'-fluoroadenosine inserts are well tolerated in the adenosine duplex at pH 4, or at neutral pH with 4.4 M NH₄Cl, however as the number of 2'-fluoroadenosine residues are increased different trends begin to become apparent. Fluoro inserts are destabilizing in acidic conditions, yet stabilizing at neutral pH in the presence of 4.4 M NH₄Cl. Similar to the dA inserts, the rfA residues are well tolerated structurally, based on crystallographic data (low pH and high ammonium concentration). The destabilization at low pH appears to be enthalpic in origin as exhibited from thermodynamic data extracted from van't Hoff plots. It is proposed that at low pH the reduced protonation of the N1 atom due to inductive effects, or a decreased 2' hydration could explain the

decrease in thermal stability. At neutral pH, 4.4 M NH₄Cl more favourable base-stacking and hydrogen bonding between the nucleobases as well as the stronger C2'-H...O4' backbone interaction could play a role in adenosine duplex thermal stability. As the pH and ammonium parameters are modified, the opposing effects appear to begin to cancel out (dependent on the degree of modification) which could be useful for the fine tuning of a molecular switch. Arabino and 2'-fluoro arabino inserts are highly destabilizing at pH 4, and there is no evidence that strands consisting entirely of the 2' epimer of ribose can form this duplex. While the 2'-*O*-methyl modifications have a minimal effect at pH 7, 4.4 M NH₄Cl, a stabilizing effect is noted in acidic conditions. Linkage by the 2'-5' phosphodiester bond is strongly destabilizing which is hypothesized to be due to a significant structural perturbation. Finally, the entropic stability expected by branched oligonucleotide was confirmed, with a 20-30°C increase in thermal stability relative to the native rA duplex.

Future Work

While having established concrete trends with various 2' inserts, the surface of modifications tolerated in the adenosine duplex has only been scratched. The most logical subsequent experiments would be to synthesize oligoadenylates 11 and 16 nucleotides in length containing arabinoadenosine inserts. Crystallizing an 11mer adenosine duplex with this modification may allow evaluation of the contribution of structural perturbations induced by alternate sugar puckers to stability. The 16mer series will allow one to evaluate trends of the arabino containing adenosine duplex at neutral pH in the presence of 4.4 M NH₄Cl. Understanding of the importance of hydration in duplex stability can be corroborated by osmotic stress

experiments.⁷⁷ The list of 2' modifications is plentiful but investigation of longer alkyl groups or even specifically reactive entities warrants investigation. To probe the weak backbone interaction a carbocyclic modification (Figure 5.41) could be employed; this would result in the elimination of the intramolecular hydrogen bond acceptor. Gonzalez and Damha⁴⁷ showed that by alternating the rfA and arafA content the backbone C-H...O interaction was neglected, and was destabilizing to a more canonical type duplex. Are biologically relevant amines potential cation stabilizers of the duplex? Preliminary research has not encountered such an amine; recent evidence of duplex formation in high concentrations of guanidinium chloride at neutral pH was negative. Potential *in vivo* applications could involve the 5' end of the strands conjugated to functional groups, and therefore a pH dependent oligonucleotide templated reaction is a possibility. Especially due to the fact that the extracellular environment of tumour cells is acidic, one could envision only drug release upon encountering regions of low pH which would overcome serious hurdles in off-target effects.

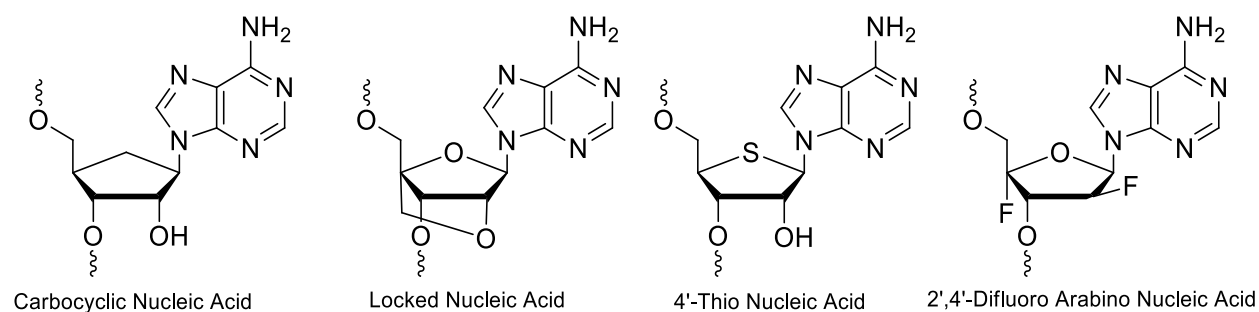


Figure 5.1: Ribose sugar modifications to investigate in adenosine duplex stability.^{78–81}

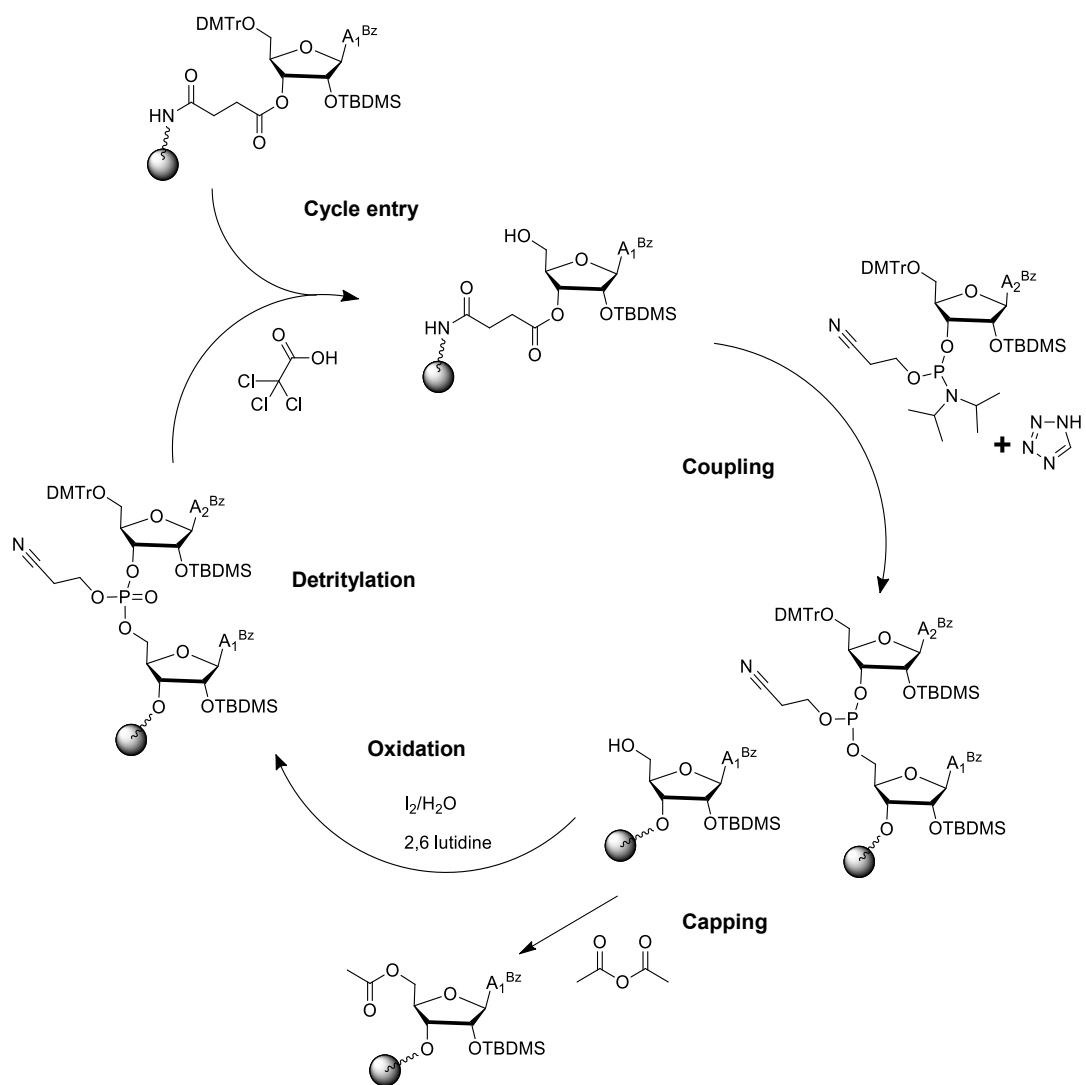
Chapter 6: Materials and Methods

6.1 Materials

All 5'-*O*-dimethoxytrityl-N-benzoyl-2'-*O*-TBDMS-3'-*O*-(2-cyanoethyl-N,N-diisopropyl)-ribonucleosides, 5'-*O*-dimethoxytrityl-N-benzoyl-2'-*O*-methyl-3'-*O*-(2-cyanoethyl-N,N-diisopropyl)-adenosine, 5'-*O*-dimethoxytrityl-N-benzoyl-2'-fluoro-3'-*O*-(2-cyanoethyl-N,N-diisopropyl)-2'-deoxyadenosine, 5'-*O*-dimethoxytrityl-N-benzoyl-2'-fluoro-3'-*O*-(2-cyanoethyl-N,N-diisopropyl)-2'-deoxyarabinoadenosine, 5'-*O*-dimethoxytrityl-N-benzoyl-2'-*O*-acetyl-3'-*O*-(2-cyanoethyl-N,N-diisopropyl)-arabinoadenosine, 5'-*O*-dimethoxytrityl-N-benzoyl-3'-*O*-(2-cyanoethyl-N,N-diisopropyl)-2'-deoxyribonucleoside phosphoramidites and appropriately functionalized CPG/universal CPG were purchased from Glen Research (Sterling, Virginia). All chemicals and solvents were purchased from the Aldrich Chemical Company (Milwaukee, Wisconsin).

6.2 Solid Phase Oligonucleotide Synthesis

All oligonucleotides were synthesized on a 1 μ mol scale on an Applied Biosystem 3400 synthesizer using standard β -cyanoethylphosphoramidite chemistry^{82,83,84} (Scheme 1) developed by Caruthers *et al.*⁸⁵ with commercially available monomers (the 2', 3'-*O*-bis-phosphoramidite for the branched molecules were prepared by Gianna Di Censo). The steps in the synthesis cycle are deprotection of the 5'OH group (detritylation), 5-thioethyl tetrazole catalyzed coupling with the incoming phosphoramidite, an acetic anhydride capping step to render unreacted 5'OH groups inactive, and finally an oxidation step to convert the phosphite to a phosphate.



Scheme 1: Steps in automated oligonucleotide synthesis *via* β -cyanoethylphosphoramidite chemistry.

6.4 Purification of Oligonucleotides

Oligonucleotides were purified by preparatory denaturing PAGE or IEX HPLC. The preparatory denaturing PAGE consisted of a 20 % acrylamide solution (19:1 acrylamide:bisacrylamide) in 1xTBE running buffer on a standard 20x20 cm glass plate at 450 V until sufficient separation was achieved. The desired band was excised and the pure oligonucleotide was extracted with 8-10 mL of 0.1 NaOAc solution on a mixer overnight. Purification by IEX was performed on a Dionex DNAPAC PA-100 column (0.4 cm x 25 cm) with a linear gradient of 0-50 % buffer B over 30 minutes (buffer A: 100 mM Tris-HCl, pH 7.5, 10 % ACN and buffer B: 100 mM Tris-HCl, pH 7.5, 10 % ACN, 1 M NaCl). The collected fraction was diluted by $\frac{1}{4}$ with 0.1 M NaOAc to ensure appropriate column affinity during desalting. Purified oligonucleotides were desalted with a C-18 SEP PAK cartridge. The cartridge was washed with 10 mL of HPLC grade ACN, followed by 50 % ACN and finally equilibrated with 0.1 M NaOAc. Extracted or collected oligonucleotide was adsorbed to the C-18 column, and salt was removed with 2x 10 mL of 18 MΩ H₂O. Flowthrough was analyzed throughout the process to verify the sample was properly adsorbed. The sample was eluted with methanol:water:ACN (2:1:1) eluent. Purity was accessed to be greater than 90 % for all oligonucleotides synthesized by an analytical denaturing PAGE or IEX HPLC.

6.5 Quantitation of Oligonucleotides

All oligonucleotides synthesized were quantitated using a Varian Cary Model 3E spectrophotometer. Single strand concentrations were calculated using the Beer-Lambert law

$A_{260} = \epsilon c l$ and the absorbance was measured at 260 nm. Molar extinction coefficients were calculated by the nearest neighbour approximation.⁸⁷ An assumption was made that the extinction coefficient for all 2' modified nucleotides was identical to their unmodified counterpart.

6.6 qTOF-ESI Mass Spectrometry

0.1 OD of oligonucleotide was dried down for analysis by electrospray ionization and the qTOF method of ion quantitation at the Concordia University Centre for Biological Applications of Mass Spectrometry (CBAMS) on a Micromass Q-ToF Ultima API. The mass spectrometer was run in full scan, negative ion detection mode.

6.7 Enzymatic Digest Characterization

0.1 OD of oligonucleotide was suspended in 17.5 μ L buffer (10 mM Tris, 2 mM MgCl₂, pH 8.1), 2 μ L of snake venom phosphodiesterase and 0.5 μ L of calf intestinal phosphatase for a minimum of 2 hours at 37°C. The constituent nucleosides were analyzed by reverse phase HPLC, on a Symmetry® C-18 5 μ m (0.46 cm x 15 cm) column with 0-60 % linear gradient of buffer B (buffer A: 50 mM sodium phosphate, pH 5.8, 2% acetonitrile and buffer B: 50 mM sodium phosphate, pH 5.8, 50% acetonitrile) with the detector set to 260 nm. The ratios were then acquired by the integrated area of each peaked divided by the molar extinction coefficient⁸⁸ of each nucleoside. Nucleoside standards were run to empirically determine the retention times. Importantly, it is believed an adenosine deaminase contamination is present in the snake venom phosphodiesterase stock, responsible for converting adenosines to inosine. Due to this, inosine, 2-

O-methyl and 2'-deoxyinosine were run as controls with retention times identical to the additional peak observed for the samples. Therefore, the sum of the integrated peaks for both adenosine and its inosine derivative were determined (after molar extinction coefficient correction) which corresponds to the adenosine content of the oligonucleotide.

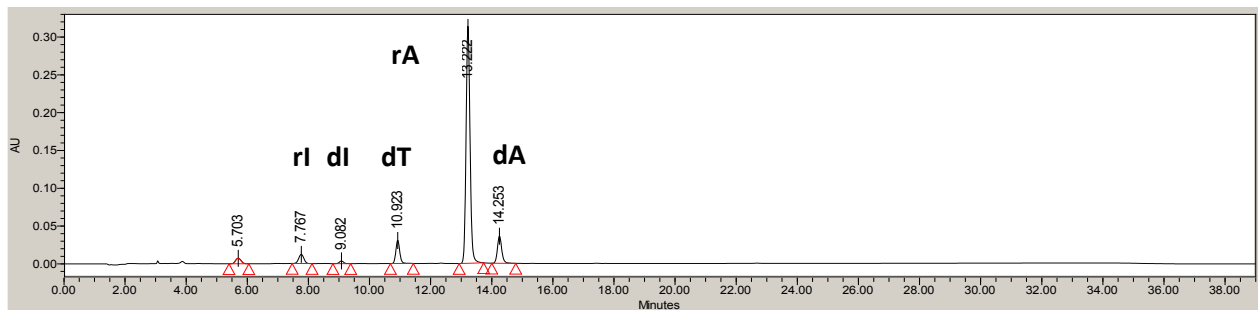


Figure 6.1: Sample chromatogram: RP HPLC trace of digest of dT-rA₄-dA-rA₃.

6.8 UV Thermal Denaturation Studies

Oligonucleotides were suspended in 1 mL of appropriate buffer, heated at 95°C for 10 minutes, slowly cooled to room temperature and incubated at 4°C overnight. In order to avoid depurination at lower pHs (<3.5), especially with dA containing oligonucleotides, the heating at 95°C step was omitted (in general). The samples were then degassed on the speed-vacuum concentrator for 2 minutes. UV thermal denaturation data was acquired on a Varian CARY Model 3E Spectrophotometer, with absorbance being measured at 260 nm (unless specified) with a heating rate at 0.5°C/min. The melting temperature (T_m) was calculated as the maximum of the first derivative ($d^2A_{260nm}/dT^2=0$) according to the method of Puglisi and Tinoco.⁶³ All data analysis was performed in Microsoft Excel™.

6.9 Van't Hoff Analysis

Extraction of thermodynamic parameters was performed by a van't Hoff analysis. 0.1, 0.5, 1.0 and 2.5 OD of oligonucleotide were dried down, and suspended in 1, 1.25, 0.5, 0.25 mL respectively of appropriate buffer. To remain in the linear range of the Beer-Lambert law, it was necessary to use a cell path length of 1 cm for 0.1 OD, 0.5 cm for 0.5 OD, 0.2 cm for 1.0 OD and 0.1 cm for 2.5 OD of sample. UV thermal denaturation studies were performed by employing the identical experimental procedure as described in section 6.8, and ΔH° , ΔS° and ΔG° were obtained by the relation between melting temperature and oligonucleotide concentration.⁸⁹

6.10 Circular Dichroism Spectroscopy

Circular dichroism experiments were performed on a Jasco J-815 spectropolarimeter equipped with a Julaba F25 circulating temperature bath. 0.5 OD of oligonucleotide was suspended in 1 mL of buffer, heated at 95°C for ten minutes, slowly cooled to room temperature and incubated at 4°C overnight. Circular dichroism spectra were scanned from 350 to 200 nm at 10°C with 5 acquisitions recorded. The Y axis is expressed in molar ellipticity (difference between absorbance of right and left handed polarized light, multiplied by 10^{-5}), with extinction coefficients calculated by the nearest neighbour approximation.

6.11 Native Polyacrylamide Gel Electrophoresis

0.1 OD of oligonucleotide was suspended in 10 μ L of phosphate-citrate sucrose loading buffer of appropriate pH. The samples were heated at 95°C for 10 mins, slowly cooled to room temperature and incubated at 4°C for one hour. Gels were prepared with 50% acrylamide/bisacrylamide (40% acrylamide, 19:1): 50% running buffer of appropriate pH. Gels were polymerized between two 7 cm x 10 cm glass plates and were prerun for 20 minutes at 80 V. It should be noted that these are general conditions and may vary depending on the experiment. For temperature controlled gels a larger gel apparatus (20 cm x 20 cm plates) and higher voltage (180 V) was used. For studies at low pH studies heating of the samples (to ensure proper annealing) was omitted to minimize acid-catalyzed depurination.

6.12 PABP RRM23 (98-269) Purification and Overexpression

Human RRM23 (Residues 98-269) with an N-terminal GST tag modification was overexpressed in *E. Coli* BL21 grown in LB rich media. The cells were lysed in PBS (19 mM Na₂HPO₄, 0.9 mM KH₂PO₄, 2.5 mM KCl, 140 mM NaCl [pH 7.0]), and the protein was isolated by affinity chromatography with glutathione-SepharoseTM beads. The GST tags were then cleaved by Protease C, and the protein was further purified by cation-exchange, anion-exchange and finally size-exclusion chromatography in buffer (10 mM HEPES, 100 mM NaCl, 2 mM DTT [pH 7.0]).

6.13 Crystal Drop Setup for X-Ray Crystallography Experiments

Crystals of necessary quality for high-resolution diffraction (rA₅-dA-rA₅, rA₅-rfA-rA₅) were grown by the sitting drop technique equilibrating 0.5 μL of RNA: RRM23 mixture (1:1 molar ratio, 0.47 mM RNA concentration, buffer: 10 mM HEPES, 100 mM NaCl, 2 mM DTT [pH 7.0]) and 0.5 μL of reservoir buffer (1.5 M (for rfA inserts) or 1.6 M NH₄Cl (for dA inserts) with 0.1 M citric acid [pH 5.0]).

References

- (1) Watson, J.; Crick, F. H. F. *Nature* **1953**, *171*, 737–738.
- (2) Saenger, W. *Principles of Nucleic Acid Structure*; Springer-Verlag: Berlin, 1984.
- (3) Blackburn, G. M.; Gait, M. J.; Loakes, J. D.; Williams, D. M. *Nucleic Acids in Chemistry and Biology*, 3rd ed.; Royal Society of Chemistry: Cambridge, UK, 2006.
- (4) Klug, A. *J. Mol. Biol.* **2004**, *335*, 3–26.
- (5) Reddy, B. S. P.; Sondhi, S. M.; Lown, J. W. *Pharmacol. Ther.* **1999**, *84*, 1–111.
- (6) Morávek, Z.; Neidle, S.; Schneider, B. *Nucleic Acids Res.* **2002**, *30*, 1182–1191.
- (7) Ussery, D. W. In *Encyclopedia of Life Sciences*; John Wiley & Sons, 2002; pp 1–11.
- (8) Arnott, S.; Chandrasekaran, R.; Millane, R. P.; Park, H.-S. *Biophys. J.* **1986**, *49*, 3–5.
- (9) Herbert, A.; Rich, A. *J. Biol. Chem.* **1996**, *271*, 11595–11598.
- (10) Sigler, P. B. *Annu. Rev. Biophys. Bioeng.* **1975**, *4*, 477–527.
- (11) Felsenfield, G.; Davies, D. R.; Rich, A. *J. Am. Chem. Soc.* **1957**, *79*, 2023–2024.
- (12) Broitman, S. L.; Im, D. D.; Fresco, J. R. *Proc. Natl. Acad. Sci. U. S. A.* **1987**, *84*, 5120–5124.
- (13) Radhakrishnan, I.; Patel, D. J. *Structure* **1993**, *1*, 135–152.
- (14) Lipsett, M. N. *J. Biol. Chem.* **1964**, *239*, 1256–1260.
- (15) Rhee, S.; Han, Z.; Liu, K.; Miles, H. T.; Davies, D. R. *Biochemistry* **1999**, *38*, 16810–16815.

- (16) Gellert, M.; Lipsett, M. N.; Davies, D. R. *Proc. Natl. Acad. Sci. U. S. A.* **1962**, *48*, 2013–2018.
- (17) Burge, S.; Parkinson, G. N.; Hazel, P.; Todd, A. K.; Neidle, S. *Nucleic Acids Res.* **2006**, *34*, 5402–5415.
- (18) Brooks, T. A.; Kendrick, S.; Hurley, L. *FEBS J.* **2010**, *277*, 3459–3469.
- (19) Gehring, K.; Leroy, J.-L.; Gueron, M. *Nature* **1993**, *363*, 561–565.
- (20) Leroy, J. L.; Guéron, M.; Mergny, J. L.; Hélène, C. *Nucleic Acids Res.* **1994**, *22*, 1600–1606.
- (21) Ding, Y.; Fleming, A. M.; He, L.; Burrows, C. J. *J. Am. Chem. Soc.* **2015**, *137*, 9053–9060.
- (22) Geinguenaud, F.; Liquier, J.; Brevnov, M. G.; Petrauskene, O. V.; Alexeev, Y. I.; Gromova, E. S.; Taillandier, E. *Biochemistry* **2000**, *39*, 12650–12658.
- (23) Mata, G.; Luedtke, N. W. *J. Am. Chem. Soc.* **2015**, *137*, 699–707.
- (24) Jin, K. S.; Shin, S. R.; Ahn, B.; Rho, Y.; Kim, S. J.; Ree, M. *J. Phys. Chem. B* **2009**, *113*, 1852–1856.
- (25) Collin, D.; Gehring, K. *J. Am. Chem. Soc.* **1998**, *120*, 4069–4072.
- (26) Seeman, N. C. *J. Theor. Biol.* **1982**, *99*, 237–247.
- (27) Chen, J.; Seeman, N. C. *Nature* **1991**, *350*, 631–633.
- (28) Rothmund, P. W. K. *Nature* **2006**, *440*, 297–302.
- (29) Goodchild, J. *Bioconjug. Chem.* **1990**, *1*, 165–187.
- (30) Edwardson, T. G. W.; Carneiro, K. M. M.; McLaughlin, C. K.; Serpell, C. J.; Sleiman, H. F. *Nat. Chem.* **2013**, *5*, 868–875.

- (31) Mao, C.; Sun, W.; Shen, Z.; Seeman, N. C. *Nature* **1999**, *397*, 144–146.
- (32) Li, J.; Lu, Y. *J. Am. Chem. Soc.* **2000**, *122*, 10466–10467.
- (33) Cuenoud, B.; Szostak, J. W. *Nature* **1995**, *375*, 611–614.
- (34) Serganov, A.; Nudler, E. *Cell* **2013**, *152*, 17–24.
- (35) Liedl, T.; Olapinski, M.; Simmel, F. C. *Angew. Chem. Int. Ed. Engl.* **2006**, *45*, 5007–5010.
- (36) Modi, S.; M G, S.; Goswami, D.; Gupta, G. D.; Mayor, S.; Krishnan, Y. *Nat. Nanotechnol.* **2009**, *4*, 325–330.
- (37) Tannock, I. F.; Rotin, D. *Cancer Res.* **1989**, *49*, 4373–4384.
- (38) Rich, A.; Davies, D. R.; Crick, F. H. C.; Watson, J. D. *J. Mol. Biol.* **1961**, *3*, 71–86.
- (39) Saha, S.; Chakraborty, K.; Krishnan, Y. *Chem. Commun.* **2012**, *48*, 2513–2515.
- (40) Chakraborty, S.; Sharma, S.; Maiti, P. K.; Krishnan, Y. *Nucleic Acids Res.* **2009**, *37*, 2810–2817.
- (41) Saha, S.; Bhatia, D.; Krishnan, Y. *Small* **2010**, *6*, 1288–1292.
- (42) Safaee, N.; Noronha, A. M.; Rodionov, D.; Kozlov, G.; Wilds, C. J.; Sheldrick, G. M.; Gehring, K. *Angew. Chem. Int. Ed. Engl.* **2013**, *52*, 10370–10373.
- (43) Ikeda, H.; Fernandez, R.; Wilk, A.; Jr, J. J. B.; Huang, X.; Marquez, V. E. *Nucleic Acids Res.* **1998**, *26*, 2237–2244.
- (44) Williams, A. A.; Darwanto, A.; Theruvathu, J. A.; Burdzy, A.; Jonathan, W.; Sowers, L. C. *Biochemistry* **2009**, *48*, 11994–12004.
- (45) Pallan, P. S.; Greene, E. M.; Jicman, P. A.; Pandey, R. K.; Manoharan, M.; Rozners, E.; Egli, M. *Nucleic Acids Res.* **2011**, *39*, 3482–3495.
- (46) Patra, A.; Paolillo, M.; Charisse, K.; Manoharan, M.; Rozners, E.; Egli, M. *Angew.*

Chemie **2012**, *124*, 12033–12036.

- (47) Martin-Pintado, N.; Deleavey, G. F.; Portella, G.; Campos-Olivas, R.; Orozco, M.; Damha, M. J.; González, C. *Angew. Chem. Int. Ed. Engl.* **2013**, *52*, 12065–12068.
- (48) Fenna, C. P.; Wilkinson, V. J.; Arnold, J. R. P.; Cosstick, R.; Fisher, J. *Chem. Commun.* **2008**, 3567–3569.
- (49) Li, Z.; Lech, C. J.; Phan, A. T. *Nucleic Acids Res.* **2014**, *42*, 4068–4079.
- (50) Watts, J. K.; Katolik, A.; Viladoms, J.; Damha, M. J. *Org. Biomol. Chem.* **2009**, *7*, 1904–1910.
- (51) Monia, B. P.; Lesnik, E. A.; Gonzalezn, C.; Liman, W. F.; Mcgee, D.; Guinosso, C. J.; Kawasaki, A. M.; Cook, P. D.; Freier, S. M. *J. Biol. Chem.* **1993**, *268*, 14514–14522.
- (52) Crooke, S. T.; Lebleu, B. *Antisense Research and Applications*; CRC Press: Boca Ranton, Ann Arbor, London, Tokyo, 1993.
- (53) Denisov, A. Y.; Noronha, A. M.; Wilds, C. J.; Trempe, J.; Pon, R. T.; Gehring, K.; Damha, M. J. *Nucleic Acids Res.* **2001**, *29*, 4284–4293.
- (54) Venkateswarlu, D.; Ferguson, D. M. *J. Am. Chem. Soc.* **1999**, *121*, 5609–5610.
- (55) Watts, J. K.; Martín-Pintado, N.; Gómez-Pinto, I.; Schwartzenruber, J.; Portella, G.; Orozco, M.; González, C.; Damha, M. J. *Nucleic Acids Res.* **2010**, *38*, 2498–2511.
- (56) Noronha, A. M.; Wilds, C. J.; Lok, C.-N.; Viazovkina, K.; Arion, D.; Parniak, M. a.; Damha, M. J. *Biochemistry* **2000**, *39*, 7050–7062.
- (57) Damha, M. J.; Wilds, C. J.; Noronha, A.; Brukner, I.; Borkow, G.; Arion, D.; Parniak, M. A. *J. Am. Chem. Soc.* **1998**, *120*, 12976–12977.
- (58) Lubini, P.; Zürcher, W.; Egli, M. *Chem. Biol.* **1994**, *1*, 39–45.
- (59) Nishizaki, T.; Iwai, S.; Ohtsuka, E.; Nakamura, H. *Biochemistry* **1997**, *36*, 2577–2585.

- (60) Sproat, B. S.; Lamond, A. I.; Beijer, B.; Neuner, P.; Ryder, U. *Nucleic Acids Res.* **1989**, *17*, 3373–3386.
- (61) Inoue, H.; Hayase, Y.; Imura, A.; Iwai, S.; Miura, K.; Ohtsuka, E. *Nucleic Acids Res.* **1987**, *15*, 6131–6148.
- (62) Lesnik, E. a; Guinosso, C. J.; Kawasaki, a M.; Sasmor, H.; Zounes, M.; Cummins, L. L.; Ecker, D. J.; Cook, P. D.; Freier, S. M. *Biochemistry* **1993**, *32*, 7832–7838.
- (63) Puglisi, J. D.; Tinoco, I. *Methods Enzymol.* **1989**, *180*, 304–325.
- (64) Acharya, P.; Cheruku, P.; Chatterjee, S.; Acharya, S.; Chattopadhyaya, J. *J. Am. Chem. Soc.* **2004**, *126*, 2862–2869.
- (65) Kejnovská, I.; Kypr, J.; Vorlícková, M. *Biochem. Biophys. Res. Commun.* **2007**, *353*, 776–779.
- (66) Kankia, B. I. *Nucleic Acids Res.* **2003**, *31*, 5101–5107.
- (67) Kool, E. T. *Chem. Rev.* **1997**, *97*, 1473–1487.
- (68) Gu, Y.; Kar, T.; Scheiner, S. *J. Am. Chem. Soc.* **1999**, *121*, 9411–9422.
- (69) Berger, I.; Egli, M.; Rich, A. *Proc. Natl. Acad. Sci. U. S. A.* **1996**, *93*, 12116–12121.
- (70) Taylor, R.; Kennard, O. *J. Am. Chem. Soc.* **1982**, *104*, 3209–3212.
- (71) Kypr, J.; Kejnovska, I.; Renciuik, D.; Vorlickova, M. *Nucleic Acids Res.* **2009**, *37*, 1713–1725.
- (72) Chatterjee, S.; Pathmasiri, W.; Plashkevych, O.; Honcharenko, D.; Varghese, O. P.; Maiti, M.; Chattopadhyaya, J. *Org. Biomol. Chem.* **2006**, *4*, 1675–1686.
- (73) Shimizu, M.; Konishi, A.; Shimada, Y.; Inoue, H.; Ohtsuka, E. *Fed. Eur. Biochem. Soc.* **1992**, *302*, 155–158.
- (74) Egli, M.; Portmann, S.; Usman, N. *Biochemistry* **1996**, *35*, 8489–8494.

- (75) Keller, W. *Cell* **1984**, *39*, 423–425.
- (76) Robidoux, S.; Klinck, R.; Gehring, K.; Damha, M. J. *J. Biomol. Struct. Dyn.* **1997**, *15*, 517–527.
- (77) Rozners, E. *Curr. Protoc. Nucleic Acid Chem.* **2010**, 43:7.14.1–7.14.13.
- (78) Marquez, V. E.; Lim, M.-I. *Med. Res Rev* **1986**, *6*, 1–40.
- (79) Jones, G. D.; Lesnik, E. A.; Owens, S. R.; Risen, L. M.; Walker, R. T. *Nucleic Acids Res.* **1996**, *24*, 4117–4122.
- (80) Martinez-Montero, S.; Deleavey, G. F.; Dierker-Viik, A.; Lindovska, P.; Ilina, T.; Portella, G.; Orozco, M.; Parniak, M. A.; Gonzalez, C.; Damha, M. J. *J. Org. Chem.* **2015**, *80*, 3083–3091.
- (81) Peterson, M.; Wengel, J. *Trends Biotechnol.* **2003**, *21*, 74–81.
- (82) Bellon, L. *Curr. Protoc. Nucleic Acid Chem.* **2000**, 1:3.6.1–3.6.13.
- (83) Beaucage, S. L.; Caruthers, M. H. *Curr. Protoc. Nucleic Acid Chem.* **2000**, 00:3.3:3.3.1–3.3.20.
- (84) Usman, N.; Ogilvie, K. K.; Jiang, M. Y.; Cedergren, R. J. *J. Am. Chem. Soc.* **1987**, *109*, 7845–7854.
- (85) Caruthers, M. H.; Barone, A. D.; Beaucage, S. L.; Dodds, D. R.; Fisher, E. F.; McBride, L. J.; Matteucci, M.; Stabinsky, Z.; Tang, J. Y. *Methods Enzymol.* **1987**, *154*, 287–313.
- (86) Guzaev, A. P.; Manoharan, M. *J. Am. Chem. Soc.* **2003**, *125*, 2380–2381.
- (87) Tataurov, A. V.; You, Y.; Owczarzy, R. *Biophys. Chem.* **2008**, *133*, 66–70.
- (88) Andrus, A.; Kuimelis, R. G. *Curr. Protoc. Nucleic Acid Chem.* **2000**, 10.6, 10.6.1–10.6.6.
- (89) Breslauer, K. J. *Methods Enzymol.* **1995**, *259*, 221–242.

(90) Seeman, N. C. *Annu. Rev. Biochem.* **2010**, *79*, 65–87.

Appendix

Snake Venom Digest Characterization Data

Sequence	Nucleoside	Expected	Calculated
dT-rA ₄ -dA-rA ₃	dT	1	1.13
	rA+rI	7	7.01
	dA+dI	1	1
dT-rA ₄ -rA ^{2'-OMe} -rA ₃	dT	1	1.05
	rA+rI	7	7.16
	rA ^{2'-OMe} +rI ^{2'-OMe}	1	1
dT-rA ^{2'-OMe} ₄ -dA-rA ^{2'-OMe} ₃	dT	1	1
	rA ^{2'-OMe} +rI ^{2'-OMe}	7	7.0
	dA+dI	1	0.95
dT-rA ₃ -dA ₂ -rA ₃	dT	1	1
	rA+rI	6	5.8
	dA+dI	2	1.9
dT-rA ₃ -dA ₃ -rA ₂	dT	1	1
	rA+rI	5	4.8
	dA+dI	3	2.8
dT-afA ₈	dT	1	1
	afA+afI	8	8.7
dT-rA ₄ -aA-rA ₃	dT	1	1
	rA+rI	7	7.4
	aA+aI	1	1
dT-aA ₈	dT	1	1
	aA+aI	8	8.8
dT-rA ₄ -rfA-rA	dT	1	NA
	rA+rI	7	NA
	rfA+rI	1	NA
rA ₅ -rfA-rA ₅	rA+rI	10	10.3
	fA+fI	1	1
rA ₁₀ -rfA-rA ₅	rA+rI	15	14.6
	fA+fI	1	1
rA ₅ -rfA ₂ -rA ₄	rA+rI	9	9.2
	fA+fI	2	2
rA ₄ -rfA ₃ -rA ₄	rA+rI	8	8.1
	fA+fI	3	3
rA ₄ -dA ₃ -rA ₄	rA+rI	8	7.8
	dA+dI	3	3
rA ₁₀ -dA-rA ₅	rA+rI	15	16.4
	dA+dI	1	1
rA ₉ -dA ₂ -rA ₅	rA+rI	14	13.8
	dA+dI	2	2
rA ₁₀ -dA-rA ₃ -dA-rA	rA+rI	14	14.3
	dA+dI	2	2
rA ₉ -dA ₃ -rA ₄	rA+rI	13	13.0
	dA+dI	3	3

$rA(rA_4-rfA-rA_3)_2$	rA+rl	15	15.2
	rfA+rfl	2	2
$rA(rfA_8)_2$	rA+rl	1	1
	rfA+rfl	16	17.2

ESI-qTOF Mass Spectrometry Characterization Data

rA+dA

Oligonucleotide	Expected (g/mol)	Experimental (m/z)
rA_{11}	3559.3	3559.6
rA_{16}	5205.4	5206.2
$dT-rA_8$	2875.9	2876.3
$rA_4-dA-rA_3$	2555.7	2556.1
$dT-rA_4-dA-rA_3$	2859.9	2860.3
$dT-rA_3-dA_2-rA_3$	2843.9	2844.3
$dT-rA_3-dA_3-rA_2$	2827.9	2828.3
$rA_5-dA_2-rA_4$	3527.3	3527.0
$rA_4-dA_3-rA_4$	3511.3	3511.0

rA+rfA

Oligonucleotide	Expected (g/mol)	Experimental (m/z)
$rA_5-rfA-rA_5$	3561.3	3561.7
$rA_5-rfA_2-rA_4$	3563.3	3563.0
$rA_4-rfA_3-rA_4$	3565.3	3565.0
$rA_{10}-rfA-rA_5$	5207.4	5208.3
rfA_8	2587.6	2587
rfA_{11}	3581.2	3581.0
rfA_{16}	5237.2	5238.4
$dT-rA_4-rfA-rA_3$	2877.9	2878.3

rA+aA+afA+rA^{2'-OMe}

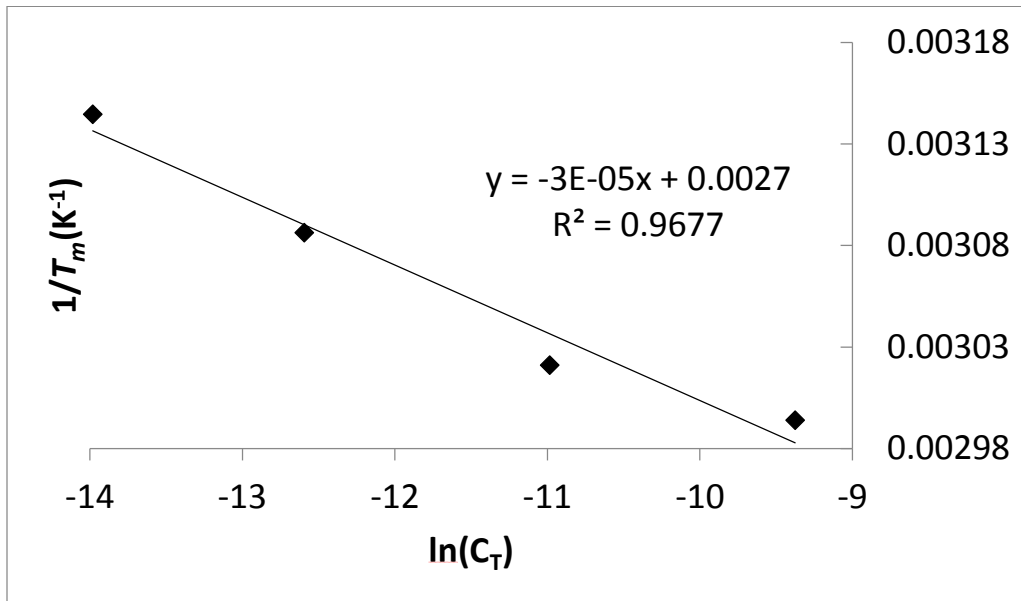
Oligonucleotide	Expected (g/mol)	Experimental (m/z)
dT-rA ₄ -afA-rA ₃	2877.9	2878.2
dT-afA ₈	2891.8	2892.0
dT-rA ₄ -aA ₈ -rA ₃	2875.9	2876.3
dT-aA ₈	2875.9	2876.2
dT-rA ₄ -rA ^{2'-OMe} -rA ₃	2889.9	2890.4
dT-rA ^{2'-OMe} ₈	2988.1	2988.5

Branched oligonucleotides

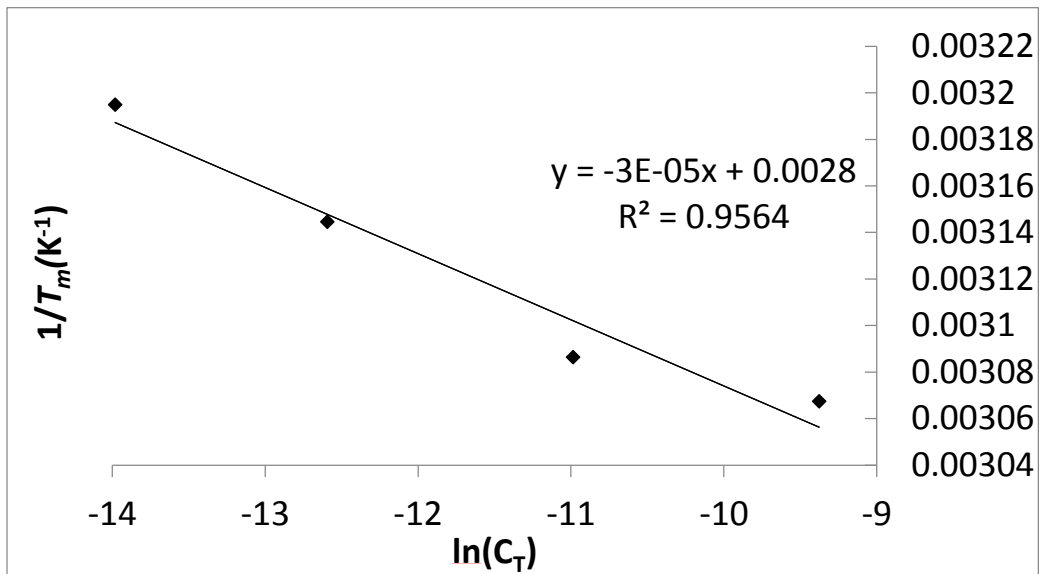
Oligonucleotide	Expected (g/mol)	Experimental (m/z)
rA-(rA ₈)	5534.6	5535
rA-(rA ₄ -dA-rA ₃)	5502.6	5502.8
rA-(rA ₄ -rfA-rA ₃)	5538.6	5539
rA-(rfA ₈)	5566.4	5567

Van't Hoff Plots

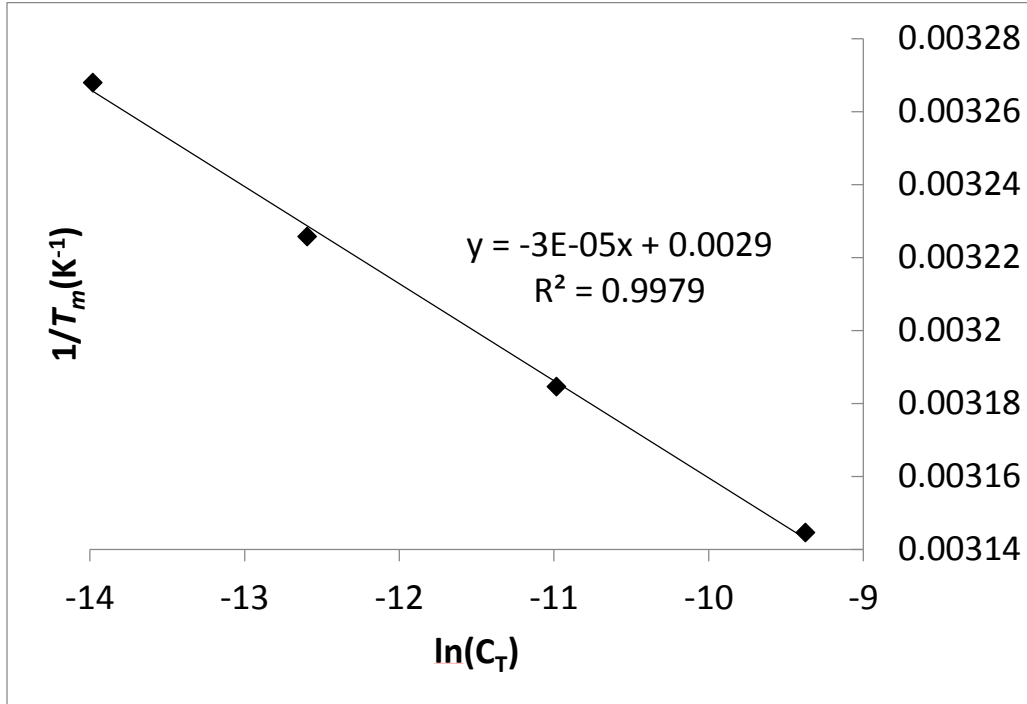
dT-rA₈



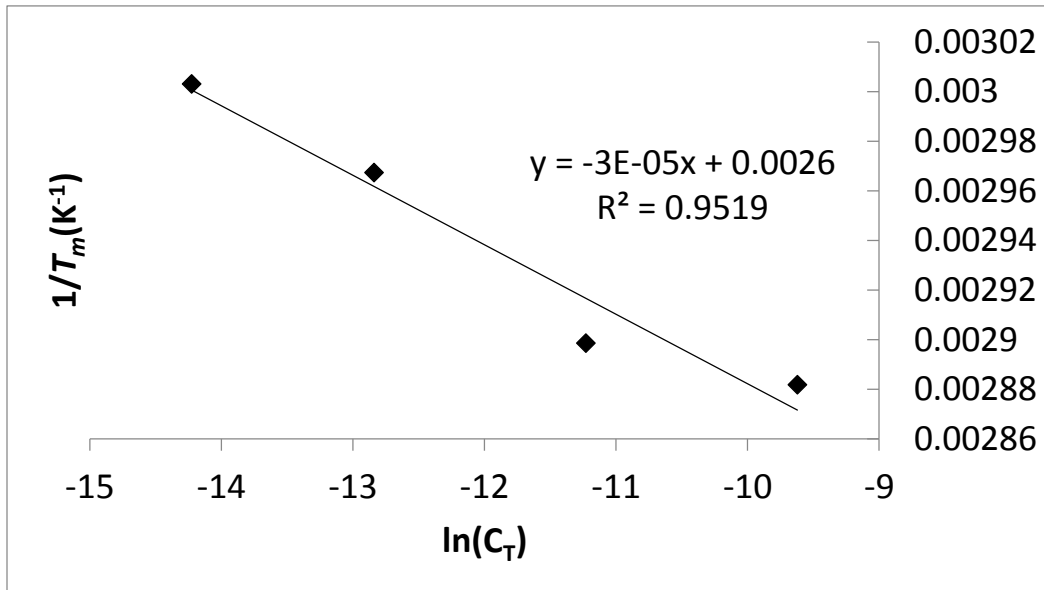
dT-rA₄-dA-rA₃



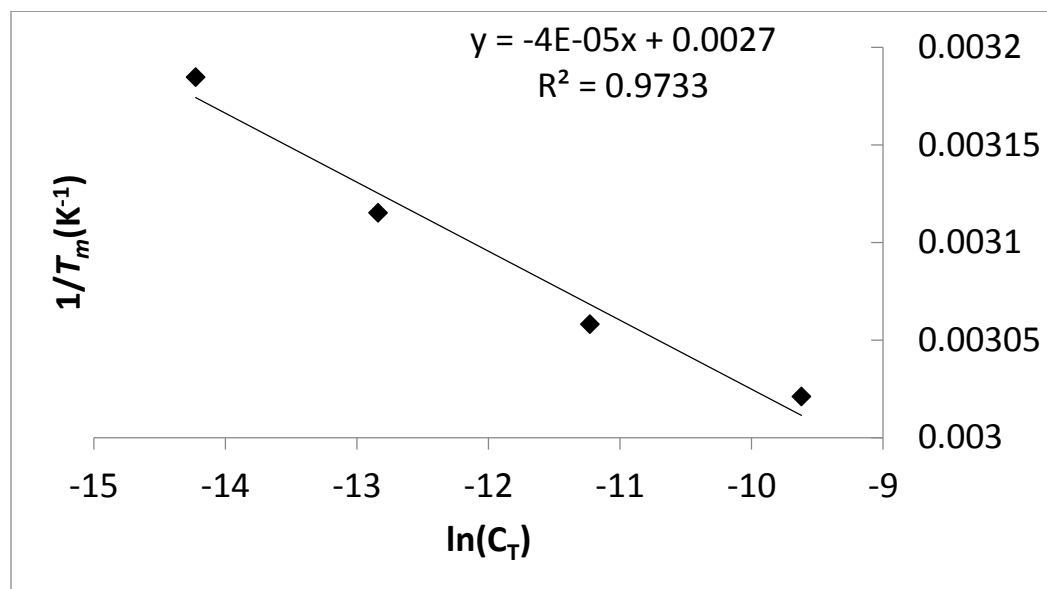
dT-rA3-dA2-rA3



rA11

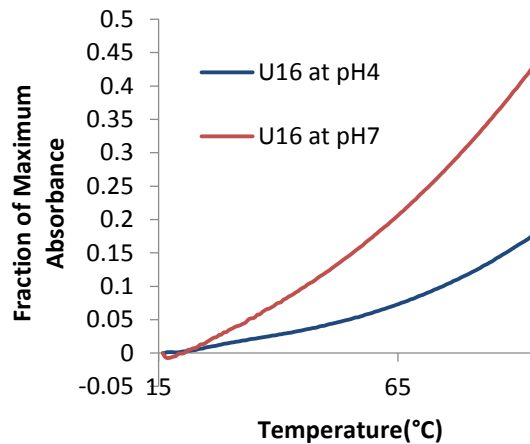
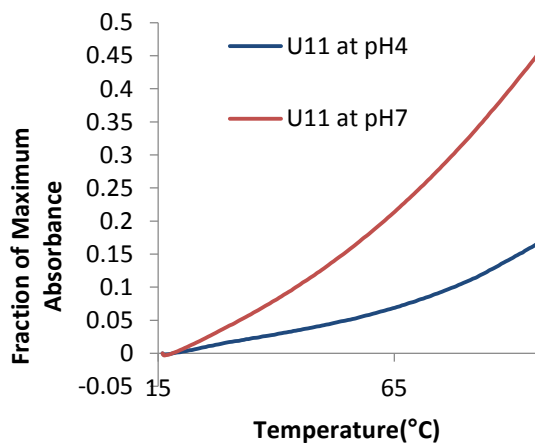


rfA₁₁



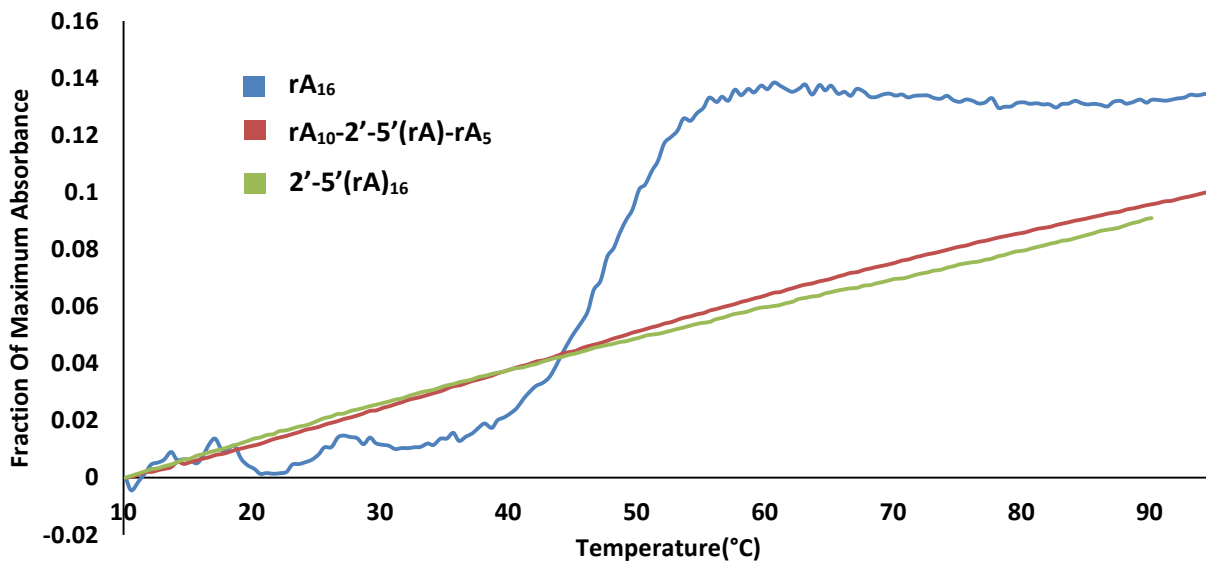
UV Thermal Denaturation Studies on rU₁₁+rU₁₆ Controls

(Buffers: 39mM Na₂HPO₄, 31 mM citric acid [pH 4]; 87 mM Na₂HPO₄, 6.5 mM citric acid [pH 7])



UV Thermal Denaturation Studies on 2'-5' Phosphodiester Bond at Neutral pH, 4.4 M NH₄Cl

Conditions: Absorbance measured at 260 nm, ramped from 10-95°C at 0.5°C/min. 0.2 OD of oligonucleotide. Buffer: 50 mM NaCaco



pH dependence of T_m for rA₁₆, rfA₁₆, rA₁₁, & rA^{2'-OMe}₁₁

Conditions: Absorbance measured at 260 nm, ramped from (15)25-95°C at 0.5°C/min. 0.2 OD of oligonucleotide. Buffer: 40 mM Na₂HPO₄, 30 mM citric acid

